KEK-TH-670
KA-TP-27-1999
UR-1601
DESY 99-201
hep-ph/0002066

One-loop sfermion corrections to $e^-e^+ \to W^-W^+$ in the MSSM

Sher Alam[1], **Kaoru Hagiwara**[1], **Shinya Kanemura**[2],
Robert Szalapski[3] and **Yoshiaki Umeda**[1,4]

[1] *Theory Group, KEK, Tsukuba, Ibaraki 305-0801, Japan*
[2] *Institut für Theoretische Physik, Universität Karlsruhe, D-76128 Karlsruhe, Germany*
[3] *Department of Physics and Astronomy, University of Rochester, Rochester, NY 14627-0171, USA*
[4] *II Institut für Theoretische Physik, Universität Hamburg, D-22761 Hamburg, Germany*

Abstract

We study one-loop effects of sfermions on helicity amplitudes for $e^-e^+ \to W^-W^+$ in the Minimal Supersymmetric Standard Model. The one-loop contributions are calculated in the $\overline{\rm MS}$ renormalization scheme. In order to verify the validity of the analytic calculation and the numerical program, the following tests are performed. (i) The BRS sum rules hold exactly among the analytic expressions of the form factors of the $e^-e^+ \to W^-W^+$ amplitude and those of the amplitudes where the external $W^\pm$ bosons are replaced by the corresponding Goldstone bosons $\chi^\pm$, hence they hold within the expected accuracy of the numerical program. (ii) The one-loop sfermion contribution to the amplitudes decouple in the heavy mass limit. This property is used to test the overall normalization of the amplitudes. In order to observe the analytically exact decoupling, the amplitudes are expanded by the $\overline{\rm MS}$ couplings of the Standard Model. (iii) The high-energy analytic formulas of the helicity amplitudes, which are verified by using the equivalence theorem analytically, are used for the numerical test of the high energy behavior of the amplitudes. We then investigate the magnitude of the one-loop effects on each helicity amplitude which may be measured by experiments at future linear colliders. Under the constraint from available precision data, the one-loop corrections to a few helicity amplitudes (for example, the longitudinal-W-pair production) can be at most from -0.8% to $+0.6\%$ in magnitude in the observables. The corrections in the helicity-summed cross sections are smaller, typically a few times $\pm 0.1\%$ at large scattering angles.

1 Introduction

As collider experiments move to higher energy and higher luminosity we are able to probe previously untested aspects of the Standard Model (SM) and to search for new physics beyond the SM. A leading candidate for the new physics is the Supersymmetric Standard Model (SUSY SM). If nature has indeed the supersymmetry broken at the weak-scale, we should expect to observe the loop level corrections due to superpartner particles as well as those from the SM particles. On the other hand, through these loop-level predictions of the SUSY the non-observation of new-physics effects may be used to place constraints on the SUSY Lagrangian. The energy upgrades of the LEP facility at CERN, LEP 2, and the possibility of a future linear collider such as JLC, NLC and TESLA motivate us to study W-boson pair production through electron-positron annihilation[1, 2].

In this paper, reflecting the above prospects, the one-loop contributions of sfermions to helicity amplitudes for $e^-e^+ \to W^-W^+$ are investigated in the Minimal Supersymmetric Standard Model (MSSM). The new physics effects on these amplitudes have been investigated in a generic framework in Refs. [3, 4, 5]. In the SM, the earliest works for the radiative corrections to $e^-e^+ \to W^-W^+$[6, 7] have been followed by authors of Refs. [8, 9, 10, 11] for the process with the on-shell W bosons. The study of radiative corrections to the off-shell W-pair production has been developed in Refs. [12, 13]. The complete SUSY corrections to the differential cross section of $e^-e^+ \to W^-W^+$ have been calculated in Ref. [14] in the model with spontaneously broken supersymmetry. The sfermion corrections to the process $e^-e^+ \to W^-W^+$ have been discussed in Ref. [15]. The trilinear gauge-boson vertices, γWW and ZWW, are the important ingredients of this process[16, 1, 17, 18]. Several authors have calculated one-loop SUSY contributions to the trilinear γWW and ZWW vertices[19].

In the calculation of the one-loop effects to the $e^-e^+ \to W^-W^+$ helicity amplitudes, a form-factor decomposition of helicity amplitudes is invaluable[16, 1, 10]. For this reason we present our results by extending the formalism of Ref. [4]. In Sec. 2, the essential aspects of the form-factor formalism and the helicity amplitudes for the process $e^-e^+ \to W^-W^+$ are reviewed. The formalism is also extended such that the unphysical scalar polarization of the final-state W bosons may be also studied[17, 20]. This will be important when we employ the BRS sum rules later for the test of the one-loop form factor calculation. A form-factor decomposition for the processes including the Nambu-Goldstone bosons ($e^-e^+ \to \chi^\mp W^\pm$ and $e^-e^+ \to \chi^- \chi^+$) is then presented along with the BRS sum rules among the form factors of W^-W^+ production and those of $W^\mp\chi^\pm$ or $\chi^-\chi^+$ production processes. In Sec. 3, we discuss the tree-level results of the helicity amplitudes. In Sec. 4, we calculate the one-loop sfermion effects on the form factors of each process in the $\overline{\mathrm{MS}}$ scheme[21]. One of the difficulties of performing loop-level calculations is determining the reliability of the results. This is especially so in the process $e^-e^+ \to W^-W^+$ where subtle cancellation among diagrams which individually grow with energy takes place. Violation of the gauge-theory cancellation due to incomplete higher-order terms can hence lead to artificially large corrections. Therefore, Sec. 5 is devoted to test our calculation by using the following three instruments:

(i) From the global BRS invariance of the electroweak theory[22], we obtain sum rules among the form factors of $e^-e^+ \to W^-W^+$ and those of the processes in which one or two external W

bosons are replaced by the corresponding Nambu-Goldstone bosons[20, 23].

(ii) After properly renormalizing the $\overline{\text{MS}}$ couplings to ensure the observed values of the low-energy electroweak observables (α, m_Z and G_F), the full one-loop amplitudes reduce to those of the SM in the large mass limit of the SUSY particles[24, 25]. By expanding the one-loop amplitudes in terms of $\overline{\text{MS}}$ couplings of the SM, the decoupling property can be observed exactly.

(iii) The analytic expressions of the amplitudes in the high-energy limit are useful to test the numerical program for the of the one-loop $e^-e^+ \to W^-W^+$ amplitudes in this limit. Such analytic expressions are confirmed by using the equivalence between the longitudinally polarized W bosons and their associated Goldstone bosons, so call the equivalence theorem[26, 27].

The test (i) ensures the gauge-theory cancellation among the one-loop corrected amplitudes, and hence shows the correctness of the loop calculation. The test (ii) ensures the validity of the renormalization scheme and shows the correctness of the overall normalization factors such as the external wave-function corrections which cannot be tested by the BRS sum rules. The test (iii) demonstrates the stability of our numerical program at high energies. A presentaion of these tests is one main part in this paper in addition to evaluation of the magnitude of the sfermion contribution. In Sec. 6, we will show our numerical results of the $e^-e^+ \to W^-W^+$ helicity amplitudes, and we will examine in which case the sfermion effects become substantial. The sfermion effects on the $e^-e^+ \to W^-W^+$ cross section are then discussed under the constraint from the direct search experiments and the electroweak precision measurements[28, 29]. In Sec. 7, we discuss the results and present our conclusion. To establish our notation and conventions, we present the relevant portions of the SUSY Lagrangian in Appendix A. This includes the sfermion–gauge boson and sfermion–Nambu-Goldstone boson interactions. Appendix B contains all the explicit formulas for the one-loop sfermion contributions to the $e^-e^+ \to W^-W^+$ form factors. In Appendix C, we calculate sfermion effects on the form factors of the processes where the Nambu-Goldstone bosons appear in external lines. Useful formulas of the loop integral functions for the heavy-mass limit and the high-energy limit are given in Appendix D.

2 The helicity amplitudes

2.1 $e^-e^+ \to W^-W^+$

The process, $e^-(k,\tau) + e^+(\overline{k},\overline{\tau}) \to W^-(p,\lambda) + W^+(\overline{p},\overline{\lambda})$, is depicted in Fig. 1. The momenta of the e^-, e^+, W^- and W^+ are k, $\overline{k}$, p and $\overline{p}$, respectively. The helicity of the incoming e^- (e^+) is given by $\frac{1}{2}\tau$ ($\frac{1}{2}\overline{\tau}$), and λ ($\overline{\lambda}$) is the helicity of the outgoing W^- (W^+). In the limit of massless electrons only $\overline{\tau} = -\tau$ helicity amplitudes survive, and they may be written for each set of $\{\tau, \lambda, \overline{\lambda}\}$ as[4, 20]

$$\mathcal{M}_\tau^{\lambda\overline{\lambda}}(e^-e^+ \to W^-W^+) = \sum_{i=1}^{16} F_{i,\tau}(s,t)\, j_\mu(k,\overline{k},\tau) T_i^{\mu\alpha\beta} \epsilon_\alpha(p,\lambda)^* \epsilon_\beta(\overline{p},\overline{\lambda})^* \,, \tag{2.1}$$

where all dynamical information is contained in the form-factors $F_{i,\tau}(s,t)$ with $s = (k+\overline{k})^2 \equiv q^2$ and $t = (k-p)^2$. The other factors in Eq. (2.1) are of a purely kinematical nature; $\epsilon_\alpha(p,\lambda)^*$ and $\epsilon_\beta(\overline{p},\overline{\lambda})^*$

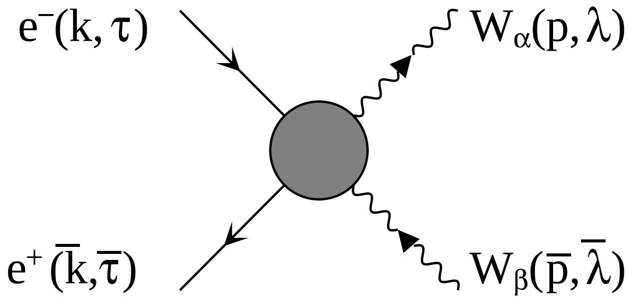

Figure 1: The process $e^-e^+ \to W^-W^+$ with momentum and helicity assignments. The momenta k and $\overline{k}$ are incoming, but p and $\overline{p}$ are outgoing. The arrows in the W boson lines indicate the flow of a negative electric charge.

	F_1	F_2	F_3	F_4	F_5	F_6	F_7	F_8	F_9
C	$+$	$+$	$+$	$-$	$-$	$+$	$+$	$+$	$-$
P	$+$	$+$	$+$	$+$	$-$	$-$	$-$	$+$	$-$
CP	$+$	$+$	$+$	$-$	$+$	$-$	$-$	$+$	$+$

Table 1: The properties of the form factors $F_{i,\tau}(s,t)$ under the discrete transformations C, P and CP. Only those which contribute to physical processes are listed.

are the polarization vectors for W^- and W^+, respectively, and $j_\mu(k,\overline{k},\tau)$ is the fermion current of massless electrons. The 16 independent basis tensors, $T_i^{\mu\alpha\beta}$, are defined by Eqs. (2.6) in Ref. [20]. For the process with physically polarized W bosons ($\lambda,\overline{\lambda} = -,+$ or 0) are decomposed by the first 9 of $T_i^{\mu\alpha\beta}$. The rest of $T_i^{\mu\alpha\beta}$ are needed for treating the process including unphysical scalar W bosons ($\lambda,\overline{\lambda} = S$). The properties of $F_{i,\tau}(s,t)$ under the discrete transformations of charge conjugation (C), parity inversion (P) and the combined transformation CP are summarized in Table 1.

Finally, the 18 physical helicity amplitudes are given in terms of the form factors ($F_{1,\tau}$ - $F_{9,\tau}$) by

$$M_\tau^{00} = -s\left[-\gamma^2\beta(1+\beta^2)F_{1,\tau} + 4\beta^3\gamma^4F_{2,\tau} + 2\beta\gamma^2F_{3,\tau} - 2\gamma^2\cos\theta F_{8,\tau}\right]\sin\theta, \tag{2.2a}$$

$$M_\tau^{\pm 0} = s\gamma\left[\beta(F_{3,\tau} - iF_{4,\tau} \pm \beta F_{5,\tau}) \pm iF_{6,\tau} \pm (\tau \mp 2\cos\theta)F_{8,\tau} \mp 4\gamma^2\beta\cos\theta F_{9,\tau}\right]\frac{(\tau\pm\cos\theta)}{\sqrt{2}}, \tag{2.2b}$$

$$M_\tau^{0\pm} = s\gamma\left[\beta(F_{3,\tau} + iF_{4,\tau} \mp \beta F_{5,\tau}) \pm iF_{6,\tau} \mp (\tau \pm 2\cos\theta)F_{8,\tau} \pm 4\gamma^2\cos\theta F_{9,\tau}\right]\frac{(\tau\mp\cos\theta)}{\sqrt{2}}, \tag{2.2c}$$

$$M_\tau^{\pm\pm} = s\left[-\beta F_{1,\tau} \mp iF_{6,\tau} \mp 4i\beta^2\gamma^2F_{7,\tau} + \cos\theta F_{8,\tau} + 4\beta\gamma^2\tau F_{9,\tau}\right]\sin\theta, \tag{2.2d}$$

$$M_\tau^{\pm\mp} = \mp s(F_{8,\tau} \pm 4\beta\gamma^2F_{9,\tau})(\tau\pm\cos\theta)\sin\theta, \tag{2.2e}$$

where the scattering angle θ is measured between the momentum vectors of the e^- and W^-, and

$$\beta = \sqrt{1 - m_W^2/E_W^2}\,, \quad \gamma = E_W/m_W\,, \quad E_W = \sqrt{s}/2\,. \tag{2.3}$$

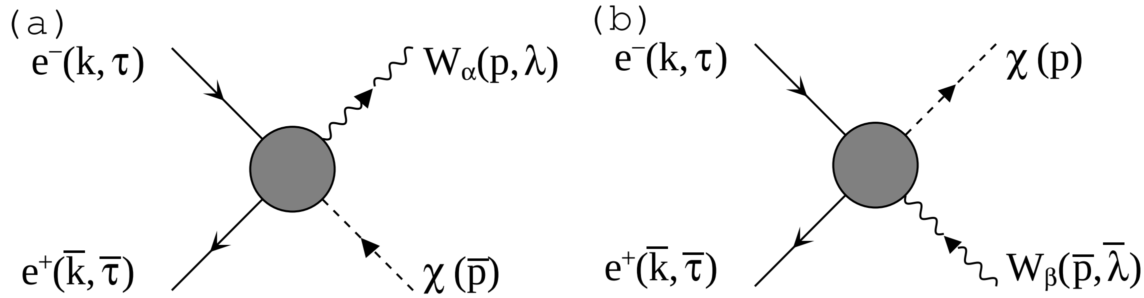

Figure 2: The processes (a) $e^-e^+ \to W^-\chi^+$ and (b) $e^-e^+ \to \chi^-W^+$ with the momentum and helicity assignments chosen to agree with those in Fig. 1. The momenta k and $\overline{k}$ are incoming, but p and $\overline{p}$ are outgoing. The arrows in the W and χ lines indicate the flow of a negative electric charge.

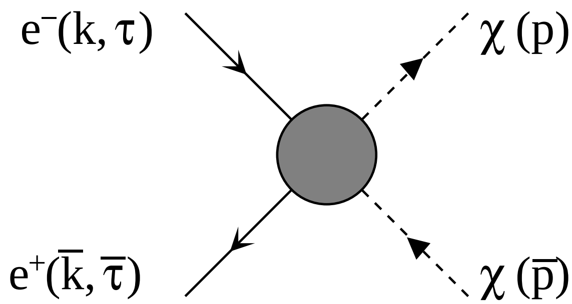

Figure 3: The process $e^-e^+ \to \chi^-\chi^+$ with momentum and helicity assignments chosen to coincide with those in Fig. 1. The momenta k and $\overline{k}$ are incoming, but p and $\overline{p}$ are outgoing. The arrows in the $\chi^\pm$ boson lines indicate the flow of a negative electric charge.

2.2 $e^-e^+ \to W^\mp\chi^\pm$ and $e^-e^+ \to \chi^-\chi^+$

The process for $e^-e^+ \to W^\mp\chi^\pm$ are shown in Figs. 2(a) and 2(b). Our phase convention for the Nambu-Goldstone bosons $\chi^\pm$ is that of Ref. [17]. We decompose the amplitudes as[20]

$$\mathcal{M}_\tau^\lambda(e^-e^+ \to W^-\chi^+) = i\sum_{j=1}^{4} H_{j,\tau}(s,t)\, j_\mu(k,\overline{k},\tau) S_j^{\mu\alpha}\epsilon_\alpha(p,\lambda)^* \; , \tag{2.4a}$$

$$\mathcal{M}_\tau^{\overline{\lambda}}(e^-e^+ \to \chi^-W^+) = i\sum_{j=1}^{4} \overline{H}_{j,\tau}(s,t)\, j_\mu(k,\overline{k},\tau) \overline{S}_j^{\mu\beta}\epsilon_\beta(\overline{p},\overline{\lambda})^* \; . \tag{2.4b}$$

In (2.4a), there are four independent basis tensors, $S_i^{\mu\alpha}$ (i = 1-4), corresponding to the four, three physical plus one scalar, polarizations of the W^- boson. The corresponding form factors are given by $H_{i,\tau}(s,t)$. A second set of four tensors, $\overline{S}_i^{\mu\beta}$, is introduced to the χ^-W^+ production. The corresponding form factors are written by $\overline{H}_{i,\tau}(s,t)$. The basis tensors $S_i^{\mu\alpha}$ and $\overline{S}_i^{\mu\beta}$ are given in Ref [20].

Next, the amplitude for the process $e^-e^+ \to \chi^-\chi^+$ shown in Fig. 3 may be expressed as

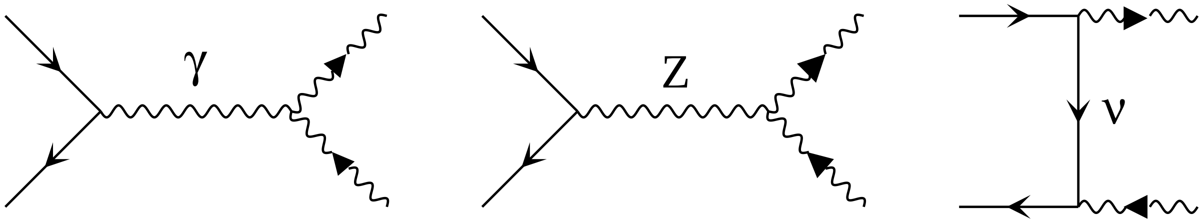

Figure 4: Tree-level Feynman diagrams for $e^-e^+ \to W^-W^+$. The arrows on the W-boson lines indicate the flow of a negative electric charge.

i	1	2	3	4	5	6	7	8	9	10	11	12	13	14	15	16
$f_i^{\gamma\,(0)}$	1		2							-1			1			
$f_i^{Z\,(0)}$	1		2							-1			1			
$f_i^{t\,(0)}$	1		2		1			1		-2			2			

Table 2: Explicit values for the $f_i^{\gamma\,(0)}$, $f_i^{Z\,(0)}$ and $f_i^{t\,(0)}$ in Eq. (3.1). Only nonzero values are shown.

$$\mathcal{M}_\tau(e^-e^+ \to \chi^-\chi^+) = P^\mu j_\mu(k, \bar{k}, \tau) R_\tau(s,t) \; . \tag{2.5}$$

Notice that there is only one form factor, $R_\tau(s,t)$, which carries an index for the electron helicity.

3 The tree-diagram contributions to the helicity amplitudes

Before going to discuss the one-loop sfermion effects, let us study the behavior of the tree-level helicity amplitudes for $e^-e^+ \to W^-W^+$. The Feynman graphs are shown in Fig. 4. The contribution of these diagrams to the form factors introduced in Sec. 2 is expressed by

$$F_{i,\tau}^{tree}(s,t) = \frac{\hat{e}^2}{s} Q_e f_i^{\gamma\,(0)} + \frac{\hat{g}^2}{s - m_W^2/\hat{c}^2}(T_e^3 - \hat{s}^2 Q_e) f_i^{Z\,(0)} + \frac{T_e^3 \hat{g}^2}{2t} f_i^{t\,(0)} \, , \tag{3.1}$$

where $Q_e = -1$ and T_e^3 are the electric charge and the third component of weak iso-spin of the electron, respectively. At tree level, we should set the Z-boson mass in the propagator as

$$m_Z^2 = \frac{m_W^2}{\hat{c}^2}, \quad \text{(tree level)}, \tag{3.2}$$

in order for the tree-level BRS sum-rules to be satisfied[20]. The coefficients $f_i^{\gamma(0)}$, $f_i^{Z(0)}$ and $f_i^{t(0)}$ are listed in Table 2.

We here take the W-boson mass m_W^2 and the $\overline{\rm MS}$ couplings $\hat{e}^2$ and $\hat{s}^2$ as the input parameters. In the SM, we can determine the $\overline{\rm MS}$ running coupling constants from the relations[31]

$$\frac{1}{\hat{\alpha}(m_Z)} = \frac{1}{\overline{\alpha}(m_Z^2)} - 0.88 + \frac{8}{9\pi}\left(1 + \frac{\alpha_s}{\pi}\right) \ln \frac{m_t}{m_Z} \, , \tag{3.3a}$$

$$\frac{\hat{s}^2(m_Z)}{\hat{\alpha}(m_Z)} = \frac{\overline{s}^2(m_Z^2)}{\overline{\alpha}(m_Z^2)} - 0.11 + \frac{1}{3\pi}\left(1+\frac{\alpha_s}{\pi}\right)\ln\frac{m_t}{m_Z}\,, \tag{3.3b}$$

where the effective charges[32] are estimated as $1/\overline{\alpha}(m_Z^2) = 128.75 \pm 0.09$[33] and $\bar{s}^2(m_Z^2) = 0.23035 \pm 0.00023$ for $m_t = 175$GeV and $m_H = 100$GeV. By inserting the mean values into Eqs. (3.3), we find

$$\frac{\hat{e}^2_{\rm SM}(m_Z)}{4\pi} = \frac{1}{128.06}, \tag{3.4a}$$

$$\hat{s}^2_{\rm SM}(m_Z) = 0.2313, \tag{3.4b}$$

for $m_t = 175$GeV and $\alpha_s = 0.118$. These couplings follow the SM renormalization group equation[1]

$$\frac{1}{\hat{e}^2_{\rm SM}(\mu)} = \frac{1}{\hat{e}^2_{\rm SM}(m_Z)} - \frac{11}{3}\frac{1}{16\pi^2}\log\frac{\mu^2}{m_Z^2}, \tag{3.5a}$$

$$\frac{1}{\hat{g}^2_{\rm SM}(\mu)} = \frac{1}{\hat{g}^2_{\rm SM}(m_Z)} + \frac{19}{6}\frac{1}{16\pi^2}\log\frac{\mu^2}{m_Z^2}. \tag{3.5b}$$

We take the value of m_W as[34]

$$m_W = 80.41\text{GeV}. \tag{3.6}$$

The $\sqrt{s}$ dependences of the tree-level helicity amplitudes at the scattering angle $\theta = 90°$ are seen in Fig. 5. At high energies where the W-boson mass is negligible, the helicity amplitudes M^{+-}, M^{-+} and M^{00} become important. The amplitudes M^{++} and M^{--} decrease as $1/s$, while M^{0+}, M^{-0}, M^{0-} and M^{+0} decrease as $1/\sqrt{s}$ at high energies. At moderately high energies, e.g. at $\sqrt{s} \sim 500$GeV, the five amplitudes, M^{+-}, M^{-+}, M^{00}, M^{0+} and M^{-0} are significant for left-handed electron ($\tau = -$), while only M^{00} is significant for right-handed electron ($\tau = +$).

4 One-loop sfermion contributions to the form factors

In this section, we calculate the one-loop contributions of squarks and sleptons to the form factors. We present the Lagrangian for the sfermion sector in Appendix A.

4.1 The scheme of the one-loop calculation

We choose our input electroweak parameters to express the tree-level amplitudes that satisfy the BRS sum rules[20]. The $\overline{\rm MS}$ couplings of the MSSM, $\hat{e}^2(\mu)$ and $\hat{g}^2(\mu)$ are used as the expansion parameters. They are related to the SM $\overline{\rm MS}$ couplings in Eqs. (3.4) by the matching condition

$$\frac{1}{\hat{e}^2(\mu)} = \frac{1}{\hat{e}^2_{\rm SM}(\mu)} - \frac{1}{16\pi^2}\left[\frac{16}{3}\log\mu^2 - \sum_f N_c^f\frac{Q_f^2}{3}\left(\log m^2_{\tilde{f}_1} + \log m^2_{\tilde{f}_2}\right)\right], \tag{4.1a}$$

$$\frac{1}{\hat{g}^2(\mu)} = \frac{1}{\hat{g}^2_{\rm SM}(\mu)} - \frac{1}{16\pi^2}\left[2\log\mu^2 - \sum_f N_c^f\frac{T^3_{f_L}Q_f}{3}\left(\cos^2\theta_{\tilde{f}}\log m^2_{\tilde{f}_1} + \sin^2\theta_{\tilde{f}}\log m^2_{\tilde{f}_2}\right)\right], \tag{4.1b}$$

[1] We note here that both the magnitudes of the $\overline{\rm MS}$ couplings in Eqs. (3.4) and the renormalization group equations in Eqs. (3.5) are for the SM with all 6 quark flavors. We include the effect of the top-quark at the m_Z-scale in order to avoid introducing the transition between the 5-quark and 6-quark regime in the SM.

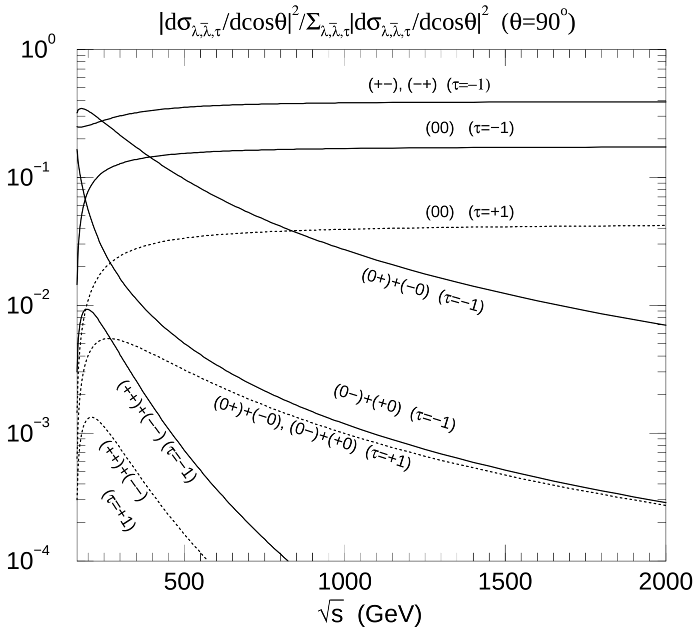

Figure 5: The ratio of the squared helicity amplitudes to the helicity sum of them at the scattering angle 90° for $\sqrt{s}$=161 - 2000 GeV.

where the color factor N_c^f is 3 for squarks and 1 for sleptons, and the other notation of the sfermion sector is defined in Appendix A. The above conditions ensure that physical observables at low energies remain the same when all the sfermion masses are large. In this paper, we do not consider contributions of the fermionic supersymmetric particles (charginos, neutralinos, and gluinos) nor those from the extra Higgs bosons. These particles are assumed to be even heavier, and we work within the effective MSSM with squarks and sleptons only. The effects of -ino particles and the extra Higgs bosons will be studied elsewhere[35]. The other $\overline{\rm MS}$ couplings are obtained from $\hat{e}^2$ and $\hat{g}^2$ as

$$\hat{s}^2(\mu) = \frac{\hat{e}^2(\mu)}{\hat{g}^2(\mu)}\,, \quad \hat{c}^2(\mu) = 1 - \hat{s}^2(\mu)\,, \quad \hat{g}_Z^2(\mu) = \frac{\hat{g}^2(\mu)}{\hat{c}^2(\mu)}\,. \tag{4.2}$$

These three input parameters $\{m_W, \hat{e}^2(\mu), \hat{s}^2(\mu)\}$ are consistently employed in the evaluation of all loop integrals and form factors. All the relevant diagrams are Taylor-expanded by the $\hat{g}^2$ (or $\hat{e}^2$) and only the terms up to $\mathcal{O}(\hat{g}^4)$ are taken into account.

The $\overline{\rm MS}$ masses of the vector bosons are defined in terms of $\hat{e}^2(= \hat{e}^2(\mu))$, $\hat{g}^2(= \hat{s}^2(\mu))$ and m_W by

$$\hat{m}_W^2 = m_W^2 + \Pi_T^{WW}(m_W^2)\,, \tag{4.3}$$

$$\hat{m}_Z^2 = \frac{\hat{m}_W^2}{\hat{c}^2} = \frac{1}{\hat{c}^2}\left\{m_W^2 + \Pi_T^{WW}(m_W^2)\right\}\,, \tag{4.4}$$

where $\Pi_T^{WW}(q^2)$ is the W-boson two-point function in the $\overline{\rm MS}$ scheme[32]. The physical mass of the Z boson is then obtained as

$$m_Z^2 = \frac{m_W^2}{\hat{c}^2} + \frac{1}{\hat{c}^2}\Pi_T^{WW}(m_W^2) - \Pi_T^{ZZ}\left(\frac{m_W^2}{\hat{c}^2}\right) \equiv \frac{m_W^2}{\hat{c}^2} + \Delta\,, \tag{4.5}$$

where deviation from the tree-level expression Eq. (3.2) is denoted by Δ. The Z-boson propagator should then be expanded and truncated as

$$\frac{1}{s-m_Z^2}=\frac{1}{s-(m_W^2/\hat{c}^2)}\left\{1+\frac{\Delta}{s-m_W^2/\hat{c}^2}\right\}\ . \tag{4.6}$$

In Ref. [20], we have demonstrated that by this scheme the BRS sum rules hold exactly.

4.2 $e^-e^+\to W^-W^+$

In the one-loop level, the form factors $F_{i,\tau}(s,t)$ defined in Eq. (2.1) may be written as

$$F_{i,\tau}=F_{i,\tau}^{(0)}+F_{i,\tau}^{(1)}, \tag{4.7}$$

where $F_{i,\tau}^{(0)}$ and $F_{i,\tau}^{(1)}$ are the $\mathcal{O}(\hat{g}^2)$ and $\mathcal{O}(\hat{g}^4)$ contributions, respectively. Although we are interested in the $e^-e^+\to W^-W^+$ amplitudes with the physically polarized external W bosons ($\lambda,\overline{\lambda}=0,\pm$), in order to test the form factors by the BRS sum rules, we have to consider the cases in which one or two external W bosons are unphysical too; *i.e.* λ and/or $\overline{\lambda}=S$. Since the BRS sum rules can test the form factors except for the contribution of overall factors such as the wave-function renormalization contribution, we divide $F_{i,\tau}^{(1)}$ into the one which is the contributions from the W-boson wave-function renormalization ($F_{i,\tau}^{(1)\mathrm{ext}}$), and the other is the rest ($F_{i,\tau}^{(1)\mathrm{int}}$). Eq. (4.7) is then rewritten as

$$F_{i,\tau}=F_{i,\tau}^{(0)}+F_{i,\tau}^{(1)\mathrm{int}}+F_{i,\tau}^{(1)\mathrm{ext}}\equiv\widetilde{F}_{i,\tau}+F_{i,\tau}^{(1)\mathrm{ext}}, \tag{4.8}$$

where $\widetilde{F}_{i,\tau}$ include all the one-loop as well as tree level contributions except for the corrections of external W-boson lines. This part will be tested by the BRS sum rules in Sec. 5.1, while the overall normalization will be verified by using the decoupling property of the sfermion contributions in the large mass limit in Sec. 5.2. For the BRS test we have to calculate all 16 of the $\widetilde{F}_{i,\tau}$ ($i=1$ - 16) for each τ, while we have only to calculate the $F_{i,\tau}^{(1)\mathrm{ext}}$ for physical external W lines ($i=1$ - 9). The form factors for the physical process, $F_{i,\tau}$ ($i=1$ - 9), are obtained by adding the $F_{i,\tau}^{(1)\mathrm{ext}}$ ($i=1$ - 9) to $\widetilde{F}_{i,\tau}$ ($i=1$ - 9) by Eq. (4.8). Let us consider each part of the form factors in order.

First, $\widetilde{F}_{i,\tau}$ are expressed by

$$\begin{aligned}\widetilde{F}_{i,\tau}(s,t)=&\frac{\hat{e}^2}{s}\left\{\Big[Q_e\Big(1-\Pi_{T,\gamma}^{\gamma\gamma}(s)+\Gamma_1^e(s)\Big)+T_e^3\,\overline{\Gamma}_2^e(s)\Big]f_i^{\gamma\,(0)}+Q_ef_i^{\gamma\,(1)}(s)\right\}\\&+\frac{\hat{g}^2}{s-(m_W^2/\hat{c}^2)}\left\{\Big[(T_e^3-\hat{s}^2Q_e)\Big(1+\frac{\Delta}{s-m_W^2/\hat{c}^2}-\Pi_{T,Z}^{ZZ}(s)+\Gamma_1^e(s)\Big)+T_e^3\Big(\hat{c}^2\overline{\Gamma}_2^e(s)+\Gamma_3^e(s)\Big)\right.\\&\qquad\left.+\Gamma_4^e(s)\Big]f_i^{Z\,(0)}+(T_e^3-\hat{s}^2Q_e)f_i^{Z\,(1)}(s)-\frac{\hat{s}}{\hat{c}}\Big[Q_e\hat{c}^2f_i^{Z\,(0)}+(T_e^3-\hat{s}^2Q_e)f_i^{\gamma\,(0)}\Big]\Pi_{T,\gamma}^{\gamma Z}(s)\right\}\\&+\frac{T_e^3\hat{g}^2}{2t}\Big[f_i^{t\,(0)}+\Gamma^{e\nu W}(t)+\overline{\Gamma}^{e\nu W}(t)\Big]+F_{i,\tau}^{[\mathrm{Box}]}(s,t)\ ,\end{aligned} \tag{4.9}$$

where $i=1$ - 16. We here have already expanded the Z-boson propagator according to Eq. (4.6).

The quantities $\Pi^{V_1V_2}_{T,V_3}(q^2)$ where V_i is γ, Z or W are defined by[32]

$$\Pi^{V_1V_2}_{T,V_3}(q^2) = \frac{\Pi^{V_1V_2}_{T}(q^2) - \Pi^{V_1V_2}_{T}(m^2_{V_3})}{q^2 - m^2_{V_3}} \;, \tag{4.10}$$

where $\Pi^{V_1V_2}_{T}$ are the propagator correction functions for the vector bosons. We present the sfermion one-loop contribution to $\Pi^{V_1V_2}_{T}(q^2)$ in Appendix B.

The vertex coefficients f_i^V are divided into the tree contribution and the one-loop vertex contribution according to Eq. (4.7),

$$f_i^V(s) = f_i^{V\,(0)} + f_i^{V\,(1)}(s) \;, \tag{4.11}$$

where $V = \gamma$ and Z. The nonzero tree-level values, $f_i^{V\,(0)}$, have been given in Table 2. In the one-loop sfermion effects, the triangle-type and the sea-gull-type diagrams for the VWW trilinear gauge vertices contribute to $f_i^{V\,(1)}(s)$, which are calculated in Appendix B.2. The triangle-type diagrams contribute only to $f_1^{V\,(0)}$, $f_2^{V\,(0)}$ and $f_3^{V\,(0)}$ among the *physical* from factor coefficients $f_1^{V\,(0)}$ - $f_9^{V\,(0)}$ and the sea-gull-type diagrams only contribute to the *unphysical* from factor coefficients.

The vertex functions for the Vee vertex, denoted by Γ^e_1, $\overline{\Gamma}^e_2$, Γ^e_3 and Γ^e_4 also appear in $e^-e^+ \to f\overline{f}$ amplitudes[32]. The vertex functions $\Gamma^{e\nu W}$ and $\overline{\Gamma}^{e\nu W}$ appear in charged current processes; they contain νeW vertex corrections as well as two-point function corrections for the external electrons and W bosons and the internal neutrino propagator. Finally, the $F^{[\mathrm{Box}]}_{i,\tau}$ terms account for contributions of box diagrams. In the limit of heavy SUSY particles except for squarks and sleptons, all these vertex and box corrections are small and we can set them to zero.

Next, as for the part of the corrections to external W-boson lines, $F^{(1)\mathrm{ext}}_{i,\tau}$, we have only to discuss the cases in which all the external W boson are physical (λ or $\overline{\lambda} = 0, \pm 1$);

$$F^{(1)\mathrm{ext}}_{i,\tau}(s,t) = \left[\frac{\hat{e}^2}{s} Q_e f_i^{\gamma\,(0)} + \frac{\hat{g}^2}{s - (m^2_W/\hat{c}^2)}(T^3_e - \hat{s}^2 Q_e) f_i^{Z\,(0)} + \frac{T^3_e \hat{g}^2}{2t} f_i^{t\,(0)}\right]\delta Z_W, \tag{4.12}$$

where $i = 1$ - 9 and δZ_W is the wavefunction-renormalization-correction factor of physical W-bosons with the helicities λ or $\overline{\lambda} = 0, \pm$, and its sfermion one-loop contribution is given in Appendix B.

We note that the sfermion one-loop contributions do not contribute to $F_{4,\tau}$, $F_{6,\tau}$, $F_{7,\tau}$ and $F_{9,\tau}$. This fact may be explained from the viewpoint of the C, P and CP property of the form factors in Table 1. Because all the contributions of the gauge-boson two-point functions are accompanied by the tree-level form-factor coefficients $f_i^{V(0)}$ and $f_i^{t(0)}$ of Table 2, nonzero contributions to $F_{4,\tau}$, $F_{6,\tau}$, $F_{7,\tau}$ and $F_{9,\tau}$ can arise only from the triangle-type diagrams[2]. Since each $\tilde{f}_i^*$-$\tilde{f}_j$-V or $\tilde{u}_i^*$-$\tilde{d}_j$-W coupling is clearly P even, these triangle diagrams have $P = +$. For the CP-violating phases that appear in the $\tilde{f}_i^*$-$\tilde{f}_j$-V and $\tilde{u}_i^*$-$\tilde{d}_j$-W couplings, we can easily see that these are cancelled out in each sfermion triangle diagram. Thus, these diagrams can contribute only to the form factors with ($P = +$, $C = +$, $CP = +$), hence $F_{4,\tau} = F_{6,\tau} = F_{7,\tau} = F_{9,\tau} = 0$ hold for the sfermion one-loop contributions.

[2] There is no contribution of the sea-gull type diagrams to F_1-F_9. (See Appendix B.2.)

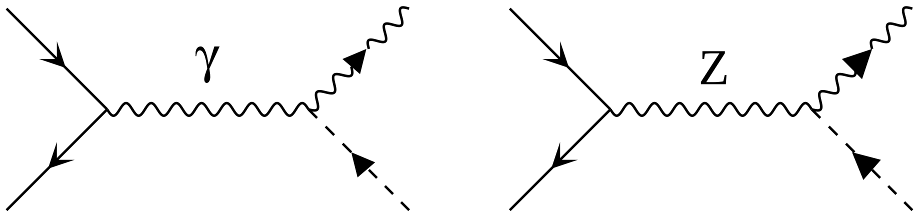

Figure 6: Tree-level Feynman diagrams contributing to $e^-e^+ \to W^-\chi^+$. The arrows in the charged boson lines indicate the flow of negative electric charge. By reversing the direction of these arrows we obtain the graphs for $e^-e^+ \to \chi^-W^+$.

4.3 $e^-e^+ \to W^\mp\chi^\pm$ and $e^-e^+ \to \chi^-\chi^+$

First, we calculate one-loop sfermion contributions to $\overset{(-)}{H}_i$ in Sec. 2.2. The results will be used for the test of the one-loop form factors of $e^-e^+ \to W^-W^+$. We have only to calculate $\overset{(-)}{H}_i$ except for the corrections to the external W- and χ-boson lines. The form factors $\overset{(-)}{H}_i$ are then expressed by

$$\begin{aligned}\overset{(-)}{H}_{i,\tau}(s,t) = \frac{\hat{e}^2}{s}\Big\{\Big[Q_e\Big(1-\Pi_{T,\gamma}^{\gamma\gamma}(s)+\Gamma_1^e(s)\Big)+T_e^3\overline{\Gamma}_2^e(s)\Big]\overset{(-)}{h}{}_i^{\gamma\,(0)}+Q_e\overset{(-)}{h}{}_i^{\gamma\,(1)}(s)\Big\} \\ +\frac{\hat{g}^2}{s-m_W^2/\hat{c}^2}\Big\{\Big[(T_e^3-\hat{s}^2Q_e)\Big(1+\frac{\Delta}{s-m_W^2/\hat{c}^2}-\Pi_{T,Z}^{ZZ}(s)+\Gamma_1^e(s)\Big)+T_e^3\Big(\hat{c}^2\overline{\Gamma}_2^e(s)+\Gamma_3^e(s)\Big) \\ +\Gamma_4^e(s)\Big]\overset{(-)}{h}{}_i^{Z\,(0)}+(T_e^3-\hat{s}^2Q_e)\overset{(-)}{h}{}_i^{Z\,(1)}(s)-\frac{\hat{s}}{\hat{c}}\Big[(T_e^3-\hat{s}^2Q_e)\overset{(-)}{h}{}_i^{\gamma\,(0)}+Q_e\hat{c}^2\overset{(-)}{h}{}_i^{Z\,(0)}\Big]\Pi_{T,\gamma}^{\gamma Z}(s)\Big\} \\ +\frac{\hat{g}^2T_e^3}{2t}\overset{(-)}{\Gamma}{}^{e\nu\chi}+\overset{(-)}{H}{}_{i,\tau}^{[\text{Box}]}(s,t)\;,\end{aligned} \tag{4.13}$$

where $\overset{(-)}{H}_{i,\tau}$, $\overset{(-)}{h}_i$ and $\overset{(-)}{\Gamma}{}^{e\nu\chi}$ should be read as $H_{i,\tau}$, h_i and $\Gamma^{e\nu\chi}$ for $e^-e^+ \to W^-\chi^+$, and $\overline{H}_{i,\tau}$, $\overline{h}_i$ and $\overline{\Gamma}^{e\nu\chi}$ for $e^-e^+ \to \chi^-W^+$, respectively. At the tree-level, Feynman graphs in Fig. 6 contribute. The expansion of $H_{i,\tau}(s,t)$ introduces the vertex form factors h_i^γ and h_i^Z, while the expansion of $\overline{H}_{i,\tau}(s,t)$ introduces $\overline{h}_i^\gamma$ and $\overline{h}_i^Z$. They are written as the sum of the tree and one-loop contributions by

$$\overset{(-)}{h}{}_i^V(s) = \overset{(-)}{h}{}_i^{V\,(0)} + \overset{(-)}{h}{}_i^{V\,(1)}(s)\;, \tag{4.14}$$

for $V=\gamma,\ Z$. The tree-level coefficients $h_i^{V\,(0)}$ are given by $h_i^{\gamma\,(0)} = -\overline{h}_i^{\gamma\,(0)} = \delta_{i\,1}$ and $h_i^{Z(0)} = -\overline{h}_i^{Z(0)} = -(\hat{s}^2/\hat{c}^2)\delta_{i\,1}$. The $\overset{(-)}{h}{}_i^{V\,(1)}(s)$ come from the one-loop 1PI $VW\chi$ vertex corrections, and their sfermion contributions are shown in Appendix C.1. The other form factor coefficients (the vertex- and the box-diagrams which connect with initial $e^\pm$) turn out to be zero for the sfermion contribution.

Second, the sfermion one-loop contributions to R_τ defined in Sec. 2.2 are expressed by

$$R_\tau(s,t) = -\frac{\hat{e}^2}{s}\Big[Q_e\Big(1-\Pi_{T,\gamma}^{\gamma\gamma}(s)+\Gamma_1^e(s)\Big)+T_e^3\overline{\Gamma}_2^e(s)+Q_e r^{\gamma\,(1)}(s)\Big]$$

$$
-\frac{\hat{g}_Z^2}{s-m_W^2/\hat{c}^2}\Bigg\{\Bigg[(T_e^3-\hat{s}^2Q_e)\left(\frac{1}{2}-\hat{s}^2\right)\Big(1+\frac{\Delta}{s-m_W^2/\hat{c}^2}-\Pi_{T,Z}^{ZZ}(s)+\Gamma_1^e(s)\Big)
$$

$$
+T_e^3\Big(\hat{c}^2\overline{\Gamma}_2^e(s)+\Gamma_3^e(s)\Big)+\Gamma_4^e(s)\Bigg]
$$

$$
+(T_e^3-\hat{s}^2Q_e)r^{Z\,(1)}(s)-\frac{\hat{s}}{\hat{c}}\Bigg[(T_e^3-\hat{s}^2Q_e)+Q_e\left(\frac{1}{2}-\hat{s}^2\right)\Bigg]\Pi_{T,\gamma}^{\gamma Z}(s)\Bigg\}+R_\tau^{[\mathrm{Box}]}(s,t)\;, \qquad (4.15)
$$

where we do not include the corrections to the external χ lines by the same reason as for the $\overset{(-)}{H}_{i,\tau}$. For the sfermion effects, we have to calculate the $V\chi\chi$-vertex corrections parametrised by $r^{V(1)}$. The results are given in Appendix C. All the other form-factor coefficients (for the one-loop vertices and the boxes that contain initial $e^\pm$ lines) turn out to be zero for the sfermion contribution.

5 Tests of the one-loop calculation

The purpose of this paper is to evaluate the sfermion one-loop effects on $e^-e^+ \to W^-W^+$. To obtain trustworthy results, we test our one-loop calculation by using the BRS invariance, the decoupling theorem, and the high energy behaviors of the theory. We show these procedure in order.

5.1 The BRS test for the $e^-e^+ \to W^-W^+$ form factors

5.1.1 The BRS sum rules

The global BRS symmetry in the quantized electroweak gauge theories gives identities between a process with scalar-polarized W bosons and one where the W bosons are replaced by the Goldstone bosons χ[23]. Regarding to our process $e^-e^+ \to W^-W^+$, we have two kind of the identities[20]; we call the first one as the single BRS identity where only one external W boson is replaced by the χ boson, and the second one as the double BRS identity where both the W bosons are replaced. From these identities for amplitudes, we obtain useful sum rules among the form factors which we introduced in Sec. 2; $\widetilde{F}_{i,\tau}$ $(i = 1$ - $16)$, $\overset{(-)}{H}_{i,\tau}$ $(i = 1$ - $4)$ and R_τ. Note that $\widetilde{F}_{1,\tau}$ - $\widetilde{F}_{9,\tau}$ are common with the physical $e^-e^+ \to W^-W^+$ amplitude (See Eq. (4.8)).

A set of the sum rules is obtained from the BRS identity between $e^-e^+ \to W^-W^+$ and $e^-e^+ \to W^-\chi^+$ amplitudes[20].

$$
-2\gamma^2\left\{\widetilde{F}_{3,\tau}(s,t)-i\,\widetilde{F}_{4,\tau}(s,t)\right\}+4\delta^2\,\widetilde{F}_{8,\tau}(s,t)+\widetilde{F}_{13,\tau}(s,t)=C_{\mathrm{mod}}^{BRS}H_{1,\tau}(s,t)\;, \qquad (5.1a)
$$

$$
-\widetilde{F}_{1,\tau}(s,t)+2\gamma^2\,\widetilde{F}_{2,\tau}(s,t)+\frac{1}{2}\widetilde{F}_{3,\tau}(s,t)+\frac{i}{2}\widetilde{F}_{4,\tau}(s,t)+\widetilde{F}_{14,\tau}(s,t)=C_{\mathrm{mod}}^{BRS}H_{2,\tau}(s,t)\;, \qquad (5.1b)
$$

$$
-\frac{1}{2}\widetilde{F}_{5,\tau}(s,t)-\frac{i}{2}\widetilde{F}_{6,\tau}(s,t)-\frac{\tau}{2}\widetilde{F}_{8,\tau}(s,t)+2\delta^2\,\widetilde{F}_{9,\tau}(s,t)+\widetilde{F}_{15,\tau}(s,t)=C_{\mathrm{mod}}^{BRS}H_{3,\tau}(s,t)\;, \qquad (5.1c)
$$

where

$$
\gamma^2=\frac{s}{4m_W^2}, \quad \text{and} \quad \delta^2=\frac{s+2t-2m_W^2}{4m_W^2}, \qquad (5.2)
$$

First BRS sum rule ($\tau = -1$)	
$\sqrt{s}$	Left-hand-side of Eq. (5.1a) Right-hand-side of Eq. (5.1a)
200GeV	$-0.1385496590672218 \times 10^{-5}$ $-0.1385496590672223 \times 10^{-5}$
500GeV	$-0.2654648169991279 \times 10^{-6}$ $-0.3685263974480902 \times 10^{-8}\, i$ $-0.2654648169991285 \times 10^{-6}$ $-0.3685263974480899 \times 10^{-8}\, i$
1000GeV	$-0.6682526871892199 \times 10^{-7}$ $-0.6849932023212376 \times 10^{-8}\, i$ $-0.6682526871892053 \times 10^{-7}$ $-0.6849932023212378 \times 10^{-8}\, i$
2000GeV	$-0.1434490310523539 \times 10^{-7}$ $-0.1201404359981963 \times 10^{-8}\, i$ $-0.1434490310523237 \times 10^{-7}$ $-0.1201404359981958 \times 10^{-8}\, i$

Table 3: The BRS test of the sfermion one-loop effects on the $e^-e^+ \to W^-W^+$ form factors by using the first BRS sum rule (5.1a). As for the MSSM parameters, Case 28 of Table 10 in Sec. 6 is used.

and

$$C^{BRS}_{\rm mod} = \frac{\hat{m}_W}{m_W}. \tag{5.3}$$

These sum rules can be used for a non-trivial test of the one-loop form factors for the physical amplitudes except for the part of the wavefunction renormalization factors. Another set of sum rules can be obtained from the 'single' BRS identity between the W^-W^+ and χ^-W^+ production. In practice, once one of the two sets of the 'single' BRS sum rules is used to verify the accuracy of a calculation, the other set is redundant. In addition, the sum rules among the $e^-e^+ \to W^-W^+$, $e^-e^+ \to W^\mp\chi^\pm$, and $e^-e^+ \to \chi^-\chi^+$ form factors are also obtained from the 'double' BRS identity, which may be useful for an independent BRS test of $\widetilde{F}_1$, $\widetilde{F}_2$, $\widetilde{F}_3$ and $\widetilde{F}_8$.

5.1.2 Numerical tests of the one-loop results for $F_{i,\tau}$ by using the BRS sum rules

The most practical application of the BRS sum rules is the numerical test of the program. In our formalization, they should hold exactly for the form factors calculated at the one-loop level. Our computational program has been tested to satisfy them with an excellent agreement.

We here test our one-loop calculation of the form factors numerically by using the BRS sum rules (5.1). In our evaluation of the scalar one-loop integral functions, we partly use the Fortran FF-package[36]. As a sample MSSM parameter choice, we take Case 28 that is defined later in Table 10 in Sec. 6[3]. We see in Tables 3 and 4 that the first sum rule (5.1a) and the second one (5.1b) hold to better than 11 digits accuracy at $\sqrt{s}$ between 200GeV and 2000GeV, respectively. As for the third one (5.1c), it turns out that the both sides are zero, so it is rather trivial.

[3] As for the renormalization scheme, in addition to the method defined in Sec. 4, the expansion by the coupling constants in the SM is employed which will be introduced a little later in Sec. 5.2.

Second BRS sum rule ($\tau = -1$)	
$\sqrt{s}$	Left-hand-side of Eq. (5.1b) Right-hand-side of Eq. (5.1b)
200GeV	$-0.2438990547345640 \times 10^{-9}$ $-0.2438990547345377 \times 10^{-9}$
500GeV	$-0.7616498712364096 \times 10^{-10}$ $-0.2662690301056969 \times 10^{-10}$ i $-0.7616498712364688 \times 10^{-10}$ $-0.2662690301056939 \times 10^{-10}$ i
1000GeV	$0.1916470996088027 \times 10^{-12}$ $-0.2445806925474609 \times 10^{-10}$ i $0.1916470996084505 \times 10^{-12}$ $-0.2445806925474613 \times 10^{-10}$ i
2000GeV	$0.3363019521319420 \times 10^{-11}$ $+0.1791648684551098 \times 10^{-11}$ i $0.3363019521319535 \times 10^{-11}$ $+0.1791648684551017 \times 10^{-11}$ i

Table 4: The BRS test of the sfermion one-loop effects on the $e^-e^+ \to W^-W^+$ form factors by using the second BRS sum rule (5.1b). As for the MSSM parameters, Case 28 of Table 10 in Sec. 6 is used.

5.2 The test by using the decoupling theorem

The second useful instrument for the test is the decoupling property of the sfermion one-loop contributions at the large mass limit, where the sfermion effects should decouple from the observable and the model should be regarded as the SM effectively by the argument of the decoupling theorem[24, 25]. To see this property at each order of perturbation, a consistent renormalization scheme must be taken, by which the one-loop result in the MSSM is coincident with that in the SM at the large mass limit. In the $\overline{\rm MS}$ scheme, the perturbation is performed by the $\overline{\rm MS}$ couplings of the MSSM. In order to obtain the one-loop expression which reduces to the SM results exactly in the large SUSY-mass limit, we expand the one-loop amplitudes by the SM $\overline{\rm MS}$ couplings by using Eqs. (4.1). By dropping the higher-order ($\mathcal{O}(\hat{g}_{\rm SM}^6)$) terms, the decoupling of the one-loop effects can be made exact.

5.2.1 The expansion by the coupling constants in the SM

In the one-loop calculation of the sfermion effects in Sec. 4, we took $\hat{e}^2(\mu)$, $\hat{s}^2(\mu)$ and m_W as the input parameters. The W-boson mass, m_W, is determined by the precision data as in Eq. (3.6). From the equations (4.1a) and (4.1b), $\hat{e}^2(\mu)$ and $\hat{g}^2(\mu)$ include higher order sfermion effects beyond the one-loop level. In order to test the decoupling property analytically, we expand the original one-loop amplitudes by the SM coupling constants $\hat{e}_{\rm SM}^2(\mu)$ and $\hat{g}_{\rm SM}^2(\mu)$:

$$\hat{e}^2(\mu) = \hat{e}_{\rm SM}^2(\mu)\left\{1 + \frac{\hat{e}_{\rm SM}^2(\mu)}{16\pi^2}\left[\frac{16}{3}\log\mu^2 - \sum_f N_c^f \frac{Q_f^2}{3}\left(\log m_{\tilde{f}_1}^2 + \log m_{\tilde{f}_2}^2\right)\right]\right\}, \tag{5.4a}$$

$$\hat{g}^2(\mu) = \hat{g}_{\rm SM}^2(\mu)\left\{1 + \frac{\hat{g}_{\rm SM}^2(\mu)}{16\pi^2}\left[2\log\mu^2 - \sum_f N_c^f \frac{T_{f_L}^3 Q_f}{3}\left(\cos^2\theta_{\tilde{f}}\log m_{\tilde{f}_1}^2 + \sin^2\theta_{\tilde{f}}\log m_{\tilde{f}_2}^2\right)\right]\right\}. \tag{5.4b}$$

Hereafter, we perform this procedure in all our calculation. All the form factors we have presented previously are now expanded by the SM couplings by using Eqs. (5.4), and we retain only terms

of $\mathcal{O}(\hat{g}_{\rm SM}^2)$ and $\mathcal{O}(\hat{g}_{\rm SM}^4)$. We then will find below that the one-loop sfermion contributions vanish exactly in the limit of infinitely heavy sfermion masses. In Sec. 7, we discuss the difference of the magnitude between the amplitude expanded by the SM couplings and that in terms of the MSSM couplings without such additional expansion. Since we do not include the SM loop contributions[8] in our analysis, the $\mathcal{O}(\hat{g}_{\rm SM}^4)$ terms are solely coming from the sfermion one-loop contributions, which decouple in the heavy sfermion mass limit ($s/m_{\tilde{f}}^2 \ll 1$) and grow logarithmically at high energies ($s/m_{\tilde{f}}^2 \gg 1$). As for the scale dependence of the SM $\overline{\rm MS}$ couplings, we set $\mu = \sqrt{s}$ for brevity.

5.2.2 The decoupling limit

The consistent calculation according to the above procedure allows us to observe the exact decoupling in the large sfermion-mass limit. In the original expression of the amplitudes which are expressed in terms of the MSSM $\overline{\rm MS}$ couplings, the amplitudes behave as

$$\delta\mathcal{M}^{\rm sfermion-loop} \sim A + B\frac{s}{m_{\tilde{f}}^2} + \mathcal{O}\left(\frac{s^2}{m_{\tilde{f}}^4}\right), \tag{5.5}$$

in the large sfermion mass limit, where the constant term, A, remains nonzero as terms of $\mathcal{O}(\hat{g}^6)$ do not cancel exactly. Contrary by taking the SM coupling constants as the expansion parameter and by truncating the expansion at the $\mathcal{O}(\hat{g}_{\rm SM}^4)$ terms, the term A in (5.5) becomes zero. This property of the exact decoupling in our scheme can be used for the excellent test of the form factors including the overall normalization factors that have not yet been tested in the BRS sum rules.

Fig. 7 shows the sfermion contribution in the helicity-summed differential cross section as a function of $1/m_{\tilde{f}}^2$ at $\sqrt{s} = 200$GeV and at the large scattering angle $\theta = 90^\circ$. We test the decoupling property in Case A and Case B; all the sfermion masses are set to M in Case A, and the sfermion masses are taken as $m_{\tilde{u}_L} = m_{\tilde{d}_L} = M$, $m_{\tilde{u}_R} = 1.1M$, $m_{\tilde{d}_R} = 1.2M$, $m_{\tilde{e}_L} = m_{\tilde{\nu}_L} = 1.3M$ and $m_{\tilde{e}_R} = 1.4M$ in Case B. In Fig. 7, we see that the both lines of Case A and Case B include the origin; the term A in Eq. (5.5) is certainly zero in our calculation of the sfermion one-loop contributions.

5.3 The high energy limit

From the full expression of the one-loop helicity amplitudes of $e^-e^+ \to W^-W^+$, compact analytic formulas in the high energy limit can be calculated, which are very useful for the test of the computational program of the full one-loop calculation. In this limit, there is the equivalence between $e^-e^+ \to W_L^- W_L^+$ and $e^-e^+ \to \chi^-\chi^+$, where $W_L^\pm$ denote the longitudinally polarized W bosons. The equivalence holds even at the loop levels with some modification, by which we can confirm the analytic formulas mentioned above. At high energy, the 00, $+-$ and $-+$ helicity sets of the W-boson pair are important as discussed in Sec. 3. Since the $+-$ and $-+$ helicity amplitudes do not suffer from subtle gauge-theory cancellation, we discuss the 00 helicity amplitude here.

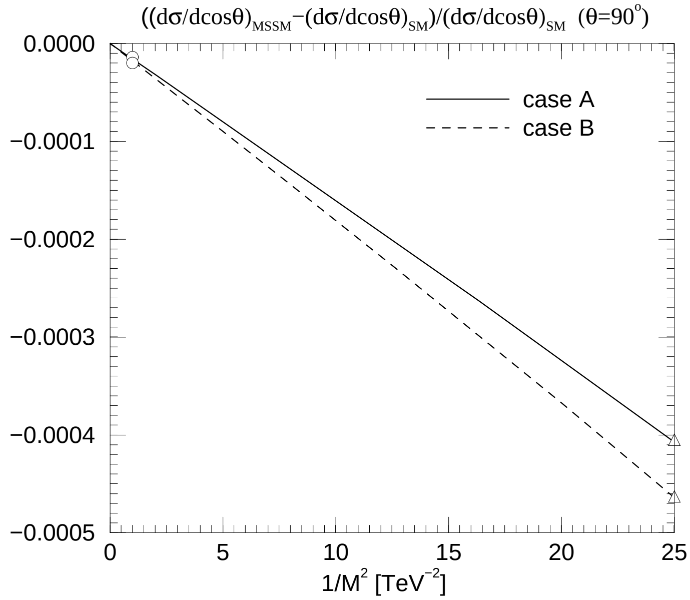

Figure 7: The test of the decoupling of the sfermion contribution. The deviation of the helicity-summed differential cross section from the SM value versus $1/M^2$ is shown at $\sqrt{s} = 200$GeV and the scattering angle $\theta = 90°$, where M is the scale of the sfermion masses. The solid line is for the case where M is the mass of all the sfermions (Case A). The dashed line is for the case where $m_{\tilde{u}_L} = m_{\tilde{u}_L} = M$, $m_{\tilde{u}_R} = 1.1M$, $m_{\tilde{d}_R} = 1.2M$, $m_{\tilde{e}_L} = m_{\tilde{\nu}_L} = 1.3M$ and $m_{\tilde{e}_R} = 1.4M$ (Case B). The symbol $\triangle$ ($\bigcirc$) on the lines is the point of $M = 200$ (1000) GeV.

5.3.1 Analytic high-energy expressions of $e^-e^+ \to W_L^- W_L^+$

By using high-energy formulas of integral functions (Appendix D), we obtain the high energy expression of the 00 helicity amplitude of $e^-e^+ \to W^-W^+$:

$$\mathcal{M}(e^-e^+ \to W_L^- W_L^+) = M_\tau^{00} \equiv Q_e M_X^{00} + T_e^3 M_Y^{00}, \tag{5.6}$$

where we denote W_L as a longitudinally polarized ($\overset{(-)}{\lambda} = 0$) W-boson, and M_X^{00} and M_Y^{00} are expressed in terms of the $\overline{\mathrm{MS}}$ coupling constants of the MSSM by

$$\begin{aligned} M_X^{00} &= \frac{\hat{e}^2(\mu)}{2\hat{c}^2(\mu)} + \sum_{\text{generation}} \frac{\hat{g}^4}{16\pi^2}\frac{\hat{s}^4}{12\hat{c}^4}\left[3\left\{\frac{11}{9}\ln\frac{s}{\mu^2} - \frac{88}{27}\right\} + \left\{\ln\frac{s}{\mu^2} - 8\right\}\right] \\ &\quad + \hat{g}^2\frac{\hat{s}^2}{2\hat{c}^2}\left(\delta Z_W + \frac{\Pi_T^{WW}(m_W^2)}{m_W^2}\right) + \mathcal{O}\left(\frac{m_W^2}{s}\right), \end{aligned} \tag{5.7a}$$

$$\begin{aligned} M_Y^{00} &= \frac{\hat{g}^2(\mu)}{\hat{c}^2(\mu)}\left(\frac{1}{2} - \hat{s}^2(\mu)\right) + \sum_{\text{generation}} \frac{\hat{g}^4}{16\pi^2}\frac{1}{12\hat{c}^4}\left[3\left\{\left(1 - 2\hat{s}^2 - \frac{2}{9}\hat{s}^4\right)\ln\frac{s}{\mu^2}\right.\right. \\ &\quad \left.\left. + \left(-1 + 2\hat{s}^2 + \frac{2}{9}\hat{s}^4\right)\frac{8}{3}\right\} + \left\{\left(1 - 2\hat{s}^2 - 2\hat{s}^4\right)\ln\frac{s}{\mu^2} + \left(-1 + \hat{s}^2 + 2\hat{s}^4\right)\frac{8}{3}\right\}\right] \end{aligned}$$

$$+\hat{g}^2\frac{1}{2\hat{c}^4}\left(\delta Z_W+\frac{\Pi_T^{WW}(m_W^2)}{m_W^2}\right)+\mathcal{O}\left(\frac{m_W^2}{s}\right), \tag{5.7b}$$

where the first curly bracket $\{\quad\}$ in RHS of each equation comes from the squark effects and the second one from the slepton effects, respectively. By using the Eqs. (5.4a) and (5.4b) we obtain the expression in terms of the SM coupling constants up to $\mathcal{O}(\hat{g}_{\rm SM}^4)$:

$$\begin{aligned}
M_X^{00} &= \frac{\hat{e}_{\rm SM}^2}{2\hat{c}_{\rm SM}^2}+\sum_{\rm generation}\frac{\hat{g}_{\rm SM}^4}{16\pi^2}\frac{\hat{s}_{\rm SM}^4}{12\hat{c}_{\rm SM}^4}\left[3\left\{\left(\frac{8}{9}-\frac{2}{3}\cos^2\theta_{\tilde{u}}\right)\ln\frac{s}{m_{\tilde{u}_1}^2}+\left(\frac{8}{9}-\frac{2}{3}\sin^2\theta_{\tilde{u}}\right)\ln\frac{s}{m_{\tilde{u}_2}^2}\right.\right.\\
&\qquad\left.+\left(\frac{2}{9}-\frac{1}{3}\cos^2\theta_{\tilde{d}}\right)\ln\frac{s}{m_{\tilde{d}_1}^2}+\left(\frac{2}{9}-\frac{1}{3}\sin^2\theta_{\tilde{d}}\right)\ln\frac{s}{m_{\tilde{d}_2}^2}-\frac{88}{27}\right\}\\
&\qquad\left.+\left\{\left(1-\cos^2\theta_{\tilde{e}}\right)\ln\frac{s}{m_{\tilde{e}_1}^2}+\left(1-\sin^2\theta_{\tilde{e}}\right)\ln\frac{s}{m_{\tilde{e}_2}^2}-8\right\}\right]\\
&\quad+\hat{g}_{\rm SM}^2\frac{\hat{s}_{\rm SM}^2}{2\hat{c}_{\rm SM}^2}\left(\delta Z_W+\frac{\Pi_T^{WW}(m_W^2)}{m_W^2}\right)+\mathcal{O}\left(\frac{m_W^2}{s}\right),
\end{aligned} \tag{5.8a}$$

$$\begin{aligned}
M_Y^{00} &= \frac{\hat{g}_{\rm SM}^2}{\hat{c}_{\rm SM}^2}\left(\frac{1}{2}-\hat{s}_{\rm SM}^2\right)+\sum_{\rm generation}\frac{\hat{g}_{\rm SM}^4}{16\pi^2}\frac{1}{12\hat{c}_{\rm SM}^4}\left[3\left\{\left(\left(1-2\hat{s}_{\rm SM}^2+2\hat{s}_{\rm SM}^4\right)\frac{2}{3}\cos^2\theta_{\tilde{u}}-\frac{8}{9}\hat{s}_{\rm SM}^4\right)\ln\frac{s}{m_{\tilde{u}_1}^2}\right.\right.\\
&\qquad+\left(\left(1-2\hat{s}_{\rm SM}^2+2\hat{s}_{\rm SM}^4\right)\frac{2}{3}\sin^2\theta_{\tilde{u}}-\frac{8}{9}\hat{s}_{\rm SM}^4\right)\ln\frac{s}{m_{\tilde{u}_2}^2}\\
&\qquad+\left(\left(1-2\hat{s}_{\rm SM}^2+2\hat{s}_{\rm SM}^4\right)\frac{1}{3}\cos^2\theta_{\tilde{d}}-\frac{2}{9}\hat{s}_{\rm SM}^4\right)\ln\frac{s}{m_{\tilde{d}_1}^2}\\
&\qquad\left.+\left(\left(1-2\hat{s}_{\rm SM}^2+2\hat{s}_{\rm SM}^4\right)\frac{1}{3}\sin^2\theta_{\tilde{d}}-\frac{2}{9}\hat{s}_{\rm SM}^4\right)\ln\frac{s}{m_{\tilde{d}_2}^2}+\left(-1+2\hat{s}_{\rm SM}^2+\frac{2}{9}\hat{s}_{\rm SM}^4\right)\frac{8}{3}\right\}\\
&\qquad+\left\{\left(\left(1-2\hat{s}_{\rm SM}^2+2\hat{s}_{\rm SM}^4\right)\cos^2\theta_{\tilde{e}}-2\hat{s}_{\rm SM}^4\right)\ln\frac{s}{m_{\tilde{e}_1}^2}\right.\\
&\qquad\left.\left.+\left(\left(1-2\hat{s}_{\rm SM}^2+2\hat{s}_{\rm SM}^4\right)\sin^2\theta_{\tilde{e}}-2\hat{s}_{\rm SM}^4\right)\ln\frac{s}{m_{\tilde{e}_2}^2}+\left(-1+\hat{s}_{\rm SM}^2+2\hat{s}_{\rm SM}^4\right)\frac{8}{3}\right\}\right]\\
&\quad+\hat{g}_{\rm SM}^2\frac{1}{2\hat{c}_{\rm SM}^4}\left(\delta Z_W+\frac{\Pi_T^{WW}(m_W^2)}{m_W^2}\right)+\mathcal{O}\left(\frac{m_W^2}{s}\right).
\end{aligned} \tag{5.8b}$$

5.3.2 The equivalence theorem

By the similarity of the polarization vectors between longitudinal and scalar W bosons, the relation

$$\mathcal{M}(e^-e^+\to W_L^-W_L^+)=\left\{iC_{\rm mod}^{ET}\right\}^2\mathcal{M}(e^-e^+\to\chi^-\chi^+)\left(1+\mathcal{O}(m_W/\sqrt{s})\right), \tag{5.9}$$

is induced from the single and double BRS identities. The modification factor $C_{\rm mod}^{ET}$, which is not unity beyond the tree level, is expressed at one-loop by

$$C_{\rm mod}^{ET}=\left(\frac{Z_W}{Z_\chi}\right)^{\frac{1}{2}}C_{\rm mod}^{BRS}, \tag{5.10}$$

in our scheme[4]. The relation (5.9) is what we call the equivalence theorem[26, 27].

We here show that the high energy expressions of the one-loop amplitudes (5.7a) and (5.7b) are tested by using the equivalence theorem. To this aim, we also calculate the high energy expression of the amplitude of $e^-e^+ \to \chi^-\chi^+$. The amplitude for $e^-e^+ \to \chi^-\chi^+$ is expressed at high energy by

$$\mathcal{M}(e^-e^+ \to \chi^-\chi^+) \equiv Q_e M_X^{\chi\chi} + T_e^3 M_Y^{\chi\chi} + \mathcal{O}\left(\frac{m_W^2}{s}\right), \tag{5.11}$$

where $M_X^{\chi\chi}$ and $M_Y^{\chi\chi}$ are expressed in terms of the MSSM couplings by

$$M_X^{\chi\chi} = -\frac{\hat{e}^2(\mu)}{2\hat{c}^2(\mu)} - \sum_{\text{generation}} \frac{\hat{g}^4}{16\pi^2}\frac{\hat{s}^4}{12\hat{c}^4}\left[3\left\{\frac{11}{9}\ln\frac{s}{\mu^2} - \frac{88}{27}\right\} + \left\{\ln\frac{s}{\mu^2} - 8\right\}\right] + \mathcal{O}\left(\frac{m_W^2}{s}\right), \tag{5.12a}$$

$$\begin{aligned} M_Y^{\chi\chi} = &-\frac{\hat{g}^2(\mu)}{\hat{c}^2(\mu)}\left(\frac{1}{2} - \hat{s}^2(\mu)\right) - \sum_{\text{generation}} \frac{\hat{g}^4}{16\pi^2}\frac{1}{12\hat{c}^4}\left[3\left\{\left(1 - 2\hat{s}^2 - \frac{2}{9}\hat{s}^4\right)\ln\frac{s}{\mu^2} + \left(-1 + 2\hat{s}^2 + \frac{2}{9}\hat{s}^4\right)\frac{8}{3}\right\}\right. \\ &\left. + \left\{\left(1 - 2\hat{s}^2 - 2\hat{s}^4\right)\ln\frac{s}{\mu^2} + \left(-1 + 2\hat{s}^2 + 2\hat{s}^4\right)\frac{8}{3}\right\}\right] + \mathcal{O}\left(\frac{m_W^2}{s}\right). \end{aligned} \tag{5.12b}$$

On the other hand, C_{mod}^{BRS} of (5.3) is expressed by

$$C_{\text{mod}}^{BRS} = 1 + \frac{1}{2m_W^2}\Pi_T^{WW}(m_W^2). \tag{5.13}$$

For the Goldstone wavefunction factors, we set $Z_\chi = 1$ when the sfermion masses are neglected. Thus, the analytic expression of the modification factor C_{mod}^{ET} is calculated as

$$C_{\text{mod}}^{ET} = 1 + \frac{1}{2}\left(\delta Z_W + \frac{\Pi_T^{WW}(m_W^2)}{m_W^2}\right). \tag{5.14}$$

By using (5.14) and the high energy expression of the amplitudes of $e^-e^+ \to W^-W^+$ (Eqs. (5.7a) and (5.7b)), and of $e^-e^+ \to \chi^-\chi^+$ (Eqs. (5.12a) and (5.12b)), one can see that the leading equation of the equivalence theorem (5.9) holds among the high energy expressions of the one-loop amplitudes.

5.3.3 Numerical test for the high energy behavior

In Fig. 8, we compare the full expressions of the one-loop 00 helicity ($W_L^-W_L^+$ production) amplitude and the high-energy expressions given by Eqs. (5.8a) and (5.8b). Figs. 8(a) and 8(c) show the amplitudes of W_LW_L production from left-handed electrons $\tau = -1$, whereas Figs. 8(b) and 8(d) show those from right-handed electrons ($\tau = +1$). In each figure, the full one-loop results are shown by solid lines, and dotted lines represent the high-energy analytic results of Eqs. (5.8). The cases with $m_{\tilde{Q}} = m_{\tilde{L}} = m_{\tilde{U}} = m_{\tilde{D}} = m_{\tilde{E}} = 500$GeV are shown in Figs. 8(a) and 8(b) ($A_f^{eff} = 0$GeV), and in Figs. 8(c) and 8(d) ($A_f^{eff} = 1500$GeV). Here the parameter A_f^{eff} give the left-right mixing

[4] In the generic renormalization scheme, C_{mod}^{ET} should be expressed by $C_{\text{mod}}^{ET} = (Z_W/Z_\chi)^{1/2} Z_{m_W}\hat{C}_0(m_W^2, \xi)$, where $\hat{C}_0(m_W^2, \xi)$ depends on the gauge parameter ξ[27] and it is 1 in our scheme.

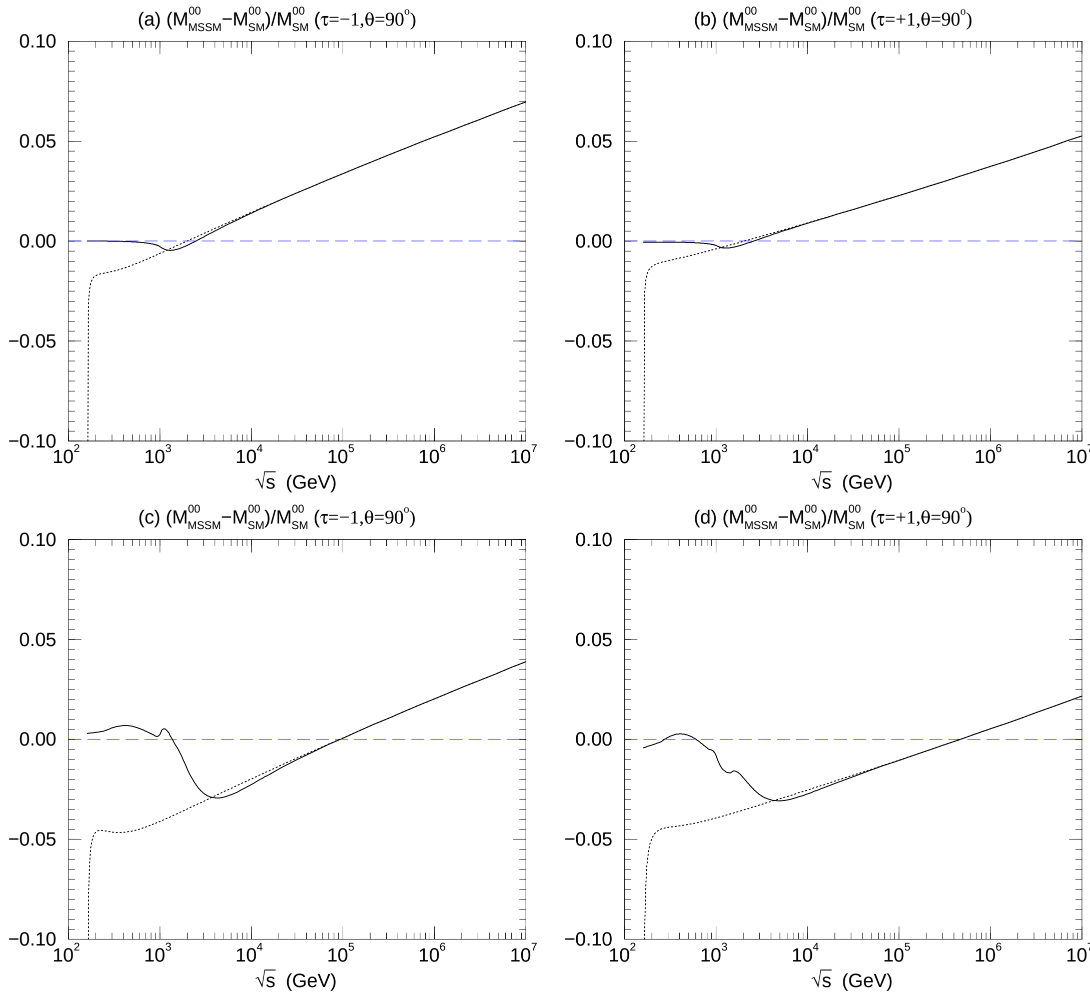

Figure 8: The high-energy behaviors of the sfermion one-loop contribution to M^{00}_{τ} at $\theta = 90°$. The solid lines show the full calculation of the sfermion one-loop contribution, while the dotted lines are of the high-energy analytic formulas (5.8). The parameters are set to $m_{\tilde{Q}} = m_{\tilde{L}} = m_{\tilde{U}} = m_{\tilde{D}} = m_{\tilde{E}} = 500$GeV for $A^{eff}_f = 0$ in (a) and (b), and for $A^{eff}_f = 1500$GeV in (c) and (d).

matrix elements of the sfermion mass matrices; see Eq. (A.5) of Appendix A. With the large value of A^{eff}_f shown in Figs. 8(c) and 8(d), there appears significant mixing in the stop sector, and the mass eigenvalues become $m_{\tilde{t}_1} = 130$GeV and $m_{\tilde{t}_2} = 736$GeV for $\tan\beta = 2$[5]. The high-energy prediction of Eqs. (5.8) is useful in understanding the normalization of the corrections at high energies for the case with the large mass mixing. We find large negative correction above the stop-pair ($\tilde{t}$-$\bar{\tilde{t}}$) production thresholds except before the asymptotic regime sets in. In the formulas (5.8), this negative correction

[5] Since we use the effective parameter A^{eff}_f of Eq. (A.5) to represent the left-right mixing term, the sfermion parameters depend on $\tan\beta$ only through the $\cos 2\beta$ terms in the diagonal mass-squark matrix elements. The $\tan\beta$ dependence from these terms are small, and we set $\tan\beta = 2$ in all the numerical results presented in this paper.

comes from the constant part,

$$\delta Z_W + \frac{\Pi_T^{WW}(m_W^2)}{m_W^2}, \tag{5.15}$$

whose magnitude grows when there is a significant mass mixing in the sfermion sector. In the full amplitudes the stop contributions around the threshold compensate for this large negative constant, which makes the correction small below the $\tilde{t}_2$-$\bar{\tilde{t}}_2$ threshold.

Therefore, the equivalence theorem is useful to confirm the high-energy formulas of the (00) amplitude, which are then used to test the stability of our numerical program at high energies and the overall normalization corrections to the amplitudes.

5.4 Summary of the tests

We have tested our one-loop calculation of the form factors by using the three methods; 1) the BRS sum rules for the test of our one-loop form factors except for the overall normalization corrections, 2) the decoupling theorem for the test of such overall normalization of our amplitudes, 3) the high-energy analytic expressions of the amplitudes for the test of the stability of the numerical program at high energies where subtle gauge-theory cancellation occurs. In the following section, we study the magnitude of the one-loop sfermion contribution to the $e^-e^+ \to W^-W^+$ helicity amplitudes in various the MSSM parameter sets.

6 The numerical evaluation of $e^-e^+ \to W^-W^+$

6.1 The helicity amplitudes

As discussed in Sec. 3, among all the tree-level helicity amplitudes, $M^{+-}_{\tau=-1}$, $M^{-+}_{\tau=-1}$ and $M^{00}_{\tau=\mp1}$ are significant for all energies: see Fig. 5. The one-loop sfermion contributions to these helicity amplitudes should be examined in detail. On the other hand, $M^{++}_{\tau=\mp1}$ and $M^{--}_{\tau=\mp1}$ reduce by $\mathcal{O}(1/s)$, while $M^{0+}_{\tau=\mp1}$, $M^{-0}_{\tau=\mp1}$, $M^{0-}_{\tau=\mp1}$ and $M^{+0}_{\tau=\mp1}$ decrease as $\mathcal{O}(1/\sqrt{s})$. Therefore, the one-loop contributions to these helicity amplitudes can be almost neglected at high energies. Note that only $M^{0+}_{\tau=-1}$ and $M^{-0}_{\tau=-1}$ are, however, larger than $M^{00}_{\tau=-1}$ for $\sqrt{s} < 274$GeV, so that the one-loop contributions to these helicity amplitudes may also be valuable to discuss at low energies. In the following, we show the sfermion one-loop contributions to $M^{+-}_{\tau=-1}$ and $M^{-+}_{\tau=-1}$, $M^{00}_{\tau=\mp1}$, $M^{0+}_{\tau=-1}$ and $M^{-0}_{\tau=-1}$, at the large scattering angle ($\theta = 90°$). The net sfermion contributions in each helicity amplitude are given by

$$\frac{{M_\tau^{\lambda\overline{\lambda}}}_{\rm MSSM} - {M_\tau^{\lambda\overline{\lambda}}}_{\rm SM}}{{M_\tau^{\lambda\overline{\lambda}}}_{\rm SM}}, \tag{6.1}$$

where ${M_\tau^{\lambda\overline{\lambda}}}_{\rm MSSM}$ are the helicity amplitudes of the MSSM in which only sfermion contributions are considered, and ${M_\tau^{\lambda\overline{\lambda}}}_{\rm SM}$ are those of the SM.

We consider the twenty cases in Tables 5, 6, 7 and 8 as parameter choice, which are categorized in the 4 groups. The first two are the following.

Set 1: Case 1 - Case 5 in Table 5, in which only the sleptons are light, and all the squarks are heavy enough. The mass eigenstates $\tilde{l}_1$ and $\tilde{l}_2$ coincident with $\tilde{l}_L$ and $\tilde{l}_R$, respectively.

Set 2: Case 6 - Case 10 in Table 6, in which only the squarks of the first and the second generations are light and all the other sfermions are heavy enough to decouple, where the mass eigenstates $\tilde{q}_1$ and $\tilde{q}_2$ coincident with $\tilde{q}_L$ and $\tilde{q}_R$, respectively.

The rest two groups are for the cases where only squarks in the third generation, which we refer to the $(\tilde{t}, \tilde{b})$ sector, are light. In this sector, the large mass mixing between $\tilde{t}_L$ and $\tilde{t}_R$ is possible by the large top quark mass.

Set 3: Case 11 - Case 15 in Table 7, where the $(\tilde{t}, \tilde{b})$ sector is considered without the $\tilde{t}_L$-$\tilde{t}_R$ mixing.

Set 4: Case 16 - Case 20 in Table 8, where the $(\tilde{t}, \tilde{b})$ sector is considered with the large mass mixing between $\tilde{t}_L$ and $\tilde{t}_R$ with the angle $\tilde{\theta}_t \sim \pi/4$.

In each parameter set, the sfermion masses that we directly do not consider should be regarded to be sufficiently large. Since we adopt the SM couplings as our expansion parameters so that the decoupling of such heavy particles is exact at the one-loop level, the contribution of these heavy sfermions can be removed simply by dropping their explicit contribution.

6.1.1 The sfermion one-loop contributions to M_τ^{+-} and M_τ^{-+}

The tree-level helicity amplitudes $M_{\tau=-1}^{+-}$ and $M_{\tau=-1}^{-+}$ are the largest of all the helicity amplitudes at the scattering angle $\theta = 90°$. Since the $(+-)$ and $(-+)$ helicity-set processes contain only the t-channel diagrams, these amplitudes contain only wavefunction renormalization factors as the sfermion one-loop contribution. Thus, they are almost independent of $\sqrt{s}$ and determined by the logarithmic function of the sfermion masses and the W-boson mass. In Table 9, we list the sfermion corrections to the $M_{\tau=-1}^{+-}$ at $\theta = 90°$ for $\sqrt{s} = 200$GeV and 1000GeV. As we expected, we see that the corrections are insensitive to $\sqrt{s}$. The magnitude of the sfermion contributions to this helicity amplitude is

Set 1:	Case 1	Case 2	Case 3	Case 4	Case 5
Input parameters					
$m_{\tilde{L}}$	100	200	300	500	1000
$m_{\tilde{E}}$	100	200	300	500	1000
A_f^{eff}	0	0	0	0	0
Output parameters					
$m_{\tilde{\nu}_e} = m_{\tilde{\nu}_\mu} = m_{\tilde{\nu}_\tau}$	85	193	295	497	999
$m_{\tilde{e}_1} = m_{\tilde{\mu}_1} \sim m_{\tilde{\tau}_1}$	105	203	302	501	1001
$m_{\tilde{e}_2} = m_{\tilde{\mu}_2} \sim m_{\tilde{\tau}_2}$	109	205	303	502	1001

Table 5: The cases where only sleptons are light. The squarks are taken to be sufficiently heavy.

Set 2:	Case 6	Case 7	Case 8	Case 9	Case 10
Input parameters					
$m_{\tilde{Q}}$	100	200	300	500	1000
$m_{\tilde{U}}= m_{\tilde{D}}$	100	200	300	500	1000
$A_{\tilde{f}}^{eff}$	0	0	0	0	0
Output parameters					
$m_{\tilde{u}_1} = m_{\tilde{c}_1}$	91	196	297	498	999
$m_{\tilde{u}_2} = m_{\tilde{c}_2}$	93	197	298	499	999
$m_{\tilde{d}_1} = m_{\tilde{s}_1}$	111	206	304	502	1001
$m_{\tilde{d}_2} = m_{\tilde{s}_2}$	103	202	301	501	1000

Table 6: Cases where only squarks from the first-two generations are light. The other sfermions are taken to be sufficiently heavy.

Set 3:	Case 11	Case 12	Case 13	Case 14	Case 15
Input parameters					
$m_{\tilde{Q}}$	100	200	300	500	1000
$m_{\tilde{U}}= m_{\tilde{D}}$	100	200	300	500	1000
$A_{\tilde{f}}^{eff}$	0	0	0	0	0
Output parameters					
$m_{\tilde{t}_1}$	197	263	345	528	1014
$m_{\tilde{t}_2}$	199	263	346	529	1015
$m_{\tilde{b}_1}$	111	206	304	502	1001
$m_{\tilde{b}_2}$	103	202	301	501	1000

Table 7: 5 sets of mass parameters of $\tilde{t}$ and $\tilde{b}$ are listed in which no mass mixing between $\tilde{t}_L$-$\tilde{t}_R$ is considered. The sfermions which we do not consider are sufficiently large.

Set 4:	Case 16	Case 17	Case 18	Case 19	Case 20
Input parameters					
$m_{\tilde{Q}}$	100	200	300	400	500
$m_{\tilde{U}}= m_{\tilde{D}}$	100	200	300	400	500
$A_{\tilde{f}}^{eff}$	168	339	625	1025	1539
Output parameters					
$m_{\tilde{t}_1}$	100	100	100	100	100
$m_{\tilde{t}_2}$	262	358	478	607	741
$m_{\tilde{b}_1}$	111	206	304	403	502
$m_{\tilde{b}_2}$	103	202	301	401	501
$\cos\theta_{\tilde{t}}$	0.710	0.708	0.708	0.708	0.707

Table 8: Cases where the squarks of the $(\tilde{t}, \tilde{b})$ sector are light with the large $\tilde{t}_L$-$\tilde{t}_R$ mass mixing. The mass of $\tilde{t}_1$ is fixed to be 100GeV in these cases. The sfermions which we do not consider are sufficiently large.

Case	$\frac{M^{+-}_{\rm MSSM}-M^{+-}_{\rm SM}}{M^{+-}_{\rm SM}}$		Case	$\frac{M^{+-}_{\rm MSSM}-M^{+-}_{\rm SM}}{M^{+-}_{\rm SM}}$	
	$\sqrt{s}=200$GeV	1000GeV		$\sqrt{s}=200$GeV	1000GeV
1	-4.5×10^{-4}	-4.4×10^{-4}	11	-1.6×10^{-4}	-1.5×10^{-4}
2	-1.1×10^{-4}	-1.1×10^{-4}	12	-1.1×10^{-4}	-1.1×10^{-4}
3	-4.8×10^{-5}	-4.7×10^{-5}	13	-6.4×10^{-5}	-6.2×10^{-5}
4	-1.7×10^{-5}	-1.7×10^{-5}	14	-2.7×10^{-5}	-2.7×10^{-5}
5	-4.3×10^{-6}	-4.2×10^{-6}	15	-7.4×10^{-6}	-7.2×10^{-6}
6	-1.5×10^{-4}	-1.5×10^{-4}	16	-8.8×10^{-5}	-8.5×10^{-5}
7	-4.2×10^{-5}	-4.1×10^{-5}	17	2.0×10^{-4}	2.0×10^{-4}
8	-1.8×10^{-5}	-1.8×10^{-5}	18	4.7×10^{-4}	4.6×10^{-4}
9	-6.8×10^{-6}	-6.7×10^{-6}	19	6.9×10^{-4}	6.7×10^{-4}
10	-1.7×10^{-6}	-1.7×10^{-6}	20	8.6×10^{-4}	8.4×10^{-4}

Table 9: The sfermion one-loop contributions to the $M^{+-}_{\tau=-1}$ amplitude are listed in Case 1 - Case 20.

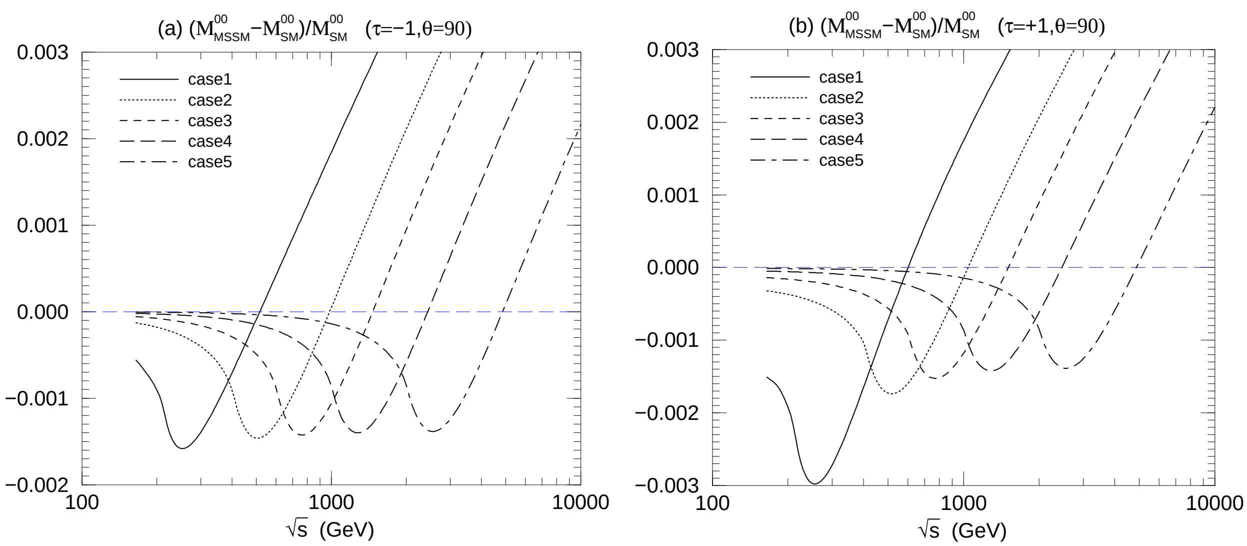

Figure 9: The sfermion one-loop corrections to M^{00}_{τ} for Set 1 (Case 1 - Case 5), in which only the sleptons are light.

rather small for all cases we consider. The contributions of the stop-sbottom sector with a large mass mixing give the biggest contribution to $M^{+-}_{\tau=-1}$, where the deviation from the SM is less than +0.1% (Case 20). The corrections to $M^{-+}_{\tau=-1}$ are the same as those to $M^{+-}_{\tau=-1}$ at $\theta=90°$.

6.1.2 The sfermion one-loop contributions to M^{00}_{τ}

We next consider the sfermion one-loop contributions to M^{00}_{τ} at $\theta=90°$, which are expected to have rich structures because M^{00}_{τ} receive contributions from all the sfermion one-loop diagrams. The slepton contributions to $M^{00}_{\tau=\mp1}$ are described by using Set 1 in Table 5 and the results are

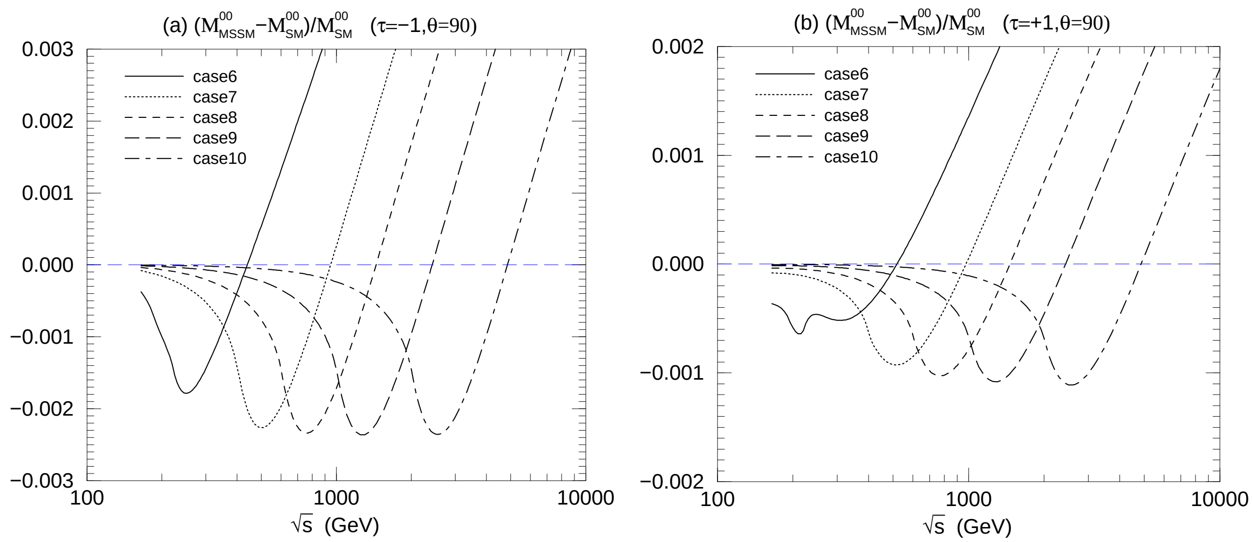

Figure 10: The sfermion one-loop corrections to M^{00}_{τ} are shown for Set 2 (Case 6 - Case 10), in which only the squarks of the first-two generations are light

shown in Figs. 9(a) and 9(b). See the $\tau = -1$ amplitude in Fig. 9(a) first. The slepton corrections contribute destructively to the SM amplitudes below the threshold of the sneutrino-pair production. The magnitude of the negative deviation from the SM reaches to its maximum slightly above the threshold, and the maximal deviation is about -0.15% in amplitudes, which is almost independent of the slepton masses. Second, for the $\tau = +1$ amplitudes shown in Fig. 9(b), the larger deviation is observed in Case 1, but it may be difficult to observe this effect because of the smallness of the $\tau = +1$ amplitudes: see Fig. 5.

The contributions of the squarks of the first-two generations, Set 2 of Table 6, are shown in Figs. 10(a) and 10(b). The qualitative behavior is quite similar to that of the slepton contributions of Set 1. The magnitude of the squark contributions per a generation is larger than that of the slepton contributions for the similar mass sets. In Fig. 10(a), the corrections to the $\tau = -1$ amplitude amount to -0.24% at the peak slightly above the thresholds of the $\tilde{u}$-pair productions and the $\tilde{c}$-pair productions. In Fig. 10(b), the contributions to the $\tau = +1$ amplitude in these cases are similar to those in Set 1, but the magnitude is smaller.

The contributions of the $(\tilde{t}, \tilde{b})$ sector are rather interesting. The cases without the $\tilde{t}_L$-$\tilde{t}_R$ mass mixing are given in Set 3 of Table 7. See the curve of Case 11 in Fig. 11(a), where the thresholds of the $\tilde{t}$-pair production are 394-398GeV and those of the sbottom-pair production are 206-222GeV. The corrections to the $\tau = -1$ amplitude are positive around the first threshold of the sbottom-pair productions and the deviation from the SM amounts to $+0.25\%$ in amplitudes at the first peak above the $\tilde{b}$-pair thresholds. Around the thresholds of the $\tilde{t}$-pair productions, the correction rapidly reduces and the deviation changes its sign from positive to negative due to the constant part (5.15) in the amplitude. Beyond the negative peak around 1000GeV, where the deviation amounts to -0.17% in amplitudes, the correction behaves asymptotically according to the analytic high-energy formulas

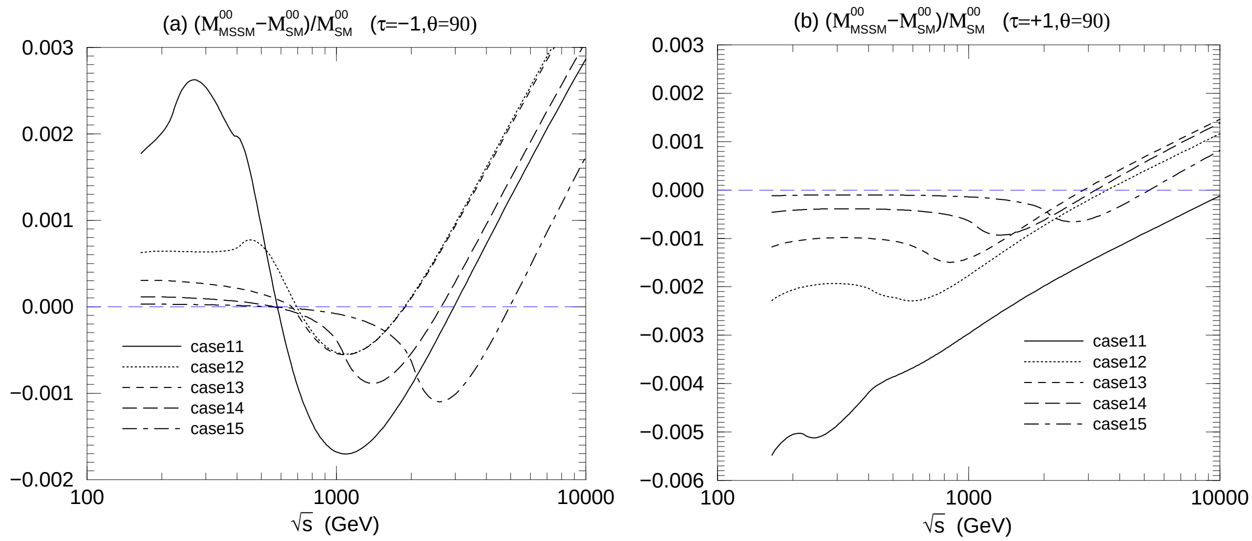

Figure 11: The sfermion one-loop contributions to M_τ^{00} are shown for Set 3 (Case 11 - Case 15), in which only the squarks of the third generation, $\tilde{t}$ and $\tilde{b}$, are light. The mixing between $\tilde{t}_L$ and $\tilde{t}_R$ is zero in these cases.

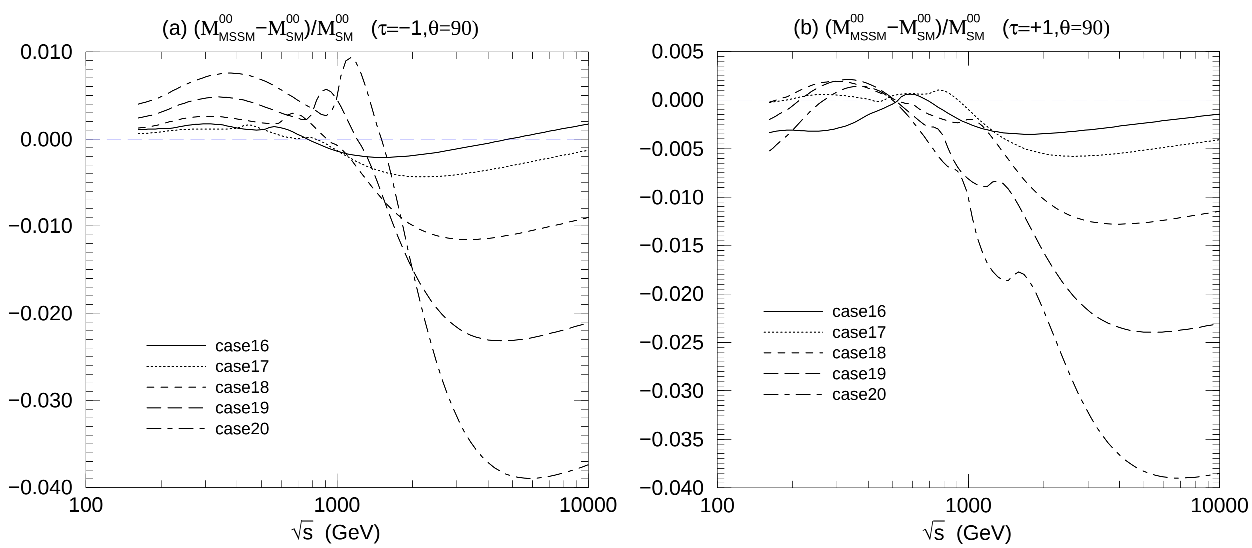

Figure 12: The sfermion one-loop contributions to M_τ^{00} for Set 4 (Case 16 - Case 20), in which only the squarks of the third generation, $\tilde{t}$ and $\tilde{b}$, are light with the nonzero mass mixing between $\tilde{t}_L$ and $\tilde{t}_R$. $m_{\tilde{t}_1}$=100GeV is fixed in these cases.

discussed in Sec. 5.3. The qualitative characteristics in Case 11 are common with the other 4 cases of Set 3 (Case 12 - Case 15), but the corrections at low energy becomes smaller as the masses of stops and sbottoms are set to be larger. For the $\tau = +1$ amplitudes in Fig. 11(b), corrections around the first threshold of the sbottom-pair production are all negative. The corrections are larger than in the $\tau = -1$ amplitudes because the constant term of (5.15) enlarges negative squark contributions.

Finally, we show the contributions of the $(\tilde{t}, \tilde{b})$ sector with the $\tilde{t}_L$-$\tilde{t}_R$ mixing described in Set 4 (Case 16 - Case 20) of Table 8, where *maximal* mixing ($\theta_{\tilde{t}} \sim \pi/4$) takes place. The mass of $\tilde{t}_1$ is fixed to be 100GeV, and the other squarks of this sector $\tilde{t}_2$, $\tilde{b}_1$ and $\tilde{b}_2$ are varied widely. First, see the $\tau = -1$ amplitude in Fig. 12(a). The largest sfermion contributions are observed in Case 20, where the smallness of $m_{\tilde{t}_1} = 100$GeV comes from the mass mixing. For this case, the corrections are positive around the $\tilde{t}_1$-pair threshold. At the first peak above this threshold, the deviation from the SM prediction can be about $+0.7\%$ in amplitudes, and it amounts to $+0.9\%$ at the second peak just above the threshold of the $\tilde{b}$-pair production. The deviation then goes to be negative drastically due to the negative constant term (5.15). The term (5.15) is enlarged by the mass difference between $\tilde{t}_1$ and the others, so that the correction reaches -3.9% in amplitudes (Case 20) before the asymptotic behavior is observed. In Case 16 - Case 19, the corrections behave in the same way as in Case 20, but the smaller corrections are observed because the mass difference between $\tilde{t}_1$ and the others is smaller. For the $\tau = +1$ amplitude, as similar to Set 3, the corrections below the threshold of $\tilde{t}_1$-pair production are negative, but the large mass difference between $\tilde{t}_1$ and the others makes the correction positive around the first peak above the threshold of the $\tilde{t}_1$-pair production.

Therefore the sfermion one-loop corrections to M_τ^{00} are sensitive to the sfermion parameter choice. The typical magnitude of the sfermion one-loop contribution, however, is a few times 0.1% in amplitudes in each part. The deviations from the SM prediction at low energies tend to be negative, but the larger mass splitting between $\tilde{t}_1$ and the other squarks of the $(\tilde{t}, \tilde{b})$ sector can induce the larger positive corrections.

6.1.3 The sfermion one-loop corrections to $M_{\tau=-1}^{0+}$ and $M_{\tau=-1}^{-0}$

The one-loop corrections to $M_{\tau=-1}^{0+}$ and M_τ^{-0} may be valuable to study only for low energies where the tree-level amplitudes are large; see Fig. 5. We here present a figure (Fig. 13) for the sfermion one-loop contributions to $M_{\tau=-1}^{0+}$, where the results for the following 5 cases are shown; Case 1 and Case 2 in Table 5, Case 7 in Table 6, Case 12 in Table 7 and Case 17 in Table 8.

In Fig. 13, we find the similar characteristics of the corrections to $M_{\tau=-1}^{00}$ which we have already discussed in detail. The deviation from the SM prediction by the slepton contributions (Case 1 and Case 2) and by the squark contributions from the first-two generations (Case 7) are negative at low energies. On the other hand, the deviation by the $(\tilde{t}, \tilde{b})$ sector (Case 12 and Case 17) is positive at low energies. In the curve of Case 17 in Fig. 13, the typical effects of the stop mass mixing seen in the study of $M_{\tau=-1}^{00}$ are also observed in $M_{\tau=-1}^{0+}$. The magnitude of the deviation from the SM prediction is smaller than that of $M_{\tau=-1}^{00}$ for each cases.

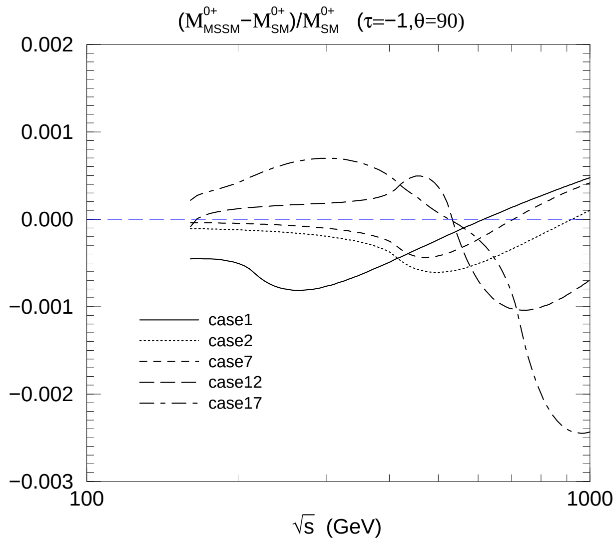

Figure 13: The sfermion one-loop contributions to $M^{0+}_{\tau=-1}$ are shown in various MSSM parameter sets; Case 1, Case 2 in Table 5, Case 7 in Table 6, Case 12 in Table 7 and Case 17 in Table 8.

6.2 The one-loop corrections to cross sections

In this subsection, we study the corrections to the helicity-summed differential cross section at the large scattering angle ($\theta = 90°$). The sfermion one-loop contributions to the helicity-summed differential cross section may be measured by

$$\frac{\left(\frac{d\sigma}{d\cos\theta}\right)_{\text{MSSM}} - \left(\frac{d\sigma}{d\cos\theta}\right)_{\text{SM}}}{\left(\frac{d\sigma}{d\cos\theta}\right)_{\text{SM}}}, \tag{6.2}$$

where $(d\sigma/d\cos\theta)_{\text{MSSM}}$ and $(d\sigma/d\cos\theta)_{\text{SM}}$ are the helicity-summed differential cross sections in the MSSM and the SM, respectively. The scattering angle is fixed at $\theta = 90°$ in the following.

Here, in order to examine combined effects including all the sfermion contributions, we dare to assume another sets of the sfermion parameters, where all the sfermion masses are not larger than about 1000GeV and the results from the direct search experiments are taken into account. The results from the direct search experiments[28] give lower bounds of the sfermion masses; all the slepton masses should not be smaller than about 100GeV, while the squarks except for the stops should be heavier than about 200GeV. As for the stop mass, it can still be about 100GeV. The sfermion mass parameter sets that we examine are defined in Table 10.

6.2.1 The cases without the mass mixing

In the first 5 cases (Case 21 - Case 25) in Table 10, we include all the sfermions but we do not consider the mass mixing by setting all the A_f^{eff} to be zero. In Case 21, the light sleptons with rather heavy squarks are assumed, while the light squarks with heavy sleptons are assumed in Case 22. In

	Case 21	Case 22	Case 23	Case 24	Case 25	Case 26	Case 27	Case 28	Case 29
Input parameters									
$m_{\tilde{Q}}$	1000	250	250	250	1000	600	600	600	600
$m_{\tilde{U}}=m_{\tilde{D}}$	1000	250	250	250	1000	540	540	540	540
$m_{\tilde{L}}$	100	1000	100	250	500	540	540	540	540
$m_{\tilde{E}}$	100	1000	100	250	100	540	540	540	540
$A_t^{eff}=A_b^{eff}=A_\tau^{eff}$	0	0	0	0	0	0	1000	1800	1950
Output parameters									
$m_{\tilde{u}_1}=m_{\tilde{c}_1}$	999	246	246	246	999	599	599	599	599
$m_{\tilde{u}_2}=m_{\tilde{c}_2}$	1000	248	248	248	1000	539	539	539	539
$m_{\tilde{d}_1}=m_{\tilde{s}_1}\sim m_{\tilde{b}_1}$	1001	254	254	254	1001	602	602	602	602
$m_{\tilde{d}_2}=m_{\tilde{s}_2}\sim m_{\tilde{b}_2}$	1000	251	251	251	1000	540	540	540	540
$m_{\tilde{e}_1}=m_{\tilde{\mu}_1}\sim m_{\tilde{\tau}_1}$	107	1001	107	253	501	541	541	541	541
$m_{\tilde{e}_2}=m_{\tilde{\mu}_2}\sim m_{\tilde{\tau}_2}$	106	1001	106	252	106	541	541	541	541
$m_{\tilde{\nu}_e}=m_{\tilde{\nu}_\mu}=m_{\tilde{\nu}_\tau}$	86	999	86	245	497	538	538	538	538
$m_{\tilde{t}_1}$	1014	302	302	302	1014	624	421	196	111
$m_{\tilde{t}_2}$	1015	304	304	304	1015	567	730	820	835
$\cos\theta_{\tilde{t}}$	1	1	1	1	1	1	0.637	0.668	0.671

Table 10: The parameter sets for the study of combined effects of sfermion contributions, which satisfies the constraint from the direct search experiments. In Case 21 - Case 25, cases without the mass mixing are assumed, while the effects of the $\tilde{t}_1$-$\tilde{t}_2$ mixing are studied by using Case 26 - Case 29.

Case 23, we can study the case where all the sfermions are light but their masses are consistent with the data from the direct search experiments. The case of the complete degeneracy of the input SUSY mass parameters $m_{\tilde{Q}}$, $m_{\tilde{U}}$, $m_{\tilde{D}}$, $m_{\tilde{L}}$ and $m_{\tilde{E}}$ is described as Case 24. Finally the case where only right-handed slepton is light and the others have heavier masses is represented by Case 25.

The corrections are shown in Fig. 14. First, see the curve of Case 21. At low energies, the slepton contributions are dominant and thus the corrections are negative around the thresholds of the slepton-pair productions. The deviation amounts at most to -0.15% at the first peak. The corrections become slightly positive below the thresholds of the squark-pair productions. Since the peak above these thresholds is negative, the combined squark effects are negative in this case. Second, see the curve of Case 22 where the combined squark effects can be seen. The corrections below and around the threshold of the squark-pair productions are also destructive and the deviation is at most about -0.1%. Third, in the Case 23, both sleptons and squarks have small masses and they are set slightly above the lower bounds from the direct search experiment. The corrections are approximately the sum of those of Case 21 and Case 22 at low energies. Forth, the large combined corrections are found in the Case 24, where the sfermions are almost mass-degenerate and all the thresholds of the sfermion-pair productions are between 490 - 610 GeV. The deviation reaches to -0.2% at the negative peak slightly above the thresholds. Finally in Case 25, the effect of the right-handed squarks is very small around the first threshold of the slepton-pair production (212 GeV); i.e. the most part of the

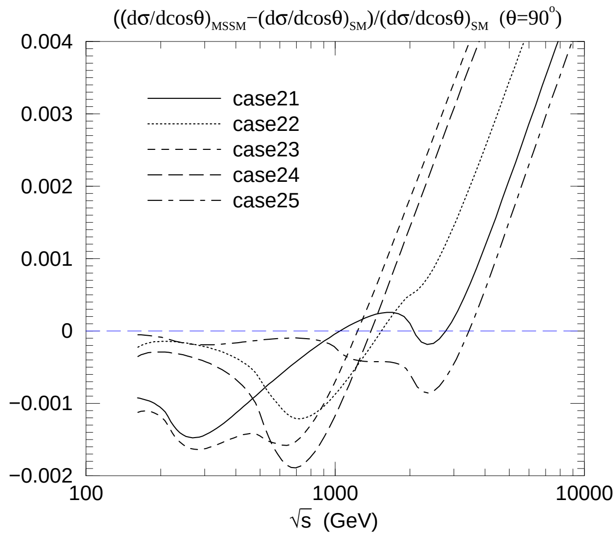

Figure 14: The sfermion one-loop corrections to the helicity-summed differential cross section are shown in Case 21 - Case 25 in Table 10. The mixing between $\tilde{t}_L$ and $\tilde{t}_R$ is zero in these cases.

slepton contributions in Case 21 comes from the left-handed sleptons.

Therefore, in these cases without the mass mixing, the combined contributions to the cross section are negative below and around the lowest threshold of the sfermion-pair production. Even in the light squark case (Case 22), the positive contributions which we have observed in $M^{00}_{\tau=-1}$ and $M^{0+}_{\tau=-1}$ are smaller than the summed negative contributions from the squarks of the first-two generations and the negative corrections in $M^{+-}_{\tau=-1}$.

6.2.2 The effects of the mass mixing

The latter 4 cases (Case 26 - Case 29) in Table 10 are introduced in order to observe the sfermion mass-mixing effects. $A_t^{eff}(= A_b^{eff} = A_\tau^{eff})$ is varied as 0, 1000GeV, 1800GeV and 1950GeV in Case 26, Case 27, Case 28 and Case 29, respectively. The larger mass splitting between $\tilde{t}_1$ and $\tilde{t}_2$ takes place for larger A_t^{eff}. In Case 25, since we put $A_t^{eff} = 0$ the mass difference between $\tilde{t}_1$ and $\tilde{t}_2$ is the smallest, while in the Case 28 with $A_t^{eff} = 1950$GeV the large stop mass-splitting takes place where $m_{\tilde{t}_1} = 111$GeV and $m_{\tilde{t}_2} = 836$GeV. The results in these cases are shown in Fig. 15.

In Case 26, there is nothing new because of $A_t^{eff} = 0$ and the curve behaves qualitatively in the same way as Cases 24 in Fig. 14. In Case 27 - Case 29, the combined sfermion contributions become positive because of the effect of nonzero A_t^{eff} values. The behaviors of the corrections are very similar to those of $M^{00}_{\tau=-1}$ and $M^{0+}_{\tau=-1}$ with the mass mixing. For large A_t^{eff}, the positive corrections maximally reach to near +0.5% (Case 28 and Case 29). The large negative correction due to the negative constant term (5.15) before the asymptotic behavior sets in is also observed, which is one of the interesting characteristics with large mass-mixing cases seen in $M^{00}_{\tau=-1}$ and $M^{0+}_{\tau=-1}$.

Therefore, in the cases with the large mass mixing, the magnitude of the positive contributions

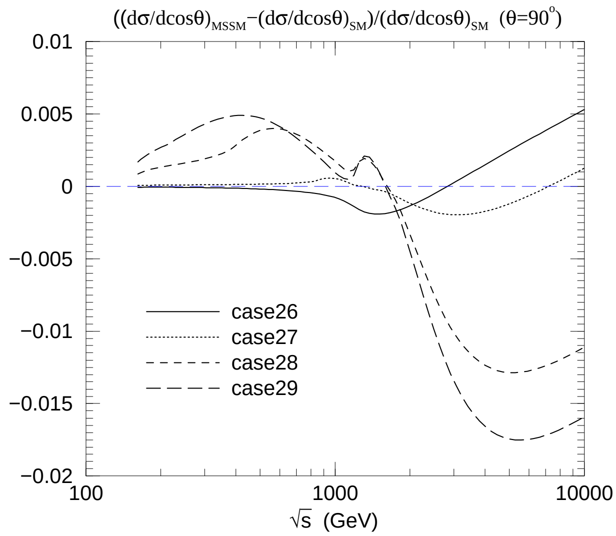

Figure 15: The sfermion one-loop corrections to the helicity-summed differential cross section are shown in Case 26 - Case 29 of Table 10. The mixing between $\tilde{t}_L$ and $\tilde{t}_R$ appears in Case 27 - Case 29.

of the $(\tilde{t}, \tilde{b})$ sector is much larger than that of the combined negative corrections from all the other sfermions. In the next section, we will see that such large corrections due to the large mass mixing are almost excluded by the constraints from the electroweak precision data.

6.3 Constraints on the sfermion sector by the electroweak precision data

We have examined in previous subsections the sfermion effects only taking into account the direct search results as experimental constraints. We here consider the constraints from the precision measurement and give a constraint on sfermion effects on $e^-e^+ \to W^-W^+$. The stringent experimental constraints on the MSSM parameters are obtained from the electroweak experiments, especially on Z-pole experiments, the m_W measurements and the low-energy neutral current experiments. The latest data on the Z parameters[37] and the W-boson mass[34] are studied in the framework of the MSSM in Ref. [29] and we use them here. We also consider the external constraints

$$\alpha_s(m_Z) = 0.119 \quad \pm 0.002, \tag{6.3a}$$

$$1/\alpha(m_Z) = 128.90 \pm 0.09, \tag{6.3b}$$

$$m_t = 174.3 \quad \pm 5.1 \text{ GeV}, \tag{6.3c}$$

referring to Ref. [28] for $\alpha_s(m_Z)$ and m_t, and Ref. [33] for $1/\alpha(m_Z)$. The new physics contributions to the three oblique parameters ΔS_Z, ΔT_Z and Δm_W of Ref. [29], which we here express by $(S_Z)_{\text{new}}$, $(T_Z)_{\text{new}}$ and $(m_W)_{\text{new}}$, are then constrained as

$$(S_Z)_{\text{new}} = -0.082 \pm 0.114, \tag{6.4a}$$

$$(T_Z)_{\text{new}} = -0.179 \pm 0.146, \tag{6.4b}$$

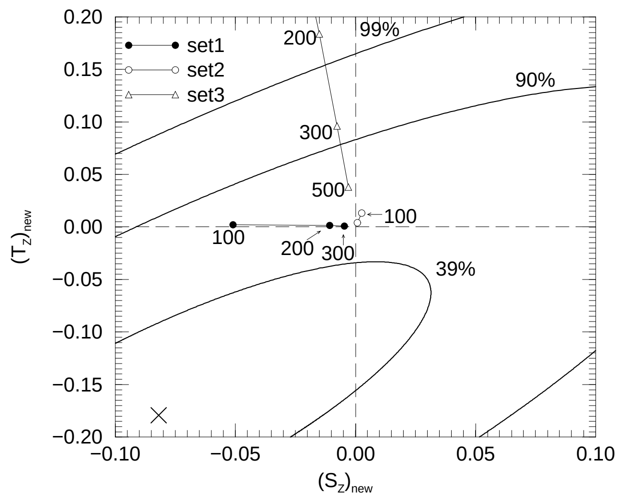

Figure 16: The constraints of $(S_Z)_{\rm new}$ and $(T_Z)_{\rm new}$ for Set 1 (Table 5), Set 2 (Table 6) and Set 3 (Table 7) from the precision data. The contour show the $(S_Z)_{\rm new}$ and $(T_Z)_{\rm new}$ fit to the all electroweak data. The point $(S_Z)_{\rm new} = (T_Z)_{\rm new} = 0$ corresponds to the SM prediction. The numbers 100, 200, ... etc in the figure are values of $m_{\tilde{L}}$ in the unit of GeV for Set 1, and those of $m_{\tilde{Q}}$ for Set 2 and Set 3.

$$(m_W)_{\rm new} = \quad 0.118 \pm 0.057, \tag{6.4c}$$

where the correlation between the first-two errors is $\rho_{\rm corr} = 0.80$. Here we choose the reference value of the SM-Higgs-boson mass as $m_H = 117$GeV, the best fit value in the SM.

On the other hand, the new physics contributions $(S_Z)_{\rm new}$, $(T_Z)_{\rm new}$ and $(m_W)_{\rm new}$ are parametrized in terms of the new physics contributions to the S, T, U and R parameters by[38]

$$(S_Z)_{\rm new} = S_{\rm new} + R_{\rm new}, \tag{6.5a}$$

$$(T_Z)_{\rm new} = T_{\rm new} + 1.49 R_{\rm new} - \frac{(\delta_G)_{\rm new}}{\alpha}, \tag{6.5b}$$

$$(m_W)_{\rm new} = -0.288 S_{\rm new} + 0.418 T_{\rm new} + 0.337 U_{\rm new} - 0.126 \frac{(\delta_G)_{\rm new}}{\alpha}, \tag{6.5c}$$

where $(\delta_G)_{\rm new}$ are the new physics contributions to the muon decay parameter, whose sfermion one-loop corrections are calculated in Ref. [39], and the $S_{\rm new}$, $T_{\rm new}$, $U_{\rm new}$ and $R_{\rm new}$ are calculated by[32]

$$S_{\rm new} = 16\pi {\rm Re} \left[\Pi_{T,\gamma}^{3Q}(m_Z^2) - \Pi_{T,Z}^{33}(0) \right], \tag{6.6a}$$

$$T_{\rm new} = \frac{4\sqrt{2} G_F}{\alpha} \left[\Pi_T^{33}(0) - \Pi_T^{11}(0) \right], \tag{6.6b}$$

$$U_{\rm new} = 16\pi {\rm Re} \left[\Pi_{T,Z}^{33}(0) - \Pi_{T,W}^{11}(0) \right], \tag{6.6c}$$

$$\begin{aligned} R_{\rm new} = 16\pi & \left[\Pi_{T,Z}^{33}(0) - \Pi_{T,Z}^{33}(q^2) - 2\hat{s}^2 \left\{ \Pi_{T,Z}^{3Q}(0) - \Pi_{T,Z}^{3Q}(q^2) \right\} \right. \\ & \left. +4\hat{s}^4 \left\{ \Pi_{T,Z}^{QQ}(0) - \Pi_{T,Z}^{QQ}(q^2) \right\} \right], \end{aligned} \tag{6.6d}$$

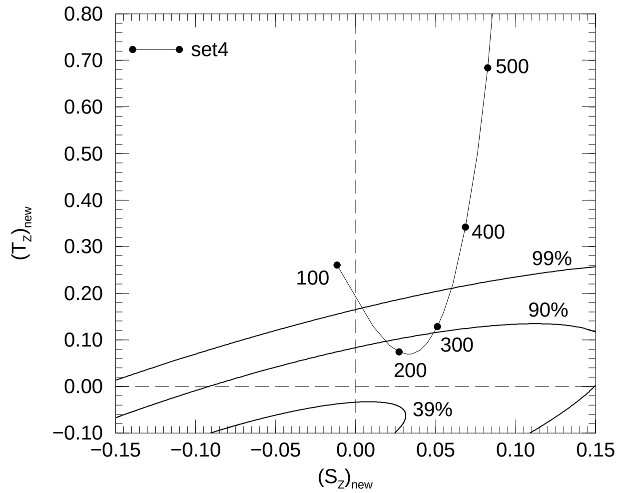

Figure 17: The constraints of $(S_Z)_{\rm new}$ and $(T_Z)_{\rm new}$ for Set 4 (Table 8) from the precision data. The point of $(S_Z)_{\rm new} = (T_Z)_{\rm new} = 0$ corresponds to the SM prediction. The numbers 100, 200, ... etc in the figure are values of $m_{\tilde{Q}}$ in the unit of GeV in each case of Set 4.

Case	$(S_Z)_{\rm new}$	$(T_Z)_{\rm new}$	$\Delta\chi^2$	Case	$(S_Z)_{\rm new}$	$(T_Z)_{\rm new}$	$\Delta\chi^2$
21	-0.052	0.012	3.4	26	-0.0035	0.028	2.5
22	-0.010	0.13	7.2	27	0.0046	0.014	2.0
23	-0.061	0.13	11	28	0.043	0.42	30
24	-0.017	0.13	8.1	29	0.080	0.81	90
25	-0.0038	0.0082	2.0				

Table 11: The values of $(S_Z)_{\rm new}$, $(T_Z)_{\rm new}$ and $\Delta\chi^2$ for Case 21 - Case 25 of Table 10.

where the sfermion one-loop corrections to the propagator functions are given in Appendix B.

Let us examine how the sfermion parameter sets in Sec. 6.1 are constrained by the precision data. We here note that Case 6 and Case 7 of Set 2 in Table 6, Case 11 and Case 12 of Set 3 in Table 7, and Case 16 and Case 17 of Set 4 in Table 8 are excluded by the results from direct search experiments. In Figs. 16 and 17, the contributions to $(S_Z)_{\rm new}$ and $(T_Z)_{\rm new}$ are shown for Set 1 - Set 4 of Tables 5 - 8 in Sec. 6.1, respectively. The origin of the plot shows the SM prediction at $m_H = 117$GeV. First, in Fig. 16, the three series of the points for the cases without the mass mixing (Case 1 - Case 15) are shown according to the three corresponding categories Set 1 (Case 1 - Case 5), Set 2 (Case 6 - Case 10), and Set 3 (Case 11 - Case 15) of Tables 5, 6 and 7. We see that all the cases of Set 1 (cases where only sleptons are light) and Set 2 (cases where only the squarks of the first-two generations are light) are in the 90% CL region. As for the cases of Set 3 (cases where only the squarks of $(\tilde{t}, \tilde{b})$ sector are light without the mass mixing), the point of cases moves outside of the 99% CL region as

the mass splitting between $\tilde{t}$ and $\tilde{b}$ grows[6]. Second, in Fig. 17, the constraint on the $(\tilde{t}, \tilde{b})$ sector with the mass mixing is shown for Set 4 (Case 16 - Case 20) of Table 8. The points of Case 16, Case 19 and Case 20 are outside of the 99% CL region and thus they are almost excluded by the precision data. In Case 19 and Case 20, the large mass splitting occurs between $\tilde{t}$ and $\tilde{b}$ because of the large off-diagonal coefficient $m_t A_t^{eff}$.

Next, we consider the constraints on the MSSM parameter sets (Case 21-Case 29) of Table 10 in Sec. 6.2 that are consistent with the results from the direct search experiments. These cases have been introduced in order to study the combined contributions of all the sfermions to the helicity-summed differential cross section. The values of $(S_Z)_{\rm new}$, $(T_Z)_{\rm new}$ and $\Delta\chi^2$, where $\Delta\chi^2 \equiv \chi^2 - \chi^2_{\rm min}$, for these cases are given in Table 11. Case 21, Case 25, Case 26 and Case 27 have their $\Delta\chi^2$ values less than 4.6 (90% CL). On the other hand, the $\Delta\chi^2$ values of Case 23, Case 28 and Case 29 are much larger than 9.2 (99% CL). Therefore, Case 23, Case 28 and Case 29 are almost excluded.

The cases allowed by the direct search experiments but strongly constrained by the precision data are Case 19 and Case 20 of Table 8, and Case 23, Case 28 and Case 29 of Table 11. Case 23 is the case with the light squarks. The others are those with the large $\tilde{t}_L$-$\tilde{t}_R$ mixing. They all have the large mass splitting between $\tilde{t}$ and $\tilde{b}$, which indicates the breakdown of the $SU(2)_V$ custodial symmetry at the sfermion sector, so that they are strongly constrained by the precision data.

6.4 Summary of the numerical results

In this section, the results of the sfermion one-loop contributions to the $e^-e^+ \to W^-W^+$ helicity amplitudes and also those to the helicity-summed differential cross sections at the large scattering angle have been presented under various sfermion parameter choices.

The contributions from each sfermion sector have been examined to the amplitudes $M^{+-}_{\tau=-1}$, $M^{00}_{\tau=\mp1}$ and $M^{0+}_{\tau=-1}$ in the various parameter sets of Tables 5 - 8. First, for the $M^{+-}_{\tau=-1}$, which is the biggest at tree level for large scattering angles, the sfermion one-loop contributions come only from the wave-function renormalization, and the corrections are found to be rather simple as seen in Table 9. The magnitude of the deviation from the SM value is very small; it is at most $\pm 0.05\%$ in amplitudes under the constraints from the direct search experiments and the precision data. Second, the rich structure of the sfermion contributions is found in M^{00}_{τ}. The deviation from the SM value tend to be negative below and around the lowest threshold of sfermion-pair productions when its corresponding fermion is light; see Figs. 9 and 10. The corrections due to the sleptons and the first-two-generation squarks do not receive severe bounds from the precision test. By including the results of the direct search experiments, the corrections amount at most to -0.15% in amplitudes by the slepton contributions and -0.25% by the squark contributions from the first-two generations. The corrections to $M^{00}_{\tau=+1}$ are the same order as those to $M^{00}_{\tau=-1}$, but they may be more difficult to be measured because of the smallness of the tree-level contribution. The large positive contributions at low energies are also observed in the $M^{00}_{\tau=-1}$ helicity amplitude by the one-loop effects from the $(\tilde{t}, \tilde{b})$ sector, where the

[6] The mass splitting between $\tilde{t}$ and $\tilde{b}$ comes from the fermion mass difference between t and b in these cases. This effect relatively becomes larger for the case with smaller SUSY masses $m_{\tilde{Q}}$, $m_{\tilde{U}}$ and $m_{\tilde{D}}$

large mass-splitting between $\tilde{t}$ and $\tilde{b}$ can occur due to the large top-quark mass; see the cases in Figs. 11(a) and 12(a). The mass mixing between $\tilde{t}_L$ and $\tilde{t}_R$ enhances such positive corrections in the $\tau = -1$ helicity amplitude as seen in Figs. 12. In Sec. 6.3, it has, however, been found that the MSSM parameter sets which give the large mass splitting between $\tilde{t}$ and $\tilde{b}$ are inconsistent with the precision data. Therefore, the large positive corrections by the $(\tilde{t}, \tilde{b})$ sector to M_τ^{00} in Fig. 12(a) are strongly bounded. Still, +0.3% of the deviation may be possible in amplitudes between the first and the second thresholds: see Case 18 in Fig. 12(a). Third, for $M_{\tau=-1}^{0+}$, which is substantial for only low energies, the structure of the sfermion contributions is similar to that of $M_{\tau=-1}^{00}$, but the magnitude is rather smaller (Fig. 13).

Next, we have examined the combined sfermion one-loop contributions to the helicity-summed differential cross section at the large scattering angle by assuming the various MSSM parameter sets in which all the masses of sfermions are not larger than $\mathcal{O}(1)$ TeV. In the case where all the sfermion masses are degenerate at slightly above the lower bound of the squarks, the summed negative contributions to the cross section amount to −0.2% at the negative peak above the thresholds of the sfermion-pair productions. The positive corrections due to the quarks of the $(\tilde{t}, \tilde{b})$ sector become at most +0.1% at the first peak.

In summary, the rich structure of the sfermion contributions has been observed in $M_{\tau=-1}^{00}$. At low energies, negative corrections to $M_{\tau=-1}^{00}$ indicate the effects of the sleptons and the squarks of the first-two generations, while the squarks from the third generation give the positive corrections. These positive corrections are enlarged by the nonzero mixing between $\tilde{t}_L$ and $\tilde{t}_R$. Since such mixing is constrained by the precision data, the magnitude of the corrections to $M_{\tau=-1}^{00}$ is at most −0.4% and +0.3% in amplitudes at low energies. In terms of the 00-helicity differential cross section, these values are counted by multiplying the factor 2. On the other hand, in the corrections to the helicity-summed differential cross section, the magnitude of the corrections becomes smaller. The magnitude of the corrections to the helicity-summed cross section is at most a few times 0.1%. These results recall to us the importance of measuring the decaying W-boson polarizations[1].

7 Discussion and Conclusion

In this paper, we have investigated the sfermion one-loop contributions to the $e^-e^+ \to W^-W^+$ helicity amplitudes in the MSSM. The calculation has been thoroughly tested by using various methods; especially by (i) the exact satisfaction of the BRS sum rules; (ii) the clear observation of the decoupling property of the sfermion effects in the low energy limit (the heavy sfermion mass limit); (iii) the coincidence in the high energy limit between the results from the full calculation program and the analytic expression of the high energy amplitude that has been verified by the one-loop version of the equivalence theorem. The BRS sum rules among the form factors have been constructed so as to hold exactly in our calculational scheme. The demonstration of the BRS test when there are left-right mass mixings in the third generation sfermions is new in this paper, while Ref. [20] showed the BRS sum rules for the sfermion one-loop contribution only for non-mixing cases. The agreement in the BRS tests has given us confidence on our one-loop calculation of the form factors except for

the overall normalization contribution. The $\overline{\mathrm{MS}}$ scheme has been employed in our calculation. In addition, all the results have been expanded by the SM $\overline{\mathrm{MS}}$ couplings, $\hat{e}^2_{\mathrm{SM}}(\mu)$ and $\hat{g}^2_{\mathrm{SM}}(\mu)$ so that we could see the exact decoupling of the sfermion effects in the low-energy limit after all the higher order terms of $\mathcal{O}(\hat{g}^6_{\mathrm{SM}})$ in amplitude are eliminated. The exact decoupling property of the sfermions effects can be used as an excellent test of the amplitudes including the overall normalization factors.

We note here that the use of the SM couplings as the expansion parameters of the MSSM amplitudes is fully justified at around and below the SUSY particle production threshold. In this paper, we adopted the SM couplings as the expansion parameters even at higher energies above the thresholds, where the use of the MSSM $\overline{\mathrm{MS}}$ coupling could re-sum the logarithms of the type $\log s/m^2_{\mathrm{SUSY}}$. We compared the results of the amplitudes expanded in terms of the MSSM couplings and those expanded in terms of the SM couplings, and found that their numerical difference is at most 0.013% or less in $M^{00}_{\tau=-1}$ for the energies below a few TeV. This means that the error in the deviation from the SM prediction can be as large as 15%.

In this paper, we have not calculated the full one-loop effects of the SM particles. Instead, we estimate the SM amplitudes by setting $\mu = \sqrt{s}$ in the SM $\overline{\mathrm{MS}}$ couplings. This may or may not be a valid approximation to the full SM amplitudes[6, 7, 8] at high energies. We therefore presented all our results for the SUSY corrections in the form of the relative correction to the SM predictions.

With the numerical program established by passing through all the tests above, we have analyzed the sfermion one-loop contributions to each helicity amplitude and also those to the helicity-summed differential cross section of $e^-e^+ \to W^-W^+$. The summary of the numerical study has been given in Sec. 6.4. The 00 helicity amplitude, $M^{00}_{\tau=-1}$, is one of the most appropriate amplitudes for the study of the sfermion one-loop contributions. The magnitude of the correction in $M^{00}_{\tau=-1}$ at low energies becomes large in the following cases; (1) the light sfermion with no-mixing cases (destructive interference with the SM amplitude), (2) the large mass mixing cases in the $(\tilde{t}, \tilde{b})$ sector (constructive interference with the SM amplitude). The experimental results of the sfermion direct search give lower bounds on the sfermion masses. By including the electroweak precision data, the $(\tilde{t}, \tilde{b})$ sector especially with the large mass mixing is strongly constrained. Under all these experimental constraints, the deviation from the SM amplitude at the peak slightly after the first thresholds of sfermion-pair productions can be at most -0.8% (in cases (1)) and $+0.6\%$ (in cases (2)) in the differential cross section of the helicity amplitude $M^{00}_{\tau=-1}$ at the large scattering angle ($\theta = 90°$). Although these characteristics of the $M^{00}_{\tau=-1}$ have been observed in the helicity-summed differential cross section, the magnitude of the corrections is smaller; typically a few times 0.1%. Therefore, it is important to measure the decaying W-boson polarizations in exploring the sfermion sector through their indirect effects on $e^-e^+ \to W^-W^+$.

In conclusion, the sfermion one-loop contributions are small (about a few times $\pm 0.1\%$ level) in the helicity-summed cross section under the constraint from the direct search results and the electroweak precision tests. In some of the helicity amplitudes such as that for the longitudinally-polarized W-boson pair, the corrections of near -0.8% and $+0.6\%$ in observables may be possible.

One-loop effects from the other sector of the MSSM will be reported elsewhere[35].

Note added

After the completion of this work, we received a preprint[40]. We confirmed the agreement with their work in the analytic results of the sfermion one-loop contributions in the gauge-boson vacuum polarizations and the trilinear vertices.

Acknowledgements

The authors would like to thank Gi-Chol Cho for his valuable contribution in the early stage of the collaboration. S. K. was supported by the Alexander von Humboldt Foundation, and Y. U. was supported by Deutsche Forschungsgemeinschaft under Contract KL 1266/1-1.

A The Lagrangian

A.1 Physical masses and mixing angles

We begin by discussing the sfermion mass-matrices. We will ignore mixing between generations, hence we need to discuss only one generation which contains the up-type squark, $\tilde{u}$, the down-type squark, $\tilde{d}$, a charged slepton, $\tilde{e}$, and its associated sneutrino, $\tilde{\nu}$. The left-handed squarks, $\tilde{u}_L$ and $\tilde{d}_L$, form an SU(2) doublet which we denote by $\tilde{Q}$. Similarly, $\tilde{\nu}_L$ and $\tilde{e}_L$ form the doublet $\tilde{L}$. As for the right-handed sfermion $\tilde{u}_R$, $\tilde{d}_R$ and $\tilde{e}_R$ are SU(2) singles which we denote by $\tilde{U}$, $\tilde{D}$ and $\tilde{E}$, respectively.

The mass matrix for the up-type squarks and the down-type squarks can be written as

$$M^2_{\tilde{u}} = \begin{pmatrix} m^2_{\tilde{Q}} + m^2_Z \cos 2\beta (T^3_{u_L} - \hat{s}^2 Q_u) + m^2_u & -m_u |A^*_u + \mu \cot\beta| e^{i\phi_{\tilde{u}}} \\ -m_u |A_u + \mu^* \cot\beta| e^{-i\phi_{\tilde{u}}} & m^2_{\tilde{U}} + m^2_Z \cos 2\beta \hat{s}^2 Q_u + m^2_u \end{pmatrix} , \tag{A.1}$$

$$M^2_{\tilde{d}} = \begin{pmatrix} m^2_{\tilde{Q}} + m^2_Z \cos 2\beta (T^3_{d_L} - \hat{s}^2 Q_d) + m^2_d & -m_d |A^*_d + \mu \tan\beta| e^{i\phi_{\tilde{d}}} \\ -m_d |A_d + \mu^* \tan\beta| e^{-i\phi_{\tilde{d}}} & m^2_{\tilde{D}} + m^2_Z \cos 2\beta \hat{s}^2 Q_d + m^2_d \end{pmatrix} . \tag{A.2}$$

where $m_{\tilde{Q}}$, $m_{\tilde{U}}$ and $m_{\tilde{D}}$ are explicit SUSY-breaking masses for the doublet $\tilde{Q}$ and the singlets $\tilde{u}_R$ and $\tilde{d}_R$, respectively. The off-diagonal elements depend upon A_u, the coefficient of the trilinear SUSY-breaking term. The parameter μ is the coefficient of the quadratic Higgs term, $H_1 \cdot H_2$, in the superpotential, and $\tan\beta$ is the ratio of the vacuum expectation values for the two Higgs doublets. The the sneutrino $\tilde{\nu}$ has only a left-handed state, whose mass is given by

$$m^2_{\tilde{\nu}_L} = m^2_{\tilde{L}} + m^2_Z \cos 2\beta (T^3_{\nu_L} - \hat{s}^2 Q_\nu) . \tag{A.3}$$

The mass-matrix for the down type sleptons is

$$M^2_{\tilde{e}} = \begin{pmatrix} m^2_{\tilde{L}} + m^2_Z \cos 2\beta (T^3_{e_L} - \hat{s}^2 Q_e) + m^2_e & -m_e |A^*_e + \mu \tan\beta| e^{i\phi_{\tilde{e}}} \\ -m_e |A_e + \mu^* \tan\beta| e^{-i\phi_{\tilde{e}}} & m^2_{\tilde{E}} + m^2_Z \cos 2\beta \hat{s}^2 Q_e + m^2_e \end{pmatrix} . \tag{A.4}$$

In this paper, we refer the off diagonal elements to

$$A^{eff}_{d,e} = A^*_{d,e} + \mu \cot\beta, \quad \text{and} \quad A^{eff}_u = A^*_u + \mu \tan\beta. \tag{A.5a}$$

After diagonalizing these matrices and finding their eigenvalues, the lighter of the two is denoted as $m^2_{\tilde{f}_1}$, while the heavier is then $m^2_{\tilde{f}_2}$. The mass matrix is diagonalized according to

$$S^\dagger_{\tilde{f}} M^2_{\tilde{f}} S_{\tilde{f}} = \mathrm{diag}(m^2_{\tilde{f}_1}, m^2_{\tilde{f}_2}) \,, \tag{A.6}$$

and the physical eigenstates are given by

$$\begin{pmatrix} \tilde{f}_L \\ \tilde{f}_R \end{pmatrix} = S_{\tilde{f}} \begin{pmatrix} \tilde{f}_1 \\ \tilde{f}_2 \end{pmatrix} . \tag{A.7}$$

The mixing matrix $S_{\tilde{f}}$ may be parametrized as

$$S_{\tilde{f}} = \begin{pmatrix} \cos\theta_{\tilde{f}} & \sin\theta_{\tilde{f}} e^{i\phi_{\tilde{f}}} \\ -\sin\theta_{\tilde{f}} e^{-i\phi_{\tilde{f}}} & \cos\theta_{\tilde{f}} \end{pmatrix} , \qquad S^\dagger_{\tilde{f}} = \begin{pmatrix} \cos\theta_{\tilde{f}} & -\sin\theta_{\tilde{f}} e^{i\phi_{\tilde{f}}} \\ \sin\theta_{\tilde{f}} e^{-i\phi_{\tilde{f}}} & \cos\theta_{\tilde{f}} \end{pmatrix} , \tag{A.8}$$

where $0 \le \cos\theta_{\tilde{f}} \le 1$ and $0 \le \sin\theta_{\tilde{f}} \le 1$. Because the mass-matrices are Hermitian, the eigenvalues are real. To prevent the breaking of SU(3) color or electric charge, none of the squared masses can be negative. If the explicit SUSY-breaking mass terms are sufficiently large, then the diagonal elements are positive for all values of $\tan\beta$. The most stringent condition, $m_{\tilde{L}} > m_Z/\sqrt{2}$, comes from the requirement $m^2_{\tilde{\nu}_L} > 0$ in the large $\tan\beta$ limit. If $\tan\beta = 1$, then $\cos 2\beta = 0$ and the diagonal terms are positive even in the limit where these mass terms vanish. As for the third family the off-diagonal entries can also be large. Assuming that the diagonal elements are positive, the condition

$$(M^2_{\tilde{f}})_{11}(M^2_{\tilde{f}})_{22} > (M^2_{\tilde{f}})_{12}(M^2_{\tilde{f}})_{21} \tag{A.9}$$

must be imposed to guarantee that $m^2_{\tilde{f}_1} > 0$ and $m^2_{\tilde{f}_2} > 0$.

A.2 Sfermion–gauge-boson interactions

The interactions of one gauge boson with two sfermions are given by

$$\begin{aligned} \mathcal{L}_{V\tilde{f}\tilde{f}} = i\Big\{ g^\gamma_{\tilde{f}_i\tilde{f}_j} A^\mu + g^Z_{\tilde{f}_i\tilde{f}_j} Z^\mu \Big\} \tilde{f}^*_i \overleftrightarrow{\partial}_\mu \tilde{f}_j + i g^Z_{\tilde{\nu}_L\tilde{\nu}_L} \tilde{\nu}^*_L \overleftrightarrow{\partial}_\mu \tilde{\nu}_L Z^\mu \\ + \Big\{ i g^W_{\tilde{u}_i\tilde{d}_j} \tilde{u}^*_i \overleftrightarrow{\partial}_\mu \tilde{d}_j W^{+\mu} + \mathrm{h.c.} \Big\} + \Big\{ i g^W_{\tilde{\nu}_L\tilde{e}_i} \tilde{\nu}^*_L \overleftrightarrow{\partial}_\mu \tilde{e}_i W^{+\mu} + \mathrm{h.c.} \Big\} , \end{aligned} \tag{A.10}$$

where summation over $\tilde{f} = \tilde{u}$, $\tilde{d}$ and $\tilde{e}$ and $i, j = 1, 2$ is implied. The couplings are then given by

$$g^\gamma_{\tilde{f}_i\tilde{f}_j} = \left[S^\dagger_{\tilde{f}} \begin{pmatrix} -\hat{e}Q_f & 0 \\ 0 & -\hat{e}Q_f \end{pmatrix} S_{\tilde{f}} \right]_{ij} = \begin{pmatrix} -\hat{e}Q_f & 0 \\ 0 & -\hat{e}Q_f \end{pmatrix}_{ij} , \tag{A.11a}$$

$$\begin{aligned} g^Z_{\tilde{f}_i\tilde{f}_j} &= \left[S^\dagger_{\tilde{f}} \begin{pmatrix} -\hat{g}_Z(T^3_{f_L} - \hat{s}^2 Q_f) & 0 \\ 0 & -\hat{g}_Z(-\hat{s}^2 Q_f) \end{pmatrix} S_{\tilde{f}} \right]_{ij} \\ &= -\,\hat{g}_Z \begin{pmatrix} (T^3_{f_L}\cos^2\theta_{\tilde{f}} - \hat{s}^2 Q_f) & T^3_{f_L}\sin\theta_{\tilde{f}}\cos\theta_{\tilde{f}} e^{i\phi_{\tilde{f}}} \\ T^3_{f_L}\sin\theta_{\tilde{f}}\cos\theta_{\tilde{f}} e^{-i\phi_{\tilde{f}}} & (T^3_{f_L}\sin^2\theta_{\tilde{f}} - \hat{s}^2 Q_f) \end{pmatrix}_{ij} , \end{aligned} \tag{A.11b}$$

$$g^Z_{\tilde{\nu}_L\tilde{\nu}_L} = -\hat{g}_Z(T^3_{\nu_L} - \hat{s}^2 Q_\nu)\ , \tag{A.11c}$$

$$g^W_{\tilde{u}_i\tilde{d}_j} = \left[S^\dagger_{\tilde{u}}\begin{pmatrix} -\hat{g}/\sqrt{2} & 0 \\ 0 & 0 \end{pmatrix} S_{\tilde{d}}\right]_{ij} = -\frac{\hat{g}}{\sqrt{2}}\begin{pmatrix} \cos\theta_{\tilde{u}}\cos\theta_{\tilde{d}} & \cos\theta_{\tilde{u}}\sin\theta_{\tilde{d}}e^{i\phi_{\tilde{d}}} \\ \sin\theta_{\tilde{u}}\cos\theta_{\tilde{d}}e^{-i\phi_{\tilde{u}}} & \sin\theta_{\tilde{u}}\sin\theta_{\tilde{d}}e^{-i(\phi_{\tilde{u}}-\phi_{\tilde{d}})} \end{pmatrix}_{ij}, \tag{A.11d}$$

$$g^W_{\tilde{\nu}_L\tilde{e}_i} = \left[\begin{pmatrix} -\frac{\hat{g}}{\sqrt{2}} & 0 \end{pmatrix} S_{\tilde{e}}\right]_i = -\frac{\hat{g}}{\sqrt{2}}\begin{pmatrix} \cos\theta_{\tilde{e}} & \sin\theta_{\tilde{e}}e^{i\phi_{\tilde{e}}} \end{pmatrix}_i\ . \tag{A.11e}$$

For the $\tilde{\nu}_L$ there is no mixing. The other couplings are expressed as 2×2 matrices.

The $VV\tilde{f}\tilde{f}$ seagull-type terms are given by

$$\begin{aligned}\mathcal{L}_{VV\tilde{f}\tilde{f}} &= \tilde{f}^*_i\tilde{f}_j\Big\{g^{\gamma\gamma}_{\tilde{f}_i\tilde{f}_j}A_\mu A^\mu + g^{\gamma Z}_{\tilde{f}_i\tilde{f}_j}A_\mu Z^\mu + g^{ZZ}_{\tilde{f}_i\tilde{f}_j}Z_\mu Z^\mu + g^{WW}_{\tilde{f}_i\tilde{f}_j}W^-_\mu W^{+\,\mu}\Big\} \\ &+ g^{ZZ}_{\tilde{\nu}_L\tilde{\nu}_L}\tilde{\nu}^*_L\tilde{\nu}_L Z_\mu Z^\mu + g^{WW}_{\tilde{\nu}_L\tilde{\nu}_L}\tilde{\nu}^*_L\tilde{\nu}_L W^+_\mu W^{-\,\mu} + \Big\{\Big[g^{W\gamma}_{\tilde{u}_i\tilde{d}_j}A^\mu + g^{WZ}_{\tilde{u}_i\tilde{d}_j}Z^\mu\Big]\tilde{u}^*_i\tilde{d}_j W^+_\mu + \text{h.c.}\Big\} \\ &+ \Big\{\Big[g^{W\gamma}_{\tilde{\nu}_L\tilde{e}_i}A^\mu + g^{WZ}_{\tilde{\nu}_L\tilde{e}_i}Z^\mu\Big]\tilde{\nu}^*_L\tilde{e}_i W^+_\mu + \text{h.c.}\Big\}\ ,\end{aligned} \tag{A.12}$$

with the following couplings:

$$g^{\gamma\gamma}_{\tilde{f}_i\tilde{f}_j} = \left[S^\dagger_{\tilde{f}}\begin{pmatrix} \hat{e}^2Q_f^2 & 0 \\ 0 & \hat{e}^2Q_f^2 \end{pmatrix} S_{\tilde{f}}\right]_{ij} = \begin{pmatrix} \hat{e}^2Q_f^2 & 0 \\ 0 & \hat{e}^2Q_f^2 \end{pmatrix}_{ij}\ , \tag{A.13a}$$

$$\begin{aligned}g^{ZZ}_{\tilde{f}_i\tilde{f}_j} &= \left[S^\dagger_{\tilde{f}}\begin{pmatrix} \hat{g}_Z^2(T^3_{f_L}-\hat{s}^2Q_f)^2 & 0 \\ 0 & \hat{g}_Z^2(-\hat{s}^2Q_f)^2 \end{pmatrix} S_{\tilde{f}}\right]_{ij} \\ &= \hat{g}_Z^2\begin{pmatrix} \Big[T^3_{f_L}(T^3_{f_L}-2\hat{s}^2Q_f)\cos^2\theta_{\tilde{f}} + \hat{s}^2Q_f^2\Big] & T^3_{f_L}(T^3_{f_L}-2\hat{s}^2Q_f)\sin\theta_{\tilde{f}}\cos\theta_{\tilde{f}}e^{i\phi_{\tilde{f}}} \\ T^3_{f_L}(T^3_{f_L}-2\hat{s}^2Q_f)\sin\theta_{\tilde{f}}\cos\theta_{\tilde{f}}e^{-i\phi_{\tilde{f}}} & \Big[T^3_{f_L}(T^3_{f_L}-2\hat{s}^2Q_f)\sin^2\theta_{\tilde{f}} + \hat{s}^2Q_f^2\Big] \end{pmatrix}_{ij},\end{aligned} \tag{A.13b}$$

$$g^{ZZ}_{\tilde{\nu}_L\tilde{\nu}_L} = \hat{g}_Z^2(T^3_{\nu_L} - \hat{s}^2Q_\nu)^2\ , \tag{A.13c}$$

$$\begin{aligned}g^{\gamma Z}_{\tilde{f}_i\tilde{f}_j} &= \left[S^\dagger_{\tilde{f}}\begin{pmatrix} 2\hat{e}\hat{g}_ZQ_f(T^3_{f_L}-\hat{s}^2Q_f) & 0 \\ 0 & 2\hat{e}\hat{g}_ZQ_f(-\hat{s}^2Q_f) \end{pmatrix} S_{\tilde{f}}\right]_{ij} \\ &= 2\hat{e}\hat{g}_Z\begin{pmatrix} Q_f(T^3_{f_L}\cos^2\theta_{\tilde{f}} - \hat{s}^2Q_f) & Q_fT^3_{f_L}\sin\theta_{\tilde{f}}\cos\theta_{\tilde{f}}e^{i\phi_{\tilde{f}}} \\ Q_fT^3_{f_L}\sin\theta_{\tilde{f}}\cos\theta_{\tilde{f}}e^{-i\phi_{\tilde{f}}} & Q_f(T^3_{f_L}\sin^2\theta_{\tilde{f}} - \hat{s}^2Q_f) \end{pmatrix}_{ij}\ ,\end{aligned} \tag{A.13d}$$

$$g^{WW}_{\tilde{f}_i\tilde{f}_j} = \left[S^\dagger_{\tilde{f}}\begin{pmatrix} \hat{g}^2/2 & 0 \\ 0 & 0 \end{pmatrix} S_{\tilde{f}}\right]_{ij} = \frac{\hat{g}^2}{2}\begin{pmatrix} \cos^2\theta_{\tilde{f}} & \sin\theta_{\tilde{f}}\cos\theta_{\tilde{f}}e^{i\phi_{\tilde{f}}} \\ \sin\theta_{\tilde{f}}\cos\theta_{\tilde{f}}e^{-i\phi_{\tilde{f}}} & \sin^2\theta_{\tilde{f}} \end{pmatrix}_{ij}\ , \tag{A.13e}$$

$$g^{WW}_{\tilde{\nu}_L\tilde{\nu}_L} = \frac{1}{2}\hat{g}^2\ , \tag{A.13f}$$

$$\begin{aligned}g^{\gamma W}_{\tilde{u}_i\tilde{d}_j} &= \left[S^\dagger_{\tilde{u}}\begin{pmatrix} \hat{g}\hat{e}(Q_u+Q_d)/\sqrt{2} & 0 \\ 0 & 0 \end{pmatrix} S_{\tilde{d}}\right]_{ij} \\ &= \frac{\hat{e}\hat{g}}{\sqrt{2}}(Q_u+Q_d)\begin{pmatrix} \cos\theta_{\tilde{u}}\cos\theta_{\tilde{d}} & \cos\theta_{\tilde{u}}\sin\theta_{\tilde{d}}e^{i\phi_{\tilde{d}}} \\ \sin\theta_{\tilde{u}}\cos\theta_{\tilde{d}}e^{-i\phi_{\tilde{u}}} & \sin\theta_{\tilde{u}}\sin\theta_{\tilde{d}}e^{-i(\phi_{\tilde{u}}-\phi_{\tilde{d}})} \end{pmatrix}_{ij}\ ,\end{aligned} \tag{A.13g}$$

$$g^{\gamma W}_{\tilde{\nu}_L\tilde{e}_i} = \left[\begin{pmatrix} \frac{\hat{g}\hat{e}}{\sqrt{2}}(Q_\nu+Q_e) & 0 \end{pmatrix} S_{\tilde{e}}\right]_i = \frac{\hat{g}\hat{e}}{\sqrt{2}}(Q_\nu+Q_e)\begin{pmatrix} \cos\theta_{\tilde{e}} & \sin\theta_{\tilde{e}}e^{i\phi_{\tilde{e}}} \end{pmatrix}_i\ , \tag{A.13h}$$

$$g^{ZW}_{\tilde{u}_i\tilde{d}_j} = \left[S^\dagger_{\tilde{u}}\begin{pmatrix} -\hat{g}\hat{g}_Z\hat{s}^2(Q_u+Q_d)/\sqrt{2} & 0 \\ 0 & 0 \end{pmatrix} S_{\tilde{d}}\right]_{ij}$$

$$= -\frac{\hat{g}\hat{g}_Z\hat{s}^2}{\sqrt{2}}(Q_u + Q_d)\begin{pmatrix} \cos\theta_{\tilde{u}}\cos\theta_{\tilde{d}} & \cos\theta_{\tilde{u}}\sin\theta_{\tilde{d}}e^{i\phi_{\tilde{d}}} \\ \sin\theta_{\tilde{u}}\cos\theta_{\tilde{d}}e^{-i\phi_{\tilde{u}}} & \sin\theta_{\tilde{u}}\sin\theta_{\tilde{d}}e^{-i(\phi_{\tilde{u}}-\phi_{\tilde{d}})} \end{pmatrix}_{ij} , \tag{A.13i}$$

$$g^{ZW}_{\tilde{\nu}_L\tilde{e}_i} = \left[\left(-\frac{\hat{g}\hat{g}_Z\hat{s}^2}{\sqrt{2}}(Q_\nu + Q_e)\ \ 0\right) S_{\tilde{e}}\right]_i = -\frac{\hat{g}\hat{g}_Z\hat{s}^2}{\sqrt{2}}(Q_\nu + Q_e)\left(\cos\theta_{\tilde{e}}\ \ \sin\theta_{\tilde{e}}e^{i\phi_{\tilde{e}}}\right)_i . \tag{A.13j}$$

A.3 Sfermion–Goldstone-boson interactions

We present only the portion of the Lagrangian which contains the interactions between one charged Goldstone boson and two scalar fermions:

$$\mathcal{L}_{\chi\tilde{f}\tilde{f}} = \left\{ig^{\chi}_{\tilde{u}_i\tilde{d}_j}\tilde{u}^*_i\tilde{d}_j\chi^+ + \text{h.c.}\right\} + \left\{ig^{\chi}_{\tilde{\nu}_L\tilde{e}_i}\tilde{\nu}^*_L\tilde{e}_i\chi^+ + \text{h.c.}\right\} , \tag{A.14}$$

where summation over $i, j = 1, 2$ is implied, and the couplings are given by

$$g^{\chi}_{\tilde{u}_i\tilde{d}_j} = \left[\frac{\hat{g}}{\sqrt{2}\hat{m}^2_W}S^\dagger_{\tilde{u}}\begin{pmatrix} m^2_W\cos 2\beta + m^2_u - m^2_d & m_d\left|A^*_d + \mu\tan\beta\right|e^{i\phi_{\tilde{d}}} \\ -m_u\left|A_u + \mu^*\cot\beta\right|e^{-i\phi_{\tilde{u}}} & 0 \end{pmatrix} S_{\tilde{d}}\right]_{ij} , \tag{A.15a}$$

$$g^{\chi}_{\tilde{\nu}_L\tilde{e}_i} = \left[\frac{\hat{g}}{\sqrt{2}\hat{m}^2_W}\left(\ m^2_W\cos 2\beta - m^2_e\quad m_e\left|A^*_e + \mu\tan\beta\right|e^{i\phi_{\tilde{e}}}\ \right) S_{\tilde{e}}\right]_i . \tag{A.15b}$$

The overall phase factors for $g^{\chi}_{\tilde{u}_i\tilde{d}_j}$ exactly parallel the phase factors for $g^{W}_{\tilde{u}_i\tilde{d}_j}$ reflected in Eq. (A.11d), while the overall phase factors for $g^{\chi}_{\tilde{\nu}_L\tilde{e}_i}$ mimic those of $g^{W}_{\tilde{\nu}_L\tilde{e}_i}$ in Eq. (A.11e).

B Sfermion effects on the form factors

B.1 Two-point functions

For the photon propagator,

$$\Pi^{\gamma\gamma}_T(q^2) = \frac{\hat{e}^2}{16\pi^2}\sum_{\substack{\tilde{f}=\tilde{u},\tilde{d},\tilde{e}\\ i=1,2}} N^f_c Q^2_f B_5(q^2; m_{\tilde{f}_i}, m_{\tilde{f}_i}) . \tag{B.1}$$

where $N^f_c = 3$ for squarks and $N^f_c = 1$ for sleptons. The function $B_5(q^2; m_1, m_2)$[32] on RHS is related to the familiar notation of Ref. [41] by

$$B_5(q^2; m_1, m_2) = A(m_1) + A(m_2) - 4B_{22}(q^2; m_1, m_2) . \tag{B.2}$$

For the γZ, ZZ and WW two-point functions, we obtain

$$\Pi^{\gamma Z}_T(q^2) = \frac{\hat{e}\hat{g}_Z}{16\pi^2}\sum_{\tilde{f}=\tilde{u},\tilde{d},\tilde{e}} N^f_c Q_f\Big\{(T^3_{f_L}\cos^2\theta_{\tilde{f}} - \hat{s}^2 Q_f)B_5(q^2; m_{\tilde{f}_1}, m_{\tilde{f}_1})$$
$$+(T^3_{f_L}\sin^2\theta_{\tilde{f}} - \hat{s}^2 Q_f)B_5(q^2; m_{\tilde{f}_2}, m_{\tilde{f}_2})\Big\} , \tag{B.3}$$

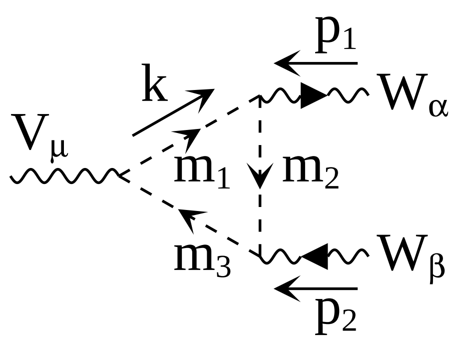

Figure 18: Mass and momentum assignments for the calculation of the sfermion triangle graph are shown. The arrows in the W lines indicate the flow of a negative electric charge.

$$\Pi_T^{ZZ}(q^2) = \frac{\hat{g}_Z^2}{16\pi^2} \sum_{\tilde{f}=\tilde{u},\tilde{d},\tilde{e}} N_c^f \Big\{ (T^3_{f_L}\cos^2\theta_{\tilde{f}} - \hat{s}^2 Q_f)^2 B_5(q^2; m_{\tilde{f}_1}, m_{\tilde{f}_1}) + (T^3_{f_L}\sin^2\theta_{\tilde{f}} - \hat{s}^2 Q_f)^2 B_5(q^2; m_{\tilde{f}_2}, m_{\tilde{f}_2})$$

$$+2(T^3_{f_L}\sin\theta_{\tilde{f}}\cos\theta_{\tilde{f}})^2 B_5(q^2; m_{\tilde{f}_1}, m_{\tilde{f}_2}) \Big\} + \frac{\hat{g}_Z^2}{16\pi^2}(T^3_{\nu_L} - \hat{s}^2 Q_\nu)^2 B_5(q^2; m_{\tilde{\nu}_L}, m_{\tilde{\nu}_L}) \ , \tag{B.4}$$

$$\Pi_T^{WW}(q^2) = \frac{\hat{g}^2/2}{16\pi^2} \Big\{ 3\cos^2\theta_{\tilde{u}}\cos^2\theta_{\tilde{d}} B_5(q^2; m_{\tilde{u}_1}, m_{\tilde{d}_1}) + 3\cos^2\theta_{\tilde{u}}\sin^2\theta_{\tilde{d}} B_5(q^2; m_{\tilde{u}_1}, m_{\tilde{d}_2}) \tag{B.5}$$

$$+ 3\sin^2\theta_{\tilde{u}}\cos^2\theta_{\tilde{d}} B_5(q^2; m_{\tilde{u}_2}, m_{\tilde{d}_1}) + 3\sin^2\theta_{\tilde{u}}\sin^2\theta_{\tilde{d}} B_5(q^2; m_{\tilde{u}_2}, m_{\tilde{d}_2})$$

$$+ \cos^2\theta_{\tilde{e}} B_5(q^2; m_{\tilde{\nu}_L}, m_{\tilde{e}_1}) + \sin^2\theta_{\tilde{e}} B_5(q^2; m_{\tilde{\nu}_L}, m_{\tilde{e}_2}) \Big\} \ . \tag{B.6}$$

The one-loop sfermion contribution to the wavefunction renormalization factor of the physical W boson is given by

$$Z_W^{\frac{1}{2}} = 1 - \frac{1}{2}\,\frac{d}{dq^2}\,\Pi_T^{WW}(q^2)\bigg|_{q^2=m_W^2} \ , \ \text{and} \ \ \delta Z_W^{\frac{1}{2}} = Z_W^{\frac{1}{2}} - 1 \ . \tag{B.7}$$

B.2 Sfermion contributions to the $e^-e^+ \to W^-W^+$

Here we show the calcuration for the form factor coefficients $f_i^{V(1)}$ $(V=\gamma, Z)$ in Sec. 4.2. First, the triangle graphs are depicted in Fig. 19. Mass and momentum assignments are as in Fig. 18. For the evaluation of the loop integrals it is convenient to have the momenta incoming, hence we use $p_1 = -p$ and $p_2 = -\overline{p}$ where p and $\overline{p}$ were defined in Fig. 1. We obtain for the γWW vertex,

$$f_i^{\gamma\,(1)\,\mathrm{SFT}} = -\frac{1}{16\pi^2\hat{e}} \Big\{ 3g^\gamma_{\tilde{u}_i\tilde{u}_i} \Big| g^W_{\tilde{u}_i\tilde{d}_j} \Big|^2 C_i^{\mathrm{SF}}(p_1, p_2, m^2_{\tilde{u}_i}, m^2_{\tilde{d}_j}, m^2_{\tilde{u}_i})$$

$$- 3g^\gamma_{\tilde{d}_i\tilde{d}_i} \Big| g^W_{\tilde{u}_j\tilde{d}_i} \Big|^2 C_i^{\mathrm{SF}}(p_1, p_2, m^2_{\tilde{d}_i}, m^2_{\tilde{u}_j}, m^2_{\tilde{d}_i}) - g^\gamma_{\tilde{e}_i\tilde{e}_i} \Big| g^W_{\tilde{\nu}_L\tilde{e}_i} \Big|^2 C_i^{\mathrm{SF}}(p_1, p_2, m^2_{\tilde{e}_i}, m^2_{\tilde{\nu}_L}, m^2_{\tilde{e}_i}) \Big\} \ , \tag{B.8}$$

where summation over $i, j = 1, 2$ is implied, and the loop-integral coefficients C_i^{SF} are defined in Ref. [20]. The photon couplings are real and the complex phases cancel between the two W-boson

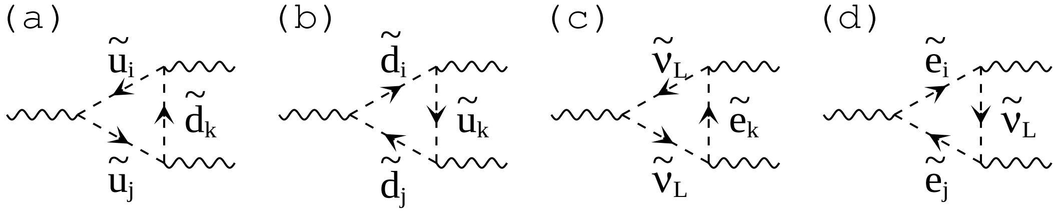

Figure 19: Feynman graphs contributing to the VWW vertex are shown. The mass and momentum assignments are shown in Fig. 18. When $V = Z$, all graphs contribute. In case of $V = \gamma$, graphs (c) do not contribute, and only $i = j$ is allowed.

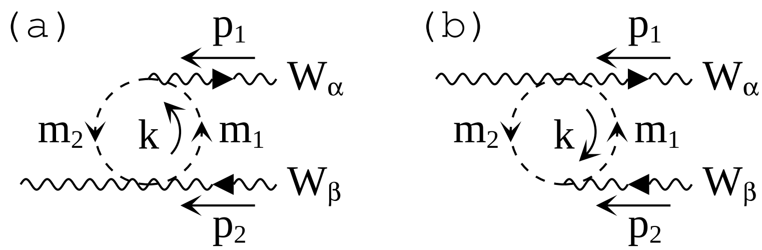

Figure 20: Mass and momentum assignments for the calculation of the sfermion graphs containing seagull coupling are shown. The arrows in the W lines indicate the flow of a negative electric charge.

vertices. For the ZWW vertex,

$$
\begin{aligned}
f_i^{Z\,(1)\,\mathrm{SFT}} &= -\frac{1}{16\pi^2 \hat{g}_Z \hat{c}^2}\Big\{ \\
&3 g^Z_{\tilde{u}_k\tilde{u}_i} g^W_{\tilde{u}_i\tilde{d}_j}\left(g^W_{\tilde{u}_k\tilde{d}_j}\right)^* C_i^{\mathrm{SF}}(p_1,p_2,m^2_{\tilde{u}_i},m^2_{\tilde{d}_j},m^2_{\tilde{u}_k}) - 3 g^Z_{\tilde{d}_i\tilde{d}_k} g^W_{\tilde{u}_j\tilde{d}_i}\left(g^W_{\tilde{u}_j\tilde{d}_k}\right)^* C_i^{\mathrm{SF}}(p_1,p_2,m^2_{\tilde{d}_i},m^2_{\tilde{u}_j},m^2_{\tilde{d}_k}) \\
&+ g^Z_{\tilde{\nu}_L\tilde{\nu}_L}\left|g^W_{\tilde{\nu}_L\tilde{e}_k}\right|^2 C_i^{\mathrm{SF}}(p_1,p_2,m^2_{\tilde{\nu}_L},m^2_{\tilde{e}_k},m^2_{\tilde{\nu}_L}) - g^Z_{\tilde{e}_i\tilde{e}_k} g^W_{\tilde{\nu}_L\tilde{e}_i}\left(g^W_{\tilde{\nu}_L\tilde{e}_k}\right)^* C_i^{\mathrm{SF}}(p_1,p_2,m^2_{\tilde{e}_i},m^2_{\tilde{\nu}_L},m^2_{\tilde{e}_k})\Big\}, \quad \text{(B.9)}
\end{aligned}
$$

where summation over $i, j, k = 1, 2$ is implied. The complex phases cancel between the three coupling factors. The superscript 'SFT' is chosen to denote 'sfermion triangle' contributions.

The second category of vertex corrections are depicted in Fig. 21. We use the momentum assignments of Fig. 20. The results for the γWW vertex and for ZWW are summarized as

$$
\begin{aligned}
f_{10}^{\gamma\,(1)\,\mathrm{SFSG}} &= \frac{1}{16\pi^2 \hat{e}}\Big\{3\left(g^{\gamma W}_{\tilde{u}_i\tilde{d}_j}\right)^* g^W_{\tilde{u}_i\tilde{d}_j}(2B_1+B_0)(m_W^2; m_{\tilde{d}_j}, m_{\tilde{u}_i}) \\
&\qquad + \left(g^{\gamma W}_{\tilde{\nu}_L\tilde{e}_j}\right)^* g^W_{\tilde{\nu}_L\tilde{e}_j}(2B_1+B_0)(m_W^2; m_{\tilde{e}_j}, m_{\tilde{\nu}_L})\Big\}, && \text{(B.10a)} \\
f_{13}^{\gamma\,(1)\,\mathrm{SFSG}} &= -f_{10}^{\gamma\,(1)\,\mathrm{SFSG}}, && \text{(B.10b)} \\
f_{10}^{Z\,(1)\,\mathrm{SFSG}} &= \frac{1}{16\pi^2 \hat{g}_Z \hat{c}^2}\Big\{3\left(g^{ZW}_{\tilde{u}_i\tilde{d}_j}\right)^* g^W_{\tilde{u}_i\tilde{d}_j}(2B_1+B_0)(m_W^2; m_{\tilde{d}_j}, m_{\tilde{u}_i}) \\
&\qquad + \left(g^{ZW}_{\tilde{\nu}_L\tilde{e}_j}\right)^* g^W_{\tilde{\nu}_L\tilde{e}_j}(2B_1+B_0)(m_W^2; m_{\tilde{e}_j}, m_{\tilde{\nu}_L})\Big\}, && \text{(B.10c)}
\end{aligned}
$$

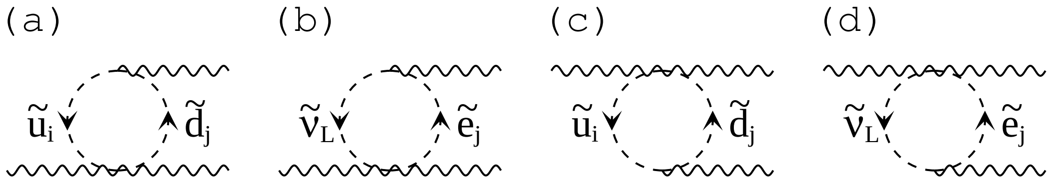

Figure 21: Feynman graphs containing seagull coupling and contributing to the γWW and ZWW vertex are shown. The mass and momentum assignments are shown in Fig. 20.

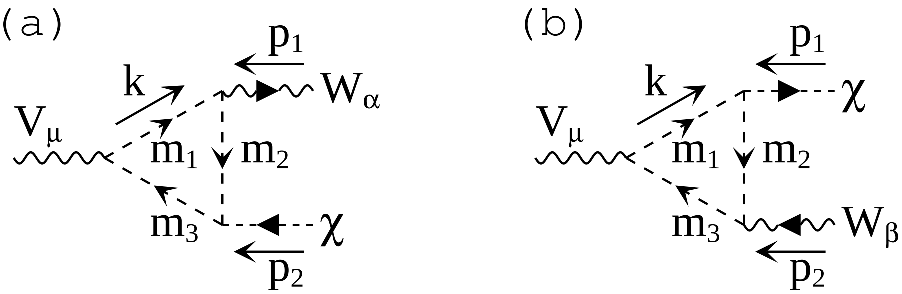

Figure 22: Mass and momentum assignments for the calculation of the sfermion triangle graphs contributing to the $VW^{\mp}\chi^{\pm}$ vertices. The arrows in the W and χ indicate the flow of a negative electric charge.

$$f_{13}^{Z\,(1)\,\mathrm{SFSG}} = -f_{10}^{Z\,(1)\,\mathrm{SFSG}}\,, \tag{B.10d}$$

where superscript 'SFSG' represents 'sfermion seagull-graph' contributions. As is clear from the above expressions, the W bosons are chosen to be on mass shell such that $p_1^2 = p_2^2 = m_W^2$.

C Sfermion effects on the $W^{\mp}\chi^{\pm}$ and $\chi^-\chi^+$ production

C.1 $e^-e^+ \to W^{\mp}\chi^{\pm}$

The one-loop level vertex coefficients $\overset{(-)}{h}{}_i^{\gamma\,(1)}$ and $\overset{(-)}{h}{}_i^{Z\,(1)}$ receive contributions from the triangle graphs in Fig. 23 and the seagull-type vertices as depicted in Fig. 25. We begin with the calculation of the triangle graphs with internal mass and momentum assignments as in Fig. 22. We obtain

$$\begin{aligned}
h_i^{\gamma\,(1)\,\mathrm{SFT}} &= -\frac{1}{16\pi^2\hat{e}}\Big\{ g^{\gamma}_{\tilde{u}_j\tilde{u}_j} g^{W}_{\tilde{u}_j\tilde{d}_k}\left(g^{\chi}_{\tilde{u}_j\tilde{d}_k}\right)^* c_i^{\mathrm{SF}}(p_1,p_2,m^2_{\tilde{u}_j},m^2_{\tilde{d}_k},m^2_{\tilde{u}_j}) \\
&+ g^{\gamma}_{\tilde{d}_j\tilde{d}_j} g^{W}_{\tilde{u}_k\tilde{d}_j}\left(g^{\chi}_{\tilde{u}_k\tilde{d}_j}\right)^* c_i^{\mathrm{SF}}(p_1,p_2,m^2_{\tilde{d}_j},m^2_{\tilde{u}_k},m^2_{\tilde{d}_j}) + g^{\gamma}_{\tilde{e}_j\tilde{e}_j} g^{W}_{\tilde{\nu}_L\tilde{e}_j}\left(g^{\chi}_{\tilde{\nu}_L\tilde{e}_j}\right)^* c_i^{\mathrm{SF}}(p_1,p_2,m^2_{\tilde{e}_j},m^2_{\tilde{\nu}_L},m^2_{\tilde{e}_j})\Big\}\,,
\end{aligned} \tag{C.1a}$$

$$\begin{aligned}
\overline{h}_i^{\gamma\,(1)\,\mathrm{SFT}} &= \frac{1}{16\pi^2\hat{e}}\Big\{ g^{\gamma}_{\tilde{u}_j\tilde{u}_j}\left(g^{W}_{\tilde{u}_j\tilde{d}_k}\right)^* g^{\chi}_{\tilde{u}_j\tilde{d}_k}\,\overline{c}_i^{\mathrm{SF}}(p_2,p_1,m^2_{\tilde{u}_j},m^2_{\tilde{d}_k},m^2_{\tilde{u}_j}) \\
&+ g^{\gamma}_{\tilde{d}_j\tilde{d}_j}\left(g^{W}_{\tilde{u}_k\tilde{d}_j}\right)^* g^{\chi}_{\tilde{u}_k\tilde{d}_j}\,\overline{c}_i^{\mathrm{SF}}(p_2,p_1,m^2_{\tilde{d}_j},m^2_{\tilde{u}_k},m^2_{\tilde{d}_j}) + g^{\gamma}_{\tilde{e}_j\tilde{e}_j}\left(g^{W}_{\tilde{\nu}_L\tilde{e}_j}\right)^* g^{\chi}_{\tilde{\nu}_L\tilde{e}_j}\,\overline{c}_i^{\mathrm{SF}}(p_2,p_1,m^2_{\tilde{e}_j},m^2_{\tilde{\nu}_L},m^2_{\tilde{e}_j})\Big\}\,,
\end{aligned} \tag{C.1b}$$

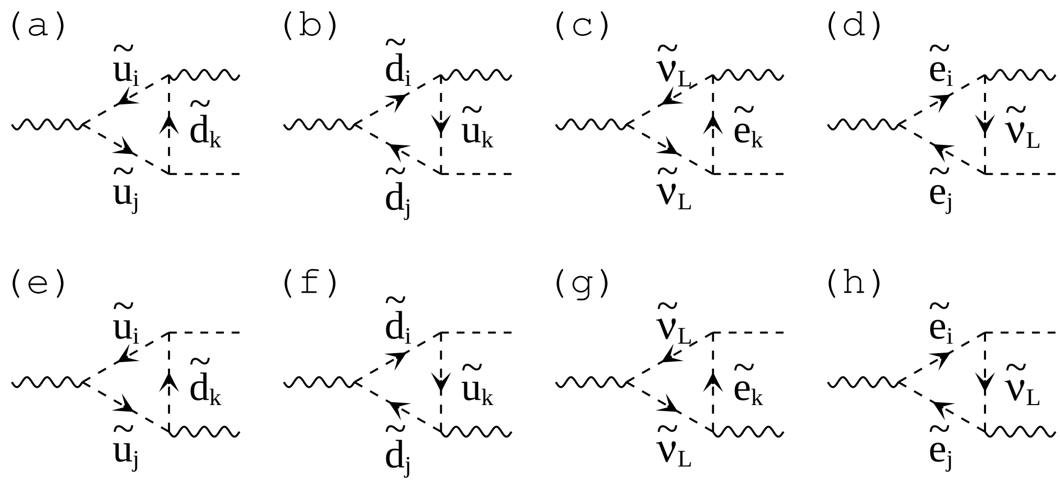

Figure 23: Feynman graphs contributing to the $VW^{\mp}\chi^{\pm}$ vertex are shown. The mass and momentum assignments are shown in Fig. 22. Feynman graphs (a)-(d) contribute to the $VW^{+}\chi^{-}$ vertex while graphs (e)-(h) contribute to the $VW^{-}\chi^{+}$ vertex. When $V = Z$, all graphs contribute. In case of $V = \gamma$, graphs (c) and (g) do not contribute, and only $i = j$ is allowed.

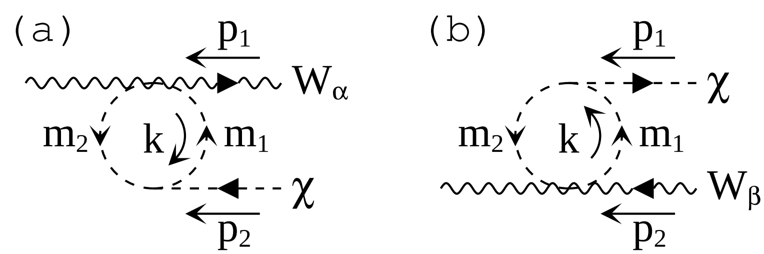

Figure 24: Mass and momentum assignments for the graphs containing seagull coupling and contributing to the $\gamma W^{\mp}\chi^{\pm}$ and $ZW^{\mp}\chi^{\pm}$ vertex are shown. The arrows in the W and χ indicate the flow of a negative electric charge.

with summation over $j, k = 1, 2$, and

$$
\begin{aligned}
h_i^{Z\,(1)\,\mathrm{SFT}} &= -\frac{1}{16\pi^2 \hat{g}_Z \hat{s}^2}\Big\{ \\
& g^Z_{\tilde{u}_j\tilde{u}_l} g^W_{\tilde{u}_j\tilde{d}_k}\left(g^\chi_{\tilde{u}_L\tilde{d}_k}\right)^* c_i^{\mathrm{SF}}(p_1, p_2, m^2_{\tilde{u}_j}, m^2_{\tilde{d}_k}, m^2_{\tilde{u}_l}) + g^Z_{\tilde{d}_j\tilde{d}_l} g^W_{\tilde{u}_k\tilde{d}_j}\left(g^\chi_{\tilde{u}_k\tilde{d}_l}\right)^* c_i^{\mathrm{SF}}(p_1, p_2, m^2_{\tilde{d}_j}, m^2_{\tilde{u}_k}, m^2_{\tilde{d}_l}) \\
&+ g^Z_{\tilde{\nu}_L\tilde{\nu}_L} g^W_{\tilde{\nu}_L\tilde{e}_k}\left(g^\chi_{\tilde{\nu}_L\tilde{e}_k}\right)^* c_i^{\mathrm{SF}}(p_1, p_2, m^2_{\tilde{\nu}_L}, m^2_{\tilde{e}_k}, m^2_{\tilde{\nu}_L}) + g^Z_{\tilde{e}_j\tilde{e}_l} g^W_{\tilde{\nu}_L\tilde{e}_j}\left(g^\chi_{\tilde{\nu}_L\tilde{e}_l}\right)^* c_i^{\mathrm{SF}}(p_1, p_2, m^2_{\tilde{e}_j}, m^2_{\tilde{\nu}_L}, m^2_{\tilde{e}_l})\Big\}\ , \qquad \text{(C.1c)} \\
\overline{h}_i^{Z\,(1)\,\mathrm{SFT}} &= \frac{1}{16\pi^2 \hat{g}_Z \hat{s}^2}\Big\{ \\
& g^Z_{\tilde{u}_j\tilde{u}_l}\left(g^W_{\tilde{u}_j\tilde{d}_k}\right)^* g^\chi_{\tilde{u}_L\tilde{d}_k} \overline{c}_i^{\mathrm{SF}}(p_2, p_1, m^2_{\tilde{u}_j}, m^2_{\tilde{d}_k}, m^2_{\tilde{u}_l}) + g^Z_{\tilde{d}_j\tilde{d}_l}\left(g^W_{\tilde{u}_k\tilde{d}_j}\right)^* g^\chi_{\tilde{u}_k\tilde{d}_l} \overline{c}_i^{\mathrm{SF}}(p_2, p_1, m^2_{\tilde{d}_j}, m^2_{\tilde{u}_k}, m^2_{\tilde{d}_l})
\end{aligned}
$$

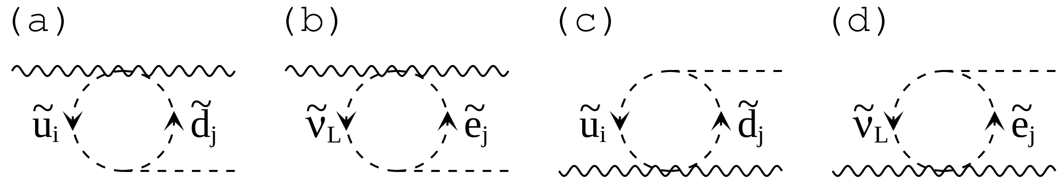

Figure 25: Feynman graphs containing seagull coupling and contributing to the $VW^{\mp}\chi^{\pm}$ vertex are shown. The mass and momentum assignments are shown in Fig. 24. Feynman graphs (a) and (b) contribute to the $VW^{+}\chi^{-}$ vertex while graphs (c) and (d) contribute to the $VW^{-}\chi^{+}$ vertex.

$$+\, g^{Z}_{\tilde{\nu}_L\tilde{\nu}_L}\left(g^{W}_{\tilde{\nu}_L\tilde{e}_k}\right)^{*} g^{\chi}_{\tilde{\nu}_L\tilde{e}_k}\overline{c}_i^{\rm SF}(p_2,p_1,m^2_{\tilde{\nu}_L},m^2_{\tilde{e}_k},m^2_{\tilde{\nu}_L}) + g^{Z}_{\tilde{e}_j\tilde{e}_l}\left(g^{W}_{\tilde{\nu}_L\tilde{e}_j}\right)^{*} g^{\chi}_{\tilde{\nu}_L\tilde{e}_l}\overline{c}_i^{\rm SF}(p_2,p_1,m^2_{\tilde{e}_j},m^2_{\tilde{\nu}_L},m^2_{\tilde{e}_l})\Big\}\,, \quad \text{(C.1d)}$$

where $j,k,l = 1,2$, and the loop-integral factors $c_i^{\rm SF}$ and $\overline{c}_i^{\rm SF}$ are defined in Ref. [20]. Next, using the assignments of Fig. 24, we calculate the contributions of the graphs in Fig. 25 with the following results:

$$h_1^{\gamma\,(1)\,\rm SFSG} = \frac{1}{16\pi^2 m_W \hat{e}}\Big\{\left(g^{\gamma W}_{\tilde{u}_j\tilde{d}_i}\right)^{*} g^{\chi}_{\tilde{u}_j\tilde{d}_i} B_0(m_W^2; m_{\tilde{d}_i}, m_{\tilde{u}_j}) + \left(g^{\gamma W}_{\tilde{\nu}_L\tilde{e}_i}\right)^{*} g^{\chi}_{\tilde{\nu}_L\tilde{e}_i} B_0(m_W^2; m_{\tilde{e}_i}, m_{\tilde{\nu}_L})\Big\}\,, \quad \text{(C.2a)}$$

$$\overline{h}_1^{\gamma\,(1)\,\rm SFSG} = -h_1^{\gamma\,(1)\,\rm SFSG}\,, \quad \text{(C.2b)}$$

$$h_1^{Z\,(1)\,\rm SFSG} = \frac{1}{16\pi^2 m_W \hat{g}_Z \hat{s}^2}\Big\{\left(g^{ZW}_{\tilde{u}_j\tilde{d}_i}\right)^{*} g^{\chi}_{\tilde{u}_j\tilde{d}_i} B_0(m_W^2; m_{\tilde{d}_i}, m_{\tilde{u}_j}) + \left(g^{ZW}_{\tilde{\nu}_L\tilde{e}_i}\right)^{*} g^{\chi}_{\tilde{\nu}_L\tilde{e}_i} B_0(m_W^2; m_{\tilde{e}_i}, m_{\tilde{\nu}_L})\Big\}, \quad \text{(C.2c)}$$

$$\overline{h}_1^{Z\,(1)\,\rm SFSG} = -h_1^{Z\,(1)\,\rm SFSG}\,, \quad \text{(C.2d)}$$

with $i,j = 1,2$. As mentioned in the previous section, our BRS sum rules effectively test the form factors except for the wavefunction renormalization corrections, so we write

$$\overset{(-)}{h}{}_i^{V\,(1)}(s) = \overset{(-)}{h}{}_i^{V\,(1)\,\rm SFT}(s) + \overset{(-)}{h}{}_i^{V\,(1)\,\rm SFSG}(s)\,. \quad \text{(C.3)}$$

C.2 $e^-e^+ \to \chi^-\chi^+$

The vertex corrections for $V\chi^-\chi^+$ ($V=\gamma$, Z) are rather simple; by taking into account the electron current conservation, we see that the sfermion sector contribute to the triangle type diagrams. The sfermion effects on the VW^-W^+ form factor coefficients are calculated as

$$\begin{aligned}
r^{\gamma(1)} = \frac{1}{16\pi^2\hat{e}}\Big\{ & 3g^{\gamma}_{\tilde{u}_i\tilde{u}_i} g^{\chi}_{\tilde{u}_i\tilde{d}_j}\left(g^{\chi}_{\tilde{u}_i\tilde{d}_j}\right)^{*}(C_{12}-C_{11})(p_1^2,p_2^2,s;m_{\tilde{u}_i},m_{\tilde{d}_j},m_{\tilde{u}_i}) \\
& -3g^{\gamma}_{\tilde{d}_i\tilde{d}_i} g^{\chi}_{\tilde{d}_i\tilde{u}_j}\left(g^{\chi}_{\tilde{d}_i\tilde{u}_j}\right)^{*}(C_{12}-C_{11})(p_1^2,p_2^2,s;m_{\tilde{d}_i},m_{\tilde{u}_j},m_{\tilde{d}_i}) \\
& -g^{\gamma}_{\tilde{e}_i\tilde{e}_i} g^{\chi}_{\tilde{e}_i\tilde{\nu}_L}\left(g^{\chi}_{\tilde{e}_i\tilde{\nu}_L}\right)^{*}(C_{12}-C_{11})(p_1^2,p_2^2,s;m_{\tilde{e}_i},m_{\tilde{\nu}_L},m_{\tilde{e}_i})\Big\}\,, \qquad \text{(C.4)} \\
r^{Z(1)} = \frac{1}{16\pi^2\hat{g}_Z}\Big\{ & 3g^{\gamma}_{\tilde{u}_k\tilde{u}_i} g^{\chi}_{\tilde{u}_i\tilde{d}_j}\left(g^{\chi}_{\tilde{u}_i\tilde{d}_k}\right)^{*}(C_{12}-C_{11})(p_1^2,p_2^2,s;m_{\tilde{u}_i},m_{\tilde{d}_j},m_{\tilde{u}_k}) \\
& -3g^{\gamma}_{\tilde{d}_k\tilde{d}_i} g^{\chi}_{\tilde{d}_i\tilde{u}_j}\left(g^{\chi}_{\tilde{d}_i\tilde{u}_k}\right)^{*}(C_{12}-C_{11})(p_1^2,p_2^2,s;m_{\tilde{d}_i},m_{\tilde{u}_j},m_{\tilde{d}_k})
\end{aligned}$$

$$+g^{\gamma}_{\tilde{\nu}_L\tilde{\nu}_L} g^{\chi}_{\tilde{\nu}_L\tilde{e}_i} \left(g^{\chi}_{\tilde{\nu}_L\tilde{e}_i}\right)^* (C_{12} - C_{11})\,(p_1^2, p_2^2, s; m_{\tilde{\nu}_L}, m_{\tilde{e}_i}, m_{\tilde{\nu}_L})$$
$$-g^{\gamma}_{\tilde{e}_i\tilde{e}_i} g^{\chi}_{\tilde{e}_i\tilde{\nu}_L} \left(g^{\chi}_{\tilde{e}_i\tilde{\nu}_L}\right)^* (C_{12} - C_{11})\,(p_1^2, p_2^2, s; m_{\tilde{e}_i}, m_{\tilde{\nu}_L}, m_{\tilde{e}_i})\Big\}\,, \tag{C.5}$$

where summation for $i, j, k = 1, 2$ is taken. The tensor coefficient functions C_{ij} follow the notation in Ref [32].

D The analytic formulas of the integral functions

We present convenient analytic formulas of the integral functions in the low- and high- energy limit. The formulas for the Passarino and Veltman's A, B_0 and C_0 functions[41] are given in the $\overline{\mathrm{MS}}$ scheme in the notation in Ref [32].

D.1 The low energy limit (heavy mass limit)

The A function does not depend on the momentum,

$$A(m) = m^2 \left(1 - \ln \frac{m^2}{\mu^2}\right). \tag{D.1}$$

The B_0 function and its first and second derivative are given for $m_1^2, m_2^2 \gg q^2$ ($m_1 \neq m_2$) by

$$B_0(q^2; m_1, m_2) = 1 - \frac{m_1^2}{m_1^2 - m_2^2} \ln \frac{m_1^2}{\mu^2} + \frac{m_2^2}{m_1^2 - m_2^2} \ln \frac{m_2^2}{\mu^2} + \mathcal{O}\left(\frac{m_i^2}{q^2}\right), \tag{D.2}$$
$$B_0'(q^2; m_1, m_2) = \frac{1}{(m_1^2 - m_2^2)^2} \left\{\frac{1}{2}(m_1^2 + m_2^2) - \frac{m_1^2 m_2^2}{m_1^2 - m_2^2} \ln \frac{m_1^2}{m_2^2}\right\} + \mathcal{O}\left(\frac{m_i^2}{q^4}\right), \tag{D.3}$$
$$B_0''(q^2; m_1, m_2) = \frac{1}{(m_1^2 - m_2^2)^2} \left\{\frac{1}{3} + 4\frac{m_1^2 m_2^2}{(m_1^2 - m_2^2)^2} - 2\frac{m_1^2 m_2^2 (m_1^2 + m_2^2)}{(m_1^2 - m_2^2)^3} \ln \frac{m_1^2}{m_2^2}\right\} + \mathcal{O}\left(\frac{m_i^2}{q^6}\right), \tag{D.4}$$

where m_i symbolizes m_1 or m_2. For the case of ($m_1 = m_2 = m$), the above expressions become

$$B_0(q^2; m, m) = -\ln \frac{m^2}{\mu^2} + \mathcal{O}\left(\frac{m^2}{q^2}\right), \tag{D.5}$$
$$B_0'(q^2; m, m) = \frac{1}{6}\frac{1}{m^2} + \mathcal{O}\left(\frac{m^2}{q^4}\right), \tag{D.6}$$
$$B_0''(q^2; m, m) = \frac{1}{30}\frac{1}{m^4} + \mathcal{O}\left(\frac{m^2}{q^6}\right). \tag{D.7}$$

The expressions of the C_0 function and its derivative are given for $p_1^2, p_2^2, q^2 = (p_1 + p_2)^2 \ll m_1^2, m_2^2, m_3^2$ by

$$C_0[123] = \frac{-1}{m_1^2 - m_3^2} \left\{\frac{1}{m_1^2 - m_2^2}(m_1^2 \ln m_1^2 - m_2^2 \ln m_2^2) - \frac{1}{m_3^2 - m_2^2}(m_3^2 \ln m_3^2 - m_2^2 \ln m_2^2)\right\} + \mathcal{O}\left(\frac{m_i^2}{q^4}\right),$$

$$\tag{D.8}$$

$$C_0'[123] = \frac{1}{(m_1^2-m_3^2)^2}\left\{1+\frac{m_2^2}{2}\frac{m_1^2+m_3^2-2m_2^2}{(m_1^2-m_2^2)(m_3^2-m_2^2)}-\frac{1}{2}\frac{m_1^2+m_3^2+2m_2^2}{m_1^2-m_3^2}\ln\frac{m_1^2}{m_3^2}\right.$$
$$\left.+\frac{1}{2}\frac{m_3^2-3m_1^2+2m_2^2}{m_1^2-m_3^2}\left(\frac{m_2^2}{m_1^2-m_2^2}\right)^2\ln\frac{m_1^2}{m_2^2}-\frac{1}{2}\frac{m_1^2-3m_3^2+2m_2^2}{m_1^2-m_3^2}\left(\frac{m_2^2}{m_3^2-m_2^2}\right)^2\ln\frac{m_3^2}{m_2^2}\right\}+\mathcal{O}\left(\frac{m_i^2}{q^6}\right), \tag{D.9}$$

where $C_0(p_1,p_2,q^2;m_i,m_j,m_k)$ is written as $C_0[ijk]$ shortly and m_i symbolizes m_1 or m_2. The formulas for $m_1^2=m_3^2$ are given by

$$C_0[121] = \frac{-1}{m_1^2-m_2^2}\left\{1-\frac{m_2^2}{m_1^2-m_2^2}\ln\frac{m_1^2}{m_2^2}\right\}+\mathcal{O}\left(\frac{m_i^2}{q^4}\right), \tag{D.10}$$

$$C_0'[121] = \frac{1}{m_1^4}\left\{-\frac{1}{12}\frac{m_1^6}{(m_1^2-m_2^2)^3}+\frac{5}{12}\frac{m_1^4m_2^2}{(m_1^2-m_2^2)^3}+\frac{1}{6}\frac{m_1^2m_2^4}{(m_1^2-m_2^2)^3}-\frac{1}{2}\frac{m_1^4m_2^4}{(m_1^2-m_2^2)^4}\ln\frac{m_1^2}{m_2^2}\right\}+\mathcal{O}\left(\frac{m_i^2}{q^6}\right). \tag{D.11}$$

Finally, for the complete degenerating case $m_1=m_2=m_3$, we have

$$C_0[111] = -\frac{1}{2}\frac{1}{m_1^2}+\mathcal{O}\left(\frac{m^2}{q^4}\right), \tag{D.12}$$

$$C_0'[111] = -\frac{1}{24}\frac{1}{m_1^4}+\mathcal{O}\left(\frac{m^2}{q^6}\right). \tag{D.13}$$

D.2 The high-energy limit

We will list formulas needed to reproduce the analytic high-energy expressions of M_τ^{00} amplitudes, Eqs. (5.7a) and (5.7b). The leading contribution of B_i-function in such cases is obtained as

$$B_0(q^2;m_1,m_2) = \ln\mu^2-\ln|q^2|+i\pi\theta(q^2)+2+\mathcal{O}\left(\frac{m_i^2}{q^2}\right), \tag{D.14}$$

$$B_1(q^2;m_1,m_2) = -\frac{1}{2}\left\{\ln\mu^2-\ln|q^2|+i\pi\theta(q^2)+2+\mathcal{O}\left(\frac{m_i^2}{q^2}\right)\right\}, \tag{D.15}$$

$$B_2(q^2;m_1,m_2) = \frac{1}{3}\left\{\ln\mu^2-\ln|q^2|+i\pi\theta(q^2)+\frac{13}{6}+\mathcal{O}\left(\frac{m_i^2}{q^2}\right)\right\}, \tag{D.16}$$

$$B_5(q^2;m_1,m_2) = \frac{q^2}{3}\left\{\ln\mu^2-\ln|q^2|+i\pi\theta(q^2)+\frac{8}{3}+\mathcal{O}\left(\frac{m_i^2}{q^2}\right)\right\}, \tag{D.17}$$

$$B_5'(q^2;m_1,m_2) \to \frac{1}{3}\left\{\ln\mu^2-\ln|q^2|+i\pi\theta(q^2)+\frac{5}{3}+\mathcal{O}\left(\frac{m_i^2}{q^2}\right)\right\}, \tag{D.18}$$

where m_i symbolizes m_1 or m_2.

References

[1] K. Hagiwara, R.D. Peccei, D. Zeppenfeld and K. Hikasa, Nucl. Phys. **B282** (1987) 253.

[2] W. Beenakker *et al.* , *WW Cross-sections and Distributions*, in *Physics at LEP2*, eds. G. Altarelli and F. Zwirner, CERN Report 1996 (`hep-ph/9602351`), and references therein.

[3] B. Holdom, Phys. Lett. **B258** (1991) 156.

[4] K. Hagiwara, T. Hatsukado, S. Ishihara and R. Szalapski, Nucl. Phys. **B496** (1997) 66.

[5] S. Alam, S. Dowson and R. Szalapski, Phys. Rev. **D57** (1998) 1577.

[6] M. Lemoine and M. Veltman, Nucl. Phys. **B164** (1980) 445.

[7] R. Philippe, Phys. Rev. **D26** (1982) 1588.

[8] M. Böhm, A. Denner, T. Sack, W. Beenakker, F. Berends and H. Kuijf, Nucl. Phys. **B304** (1988) 463.

[9] C. Ahn, M.E. Peskin, B.W.Lynn and S. Selipsky, Nucl. Phys. **B309** (1988) 221.

[10] J. Fleischer, F. Jegerlehner and M. Zralek, Z. Phys. **C42** (1989) 409; J. Fleischer, K. Kolodziej and F. Jegerlehner, Phys. Rev. **D47** (1993) 830.

[11] W. Beenakker, A. Denner, S. Dittmaier, R. Mertig and T. Sack, Nucl. Phys. **B410** (1993) 245; W. Beenakker, A. Denner, S. Dittmaier and R. Mertig, Phys. Lett. **B317** (1993) 622.

[12] A. Denner and T. Sack, Z. Phys. **C45** (1990) 439; D. Bardin, W. Beenakker and A. Denner, Phys. Lett. **B317** (1993) 213; R.G. Stuart, Phys. Lett. **B262** (1991) 113, A. Aeppli, G.J. van Oldenborgh, D. Wyler, Nucl. Phys. **B428** (1994) 126; K. Melnikov, O. Yakovlev, Nucl. Phys. **B471** (1996) 90; W. Beenakker, A.P. Chapovsky, F.A. Berends, Phys. Lett. **B411** (1997) 203; A. Denner, S. Dittmaier and M. Roth, Nucl. Phys. **B519** (1998) 39, Phys. Lett. **B429** (1998) 145; W. Beenakker, F.A. Berends, A.P. Chapovsky, Nucl. Phys. **B548** (1999) 3; A. Denner, S. Dittmaier, M. Roth and D. Wackeroth, Nucl. Phys. **B560** (1999) 33, Phys. Lett. **B475** (2000) 127.

[13] W. Beenakker and A. Denner, Int. J. Mod. Phys. **A9** (1994) 4837.

[14] S. Alam, Phys. Rev. **D50** (1994) 124, 148, and 174.

[15] R. Hempfling, Proceedings of the XXXI Rencontres de Moriond, France March 16-13, 1996 (`hep-ph/9605394`).

[16] K.J.F. Gaemers, G.J. Gounaris, Z. Phys. **C1** (1979) 259.

[17] K. Hagiwara, S. Ishihara, R. Szalapski and D. Zeppenfeld, Phys. Rev. **D48** (1993) 2182.

[18] G. Gounaris *et al.* , *Triple Gauge Boson Couplings*, in *Physics at LEP2*, eds. G. Altarelli and F. Zwirner, CERN Report 1996 (`hep-ph/9601233`), and references therein.

[19] A. Arhrib, J.-L. Kneur and G. Moultaka, Phys. Lett. **B376** (1996) 127; E.N. Argyres, A.B. Lahanas, C.G. Papadopoulos, and V.C. Spanos, Phys. Lett. **B383** (1996) 63.

[20] S. Alam, K. Hagiwara, S. Kanemura, R. Szalapski and Y. Umeda, Nucl. Phys. **B541** (1999) 50.

[21] O.V. Tarasov, A.A. Vladimirov and A.Yu Zharkov, Phys. Lett. **93B** (1980) 429; K.G. Chetyrkin, A.L. Kataev and F.V. Tkachev, Nucl. Phys. **B174** (1980) 345.

[22] C. Becchi, A. Rouet, R. Stora, Ann. Phys. **98** (1976) 287.

[23] G.J. Gounaris, R. Kögerler and H. Neufeld, Phys. Rev. **D34** (1986) 3257.

[24] T. Appelquist and J. Carazzone, Phys. Rev. **D11** (1975) 2856.

[25] A. Dobado, M.J. Herrero and S. Peñaranda, Eur. Phys. J. **C7** (1999) 313, *ibid.* **C12** (2000) 673.

[26] J.M. Cornwall, D.N. Levin and G. Tiktopoulos, Phys. Rev. Lett. **30** (1973) 1268; Phys. Rev. **D10** (1974) 1145; B.W. Lee, C. Quigg and H.B. Thacker, Phys. Rev. **D16** (1977) 1519.

[27] M.S. Chanowitz and M.K. Gaillard, Nucl. Phys. **B261** (1985) 379; H. Veltman, Phys. Rev. **D41** (1990) 2294; J. Bagger and C. Schmidt, Phys. Rev. **D41** (1990) 264; H.-J. He, Y.-P. Kuang and X. Li, Phys. Rev. Lett. **69** (1992) 2619; Phys. Rev. **D49** (1994) 4842.

[28] Particle Data Group, C. Caso *et al.* , Eur. Phys. J. **C3** (1998) 1.

[29] G.C. Cho and K. Hagiwara, to appear in Nucl. Phys. **B** (`hep-ph/9912260`).

[30] K. Hagiwara and D. Zeppenfeld, Nucl. Phys. **B274** (1986) 1.

[31] K. Hagiwara, Ann. Rev. Nucl. Part. Sci. **48**, 463 (1998).

[32] K. Hagiwara, D. Haidt, C. S. Kim and S. Matsumoto, Z. Phys. **C64** (1994) 559, Erratum, *ibid.* **C68** (1995) 352.

[33] S. Eidelman and F. Jegerlehner, Z. Phys. **C67** (1995) 585.

[34] I. Riu, Talk given at the XXXIVth Rencontres de Moriond, March 13-20, 1999.

[35] K. Hagiwara, S. Kanemura, M. Klasen and Y. Umeda, In preparation.

[36] G.J. van Oldenborgh, Comput. Phys. Commun. **66** (1991) 1.

[37] The LEP Collaborations ALEPH, DELPHI, L3, OPAL, the LEP Electroweak Working Group and the SLD Heavy Flavor Group, CERN-EP/99-15.

[38] K. Hagiwara, D. Haidt and S. Matsumoto, Eur. Phys. J. **C2** (1998) 95; Y. Umeda, G.C. Cho and K. Hagiwara, Phys. Rev. **D58** (1998) 115008; G.C. Cho, K. Hagiwara and Y. Umeda, Nucl. Phys. **B531** (1998) 65; **B555** (1999) 651 (E).

[39] K. Hagiwara, S. Matsumoto and Y. Yamada, Phys. Rev. Lett. **75** (1995) 3605.

[40] A.A. Barrientos Bendezú, K.-P.O. Diener and B.A. Kniehl, DESY 99-189, MPI/PhT/99-59.

[41] G. Passarino and M. Veltman, Nucl. Phys. **B160** (1979) 151.

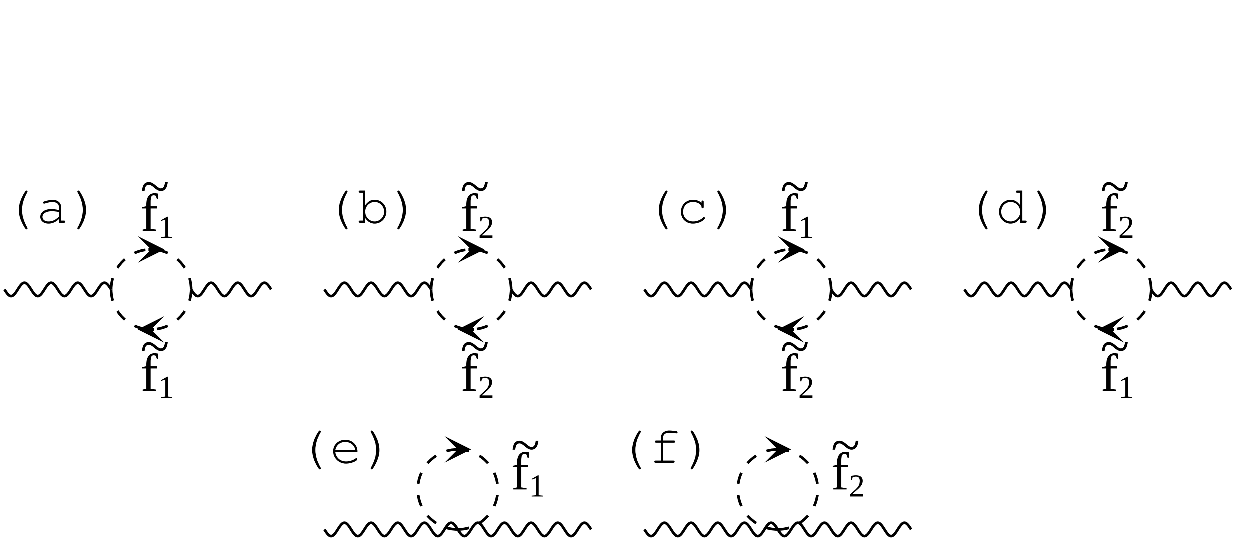

(a)
$\tilde{f}_1$
$\tilde{f}_1$
(b)
$\tilde{f}_2$
$\tilde{f}_2$
(c)
$\tilde{f}_1$
$\tilde{f}_2$
(d)
$\tilde{f}_2$
$\tilde{f}_1$
(e)
$\tilde{f}_1$
(f)
$\tilde{f}_2$